UNIVERSITAT POLITÈCNICA DE CATALUNYA BARCELONATECH

A virtual environment to evaluate and predict recovery of human hand motion post-stroke

Jesús Fernando Padilla Magaña

UNIVERSITAT POLITÈCNICA DE CATALUNYA

Programa de Doctorat:

AUTOMÀTICA, ROBÒTICA I VISIÓ

Tesi Doctoral

A Virtual Environment to evaluate and predict recovery of Human hand motion Post-stroke

Jesús Fernando Padilla Magaña

Director de tesi:

Dr. Esteban Peña Pitarch

Dra. Neus Tico Falguera

Juny de 2022

Dedicated to

My parents Jesús and Dolores, my wife Lupita, and my little daughter Nathalie, who are my inspiration and my greatest motivation.

ACKNOWLEDGMENTS

I would like to thank my advisors, Dr. Esteban Peña and Dra. Neus Tico, for their trust in allowing me to work with them on this research. I would also like to thank them for their patience, willingness, advice, and comments during my doctoral studies.

I would also like to thank the National Council of Science and Technology of Mexico (CONACYT) for the scholarship granted to obtain my Ph.D. degree.

I would also like to thank my wife for being my partner in this adventure, helping me in this research, and giving me her support. Also, I thank my parents for their unconditional support and love. I thank my siblings and aunt Carmen for their advice and encouragement in carrying out this research. I also thank my niece Elizabeth for helping me with the English editing.

Finally, I would like to thank Dr. Isahi Sanchez for his advice on this research and for motivating me to pursue a Ph.D.

ABSTRACT

The Action Research Arm Test (ARAT) is a measurement tool to assess post-stroke upper extremities motor function. However, ARAT scoring can be subjective and limited only to determining performance quality. Therefore, in this thesis, we presented a novelty hand motion system to improve the evaluation with the ARAT. The hand motion system is composed of a data glove CyberGlove II®, a Finger force sensing module, and a Graphical User Interface (GUI). In this thesis, three studies were conducted to evaluate whether the hand motion system improved the assessment with the ARAT.

Firstly, in Chapter 4, we performed an analysis on healthy subjects using the hand motion system during the performance of the ARAT. We determined the fingertip force and the flexion angles of the metacarpophalangeal (MCP) and proximal interphalangeal (PIP) joints of the fingers (index, middle, ring, and little) and carpometacarpal (CMC), MCP, and interphalangeal (IP) for the thumb. The results showed that the flexion angles and the finger force depend on the object size and the type of grasp used (power, grip, or pinch). In addition, an important database of the range of motion of the finger joints and finger forces was obtained.

Secondly, Chapter 5 evaluated post-stroke patients with right (RH) and left (LH) hemiparesis to identify joint impairments and compensatory grasping strategies. For this purpose, an experimental study was carried out with 12 patients six months after a stroke with a global ARAT score ≥ 10. The range of motion (ROM) of the finger joints in stroke patients was compared with the data obtained in Chapter 4. Stroke patients with LH and RH showed significantly lower flexion angles in the MCP joints of the Index and Middle fingers than the Control group. However, RH patients showed larger flexion angles in the PIP joints of the Index, Middle, Ring, and Little fingers. In contrast, LH patients showed larger flexion angles in the PIP joints of the Middle and Little fingers. Therefore, the results showed that RH and LH patients used compensatory strategies involving increased flexion at the PIP joints for decreased flexion in the MCP joints. In addition, the hand motion system allows the detection of finger joint impairments in stroke patients that are not visible from ARAT scores.

Finally, in Chapter 6, we developed classification models to predict whether activities with similar ARAT scores were performed by a healthy subject or by a subject with stroke. For this purpose, we used three classification algorithms: Support Vector Machine (SVM), Random Forest (RF), and K-N Neighbors (KNN). The results showed that the SVM classifier had the best performance, with a precision of 98.3% and an accuracy of 94.5 %. However, the dataset showed class imbalance and the classification models presented a low recall, especially in the stroke class. Therefore, we implemented class balance using the technique Borderline-SMOTE (BSM). After data balancing, the models showed a significantly higher

accuracy, recall, f1-score, and AUC. The SVM classifier showed a higher performance with a precision of 98% and a recall of 97.5% after data balancing. Hence, the results showed that classification models based on human hand motion features combined with BSM achieve higher performance.

Therefore, we conclude that integrating the hand motion system during the performance of the ARAT allows for a quantitative, accurate, and sensitive assessment. Furthermore, the proposed method is of clinical relevance as it will help health care professionals to create more specific and effective rehabilitation programs for functional recovery of the hand in patients with stroke and other chronic diseases.

Keywords: finger joints; finger force; ARAT; stroke; CyberGlove II; machine learning; hand; rehabilitation

RESUMEN

El Action Research Arm Test (ARAT) es una herramienta para evaluar la función motora de las extremidades superiores después de un ictus. Sin embargo, la puntuación del ARAT puede ser subjetiva y limitarse a evaluar solamente la calidad del rendimiento de la tarea. Por lo tanto, en esta tesis presentamos un novedoso sistema de movimiento de la mano para mejorar la evaluación con el ARAT. El sistema está compuesto por un guante de datos CyberGlove II®, un módulo de detección de fuerza de los dedos y una interfaz gráfica de usuario. En esta tesis, se realizaron tres estudios para determinar si el sistema propuesto mejoraba la evaluación con el ARAT.

En primer lugar, en el Capítulo 4 se realizó un estudio en sujetos sanos utilizando el sistema de movimiento de la mano durante la realización de la ARAT. Se determino la fuerza de los dedos y los ángulos de flexión de las articulaciones metacarpofalángicas (MCP) e interfalángicas proximales (PIP) de los dedos (índice, medio, anular y meñique) y carpometacarpiana (CMC), MCP e interfalángica (IP) del pulgar. Los resultados mostraron que los ángulos de flexión y la fuerza de los dedos dependen del tamaño del objeto y del tipo de agarre utilizado.

En segundo lugar, en el Capítulo 5 se evaluaron pacientes con ictus con hemiparesia derecha e izquierda para identificar deficiencias articulares y estrategias de agarre compensatorias. Para ello, se realizó un estudio experimental con 12 pacientes seis meses después de un ictus con una puntuación ARAT global ≥ 10. El rango de movimiento (ROM) de las articulaciones de los dedos en los pacientes con ictus se comparó con los datos del Capítulo 4. Los pacientes con ictus con LH y RH mostraron ángulos de flexión significativamente menores en las articulaciones MCP de los dedos índice y medio que el grupo de control. Sin embargo, los pacientes con RH mostraron mayores ángulos de flexión en las articulaciones PIP de los dedos índice, medio, anular y meñique. Por el contrario, los pacientes del grupo LH mostraron mayores ángulos de flexión en las articulaciones PIP de los dedos medio y meñique. Por lo tanto, los resultados mostraron que los pacientes RH y LH utilizaron estrategias compensatorias que implicaban un aumento de la flexión en las articulaciones PIP debido a la disminución de flexión en las articulaciones MCP. Además, el sistema permitió detectar deficiencias en las articulaciones de los dedos que no son visibles con el ARAT.

Por último, en el Capítulo 6, se desarrollaron modelos de clasificación para predecir actividades con puntuaciones ARAT similares de sujeto sanos y sujetos con ictus. Para ello, se utilizaron tres algoritmos de clasificación: Maquinas de vector soporte (SVM), Bosques aleatorios (RF) y K vecinos más cercanos (KNN). Los datos mostraban un desbalanceo de clases y los clasificadores presentaron una baja exhaustividad, especialmente en la clase de ictus. Por lo tanto, se implementó el balanceo de clases con la técnica

Borderline-SMOTE (BSM). Después de equilibrar los datos, los clasificadores mostraron una precisión, una exhaustividad, una puntuación f1 y un AUC significativamente mayores. El clasificador SVM mostró el mayor rendimiento con una precisión de 98% y una exhaustividad de 97.5%. Por lo tanto, los resultados mostraron que los clasificadores basados en características del movimiento de la mano humana combinados con el algoritmo BSM lograron un mayor rendimiento.

Por lo tanto, concluimos que la integración del sistema de movimiento de la mano durante la realización del ARAT permite una evaluación cuantitativa, precisa y sensible. Además, el método propuesto es de relevancia clínica ya que ayudará a los profesionales de la salud a crear programas de rehabilitación más específicos y eficaces para la recuperación funcional de la mano en pacientes con ictus y otras enfermedades crónicas.

Palabras clave: articulaciones de los dedos; fuerza de los dedos; ARAT; ictus; CyberGlove II; aprendizaje automático; mano; rehabilitación

CONTENTS

ACKNOWLEDGMENTS ..... *I*

ABSTRACT ..... *II*

RESUMEN ..... *IV*

CONTENTS ..... *VI*

List of Figures ..... *X*

List of Tables ..... *XIII*

List of Abbreviations ..... *XV*

CHAPTER 1 ..... *1*

Introduction *1*

1.1 Motivation **1**

1.2 State of Art **2**

1.2.1 Data Glove based capturing 2

1.2.2 Force sensing 3

1.2.3 Sensors for stroke rehabilitation 4

1.2.4 Incorporation of sensors in the Action Research Arm Test (ARAT) 4

1.2.5 Machine Learning and ARAT test 5

1.2.6 Machine Learning in Clinical Measures of Upper extremities 5

1.3 Thesis Objectives **6**

1.4 Outline of the Thesis **6**

CHAPTER 2 ..... *8*

Anatomy of the Hand *8*

2.1 Basic Hand Anatomy **8**

2.1.1 Finger Joints 9

2.1.2 Palm Arch 10

2.1.3 Normal Range of motion 11

2.1.4 Muscular Hand Function 13

2.2 Methods of ROM Measurement **13**

2.2.1 Goniometer 13

2.2.2 Inclinometer 14

2.2.3 Electrogoniometers 14

2.2.4 Radiography and Photography 14

2.3 Types of human grip **14**

2.3.1 Power Grip 14

2.3.2 Precision Grip 15

2.4 Hand force measurement methods **15**

2.4.1 Dynamometer 15

CHAPTER 3 ..... *16*

Human Hand Motion System *16*

3.1 Overview **16**

3.2 Introduction **16**

3.3 Data Glove **17**

3.3.1 Calibration 17

3.4 Force sensing module **19**

3.4.1 Force Sensors 19

3.4.2 Signal conditioning 22

3.4.3 Signal filtering 25

3.4.4 Data Acquisition 27

3.4.5 Graphical User Interface 28

3.4.6 Digital Filter 30

3.5 Hand Model and Simulation **31**

3.5.1 Hand model 31

3.5.2 Simulation 34

3.6. Conclusions **34**

CHAPTER 4 ..... *35*

Hand Motion Analysis in Healthy Subjects during the performance of the Action Research Arm Test *35*

4.1. Overview **35**

4.2. Introduction **35**

4.3 Materials and Methods **37**

4.3.1. Action Research Arm Test 37

4.3.2. Participants 38

4.3.3. Experimental Setup 39

4.3.4. Statistical Analysis 40

4.4. Results **40**

4.4.1. Finger Joints Flexion Angles 40

4.4.2. Pinch Subtest t-Test 41

4.4.3. Grasp, Grip, and Pinch Subtests 42

4.4.4. Flexion Angle of Each Finger Joint during the 16 Tests 45

4.4.5. Differences in the Flexion Angles Respect to Age and Hand Length Groups 47

4.4.6. Fingertip Forces 49

4.4.7. Differences in Fingertip Force with Respect to Age Groups 50

4.5. Discussion **51**

4.6. Limitations **53**

4.7. Conclusions **53**

CHAPTER 5 ..... *54*

Quantitative Assessment of Hand Function in Healthy Subjects and Post-Stroke Patients with the Action Research Arm Test *54*

5.1. Overview **54**

5.2. Introduction **54**

5.3. Methods ... **56**
5.3.1. Subjects ... 56
5.3.2. Experimental Protocol ... 57
5.3.3. Experimental Equipment ... 57
5.3.4. Data Analysis ... 58
5.4. Results ... **59**
5.4.1. Functional Range of Motion of the Finger Joints ... 59
5.4.2. Range of Motion of the Finger Joints in the Stroke Group with Right Hemiparesis ... 60
5.4.3. Range of Motion of the Finger Joints in the Stroke Group with Left Hemiparesis ... 61
5.4.4. Comparison of the Range of Motion between the Stroke Groups ... 63
5.5 Discussion ... **63**
5.6. Limitations ... **66**
5.7. Conclusions ... **66**
CHAPTER 6 ... ***68***
Classification Models in Post-stroke patients based in Human Hand Motion ... ***68***
6.1. Overview ... **68**
6.2. Introduction ... **68**
6.2. Basic Concepts ... **69**
6.2.1. Machine Learning ... 69
6.2.2. Classification Models ... 69
6.2.3. Support vector machine (SVM) ... 70
6.2.4. K-Nearest Neighbor Classification ... 73
6.2.5. Random Forest ... 74
6.3 Methods ... **75**
6.3.1. Programming Language ... 75
6.3.2. Data pre-processing ... 76
6.3.3. Training and testing sets ... 76
6.3.4. Tuning hyperparameters ... 77
6.3.5. Classification metrics ... 77
6.3.6. Over-sampling Data ... 80
6.3.7. Statistical Analysis ... 81
6.4. Results ... **81**
6.4.1. Hyperparameters selection ... 82
6.4.2. Performance of the Classification Models in the Dataset ... 82
6.4.3 Comparison of classification models ... 84
6.4.4. Classification Models with Borderline-SMOTE ... 85
6.4.5. Performance Comparison between Classifiers after Borderline-SMOTE ... 86
6.4.6. Performance comparison of the Classifiers before and after data balancing ... 87
6.5. Discussion ... **89**
6.6 Limitations ... **91**
6.7. Conclusions ... **92**
CHAPTER 7 ... ***93***
Conclusions and Future Work ... ***93***
7.1 Conclusions ... **93**

7.2 Future Work **94**

Bibliography ***95***

List of Publications ***103***

Journals **103**

Conference Papers **103**

Appendix A ***104***

Supplementary material for Chapter 5 ..... **104**

Appendix B ***108***

Supplementary material for Chapter 6 ..... **108**

Appendix C ***110***

Participant Information Sheet **110**

Consent Form **112**

List of Figures

Figure 2.1. Bones of the Human Hand.....8

Figure 2.2. Finger Joints of the Index Finger and the Thumb. 10

Figure 2.3. The three arches supporting the palm of the hand: one longitudinal and two transverse.....11

Figure 2.4. Abduction/adduction(Ab/Ad) (left); Flexion/extension (F/E) for one finger(right) 11

Figure 2.5. Radial/ulnar deviation of the wrist (left); Flexion/extension of the wrist (right) 12

Figure 3.1. Diagram of the Hand motion system. 16

Figure 3.2. A subject wearing the CyberGlove II.....17

Figure 3.3. Dorsal view of the model of the right hand with 25 degrees of freedom. 17

Figure 3.4. Numbering of the sensors used (CyberGlove II®) 18

Figure 3.5. Basic schematic of the force sensing resistor (FSR).....20

Figure 3.6. The Force sensing resistors family of Ohmite (Manufacturing Company, USA).....20

Figure 3.7. Force Sensing Resistor FSR07. 21

Figure 3.8. Curve of Resistance vs Force.....21

Figure 3.9. Curve of Conductance vs Force.....22

Figure 3.10. Circuit of a voltage divider for a force sensing resistor (FSR).....22

Figure 3.11. Characteristic curves for a FSR Voltage Divider with different RG resistor values.....23

Figure 3.12. Inverting operational amplifier circuit diagram for an FSR.....24

Figure 3.13. Characteristic curves for a FSR Inverting Operational Amplifier with different RG resistor values.....24

Figure 3.14. Circuit diagram of the force sensing module; configuration for a single FSR is shown.....26

Figure 3.15. Calibration curve of a single FSR. 27

Figure 3.16. Schematic circuit of the Arduino Nano.....28

Figure 3.17. Main menu scene of the Graphical User Interface (GUI).....29

Figure 3.18. ARAT menu scene of the Graphical User Interface.....30

Figure 3.19. Butterworth filter gain at distinct orders. 30

Figure 3.20. Parametric length for a hand. 31

Figure 3.21. Parametric length for a finger.....32

Figure 3.22. Parametric length for the Thumb.....32

Figure 3.23. Hand model created in Blender with parametric lengths. 33

Figure 3.24. Hand model in the Unity Scene. 34

Figure 4.1. A participant is wearing the hand motion system, performing the Action Research Arm test (ARAT).....39

Figure 4.2. Welch's ANOVA and post hoc results; Comparison of flexion angles of the Thumb joints concerning the three Subtests of the ARAT.. 43

Figure 4.3. Welch's ANOVA and post hoc results; Comparison of flexion angles of the Index and Middle joints concerning the three Subtests of the ARAT.. 44

Figure 4.4. Welch's ANOVA and Post hoc results; Comparison of flexion angles of the Ring and Little joints concerning the three Subtests of the ARAT.. 45

Figure 4.5. Welch's ANOVA and Post hoc results; Comparison flexion angles concerning the finger joints, during the 16 tests of the ARAT. 46

Figure 4.6. Mann–Whitney U test flexion angle of the finger joints with respect to different age groups 47

Figure 4.7. Mann–Whitney U test of flexion angle in finger joints with respect to different hand length groups. 48

Figure 4.8. Mann–Whitney U test of flexion angle in finger joints with respect to different hand length groups. 49

Figure 5.1. Functional range of motion in each finger joint. 59

Fig 6.1. Illustration of data with Linear Separation (left); Illustration of data with Non-linear Separation (right). 70

Fig 6.2. Example of different separation hyperplanes (left); Example of over-fitting problem with training and classification data (highlighted in yellow) (right). 71

Fig 6.3. Example of Optimal Separating Hyperplane and its associated maximum margin; Hyperplane and decision boundary are equivalent at small dimension space. 71

Fig 6.4. Example of Soft-Margin in SVM. 72

Fig 6.5. Example of Non-Linear SVM; Kernel= Radial basis function (RBF). 73

Fig 6.6. Illustration example of K-Nearest Neighbor (KNN) algorithm. 74

Fig 6.7. Conceptual diagram of the Random Forest algorithm. 75

Figure 6.8. Confusion Matrix Binary Classification. 78

Figure 6.9. Example of distinct receiver operating characteristic curves (ROC). 80

Fig 6.10. Random Forest (RF) Confusion Matrix 82

Fig 6.11. K-nearest neighbor (KNN) Confusion Matrix. 83

Fig 6.12. Support Vector Machine Confusion Matrix. 84

Figure 6.13. The receiver operating characteristic curves (ROC) of the three classification models in the test set. 84

Figure 6.14 Distribution of each class in the dataset; 0=Control and 1=Stroke. 85

Figure 6.15. Distribution of each class in the dataset after Borderline-SMOTE. 85

Fig 6.16. The receiver operating characteristic curves (ROC) of the three classification models with Borderline-SMOTE 86

Figure 6.17. Comparison of Precision between Classification models with imbalanced and oversampled data 87

Figure 6.18. Comparison of Accuracy between Classification models with imbalanced and oversampled data. 88

Figure 6.19. Comparison of Recall between Classification models with imbalanced and oversampled data 88

Figure 6.20. Comparison of F1-score between Classification models with imbalanced and oversampled data 89

Figure 6.21. Comparison of AUC between Classification models with imbalanced and oversampled data 89

Fig B1. Random Forest Confusion Matrix after Borderline-SMOTE.....108

Fig B2. K-nearest neighbor Confusion Matrix after Borderline-SMOTE. 108

Fig B3. Support Vector Machine Confusion Matrix after Borderline-SMOTE 109

List of Tables

Table 2.1. Range of Motion for the joints of the Hand 12

Table 3.1 Calibration equations for finger joints. 19

Table 3.2. Formulas for determining metacarpal and phalangeal bone lengths 32

Table 3.3. Lengths for the metacarpal and phalangeal bones of the hand model 33

Table 4.1. Materials and test description of the Action Research Arm Test 38

Table 4.2. Descriptive data of the subjects. 38

Table 4.3. Descriptive statistics of flexion angles required to perform ARAT test. 41

Table 4.4. Independent samples t-test for comparison flexion angles with respect to Test 12 and Test 14. 42

Table 4.5. Independent samples t-test for comparison flexion angles with respect to Test 13 and Test 16. 42

Table 4.6. Independent samples t-test for comparison flexion angles with respect to Test 11 and Test 15. 42

Table 4.7. Descriptive statistics of fingertip forces during the performance of the ARAT test. 50

Table 4.8. Independent samples t-test for comparison finger forces in grasp subtest, with respect to different groups of age (18–32 years) and (45–72 years). 50

Table 4.9. Independent samples t-test for comparison finger force in grip subtest, with respect to different groups of age (18–32 years) and (45–72 years). 51

Table 5.1. Characteristics of the groups. 57

Table 5.2. Flexion angles of the functional range of motion (FROM) during 14 tests. 60

Table 5.3. Range of motion (ROM) during the sixteen activities (control and right hemiparesis). 60

Table 5.4. Results of Mann–Whitney test of the ROM with respect to the control and right hemiparesis groups. 61

Table 5.5. Range of motion (ROM) during the sixteen activities (control and left hemiparesis). 62

Table 5.6. Results of Mann–Whitney test of the ROM with respect to the control and left hemiparesis groups. 62

Table 5.7. Results of Mann–Whitney test of the ROM with respect to the stroke groups (left hemiparesis vs. right hemiparesis). 63

Table 6.1 Dataset variables 76

Table 6.2. Random Forest model classification report 82

Table 6.3. K-nearest neighbor model classification report 83

Table 6.4. Support Vector Machine model classification report 83

Table 6.5. Comparison of classification models in different evaluation metrics 84

Table 6.6. Classification Report of the three classification models after data balancing (Borderline-SMOTE) *86*

Table 6.7. Comparison of classification models after Borderline-SMOTE in different evaluation metrics ..*87*

Table A1.1. Results of Mann–Whitney test of the arc of motion (AROM) with respect to the Control and Right hemiparesis groups. *104*

Table A1.2. Results of Mann–Whitney test of the AROM with respect to the Control and Left hemiparesis groups. *104*

Table A1.3. Results of Mann–Whitney test of the AROM with respect to the Stroke groups (Left hemiparesis vs Right hemiparesis). *105*

Table A1.4. Functional Range of Motion (FROM) for each finger joint *106*

Table A1.5. Subtest Range of Motion (sROM) during the performance of the Grasp Subtest (All groups) *106*

Table A1.6. Subtest Functional Range of Motion (sROM) during the performance of the Grip Subtest (All groups) *107*

Table A1.7. Subtest Functional Range of Motion (sROM) during the performance of the Pinch Subtest (All groups) *107*

Table B1.1. Random Forest Paired t-test *109*

Table B1.2. Support Vector Machine Paired t-test *109*

Table B1.3. K-nearest Neighbors Paired t-test *109*

List of Abbreviations

Ab/Ad	Abduction/Adduction
ARAT	Action Research Arm Test
ADLs	Activities of daily living
ANOVA	Analysis of Variance
aROM	Arc of motion
AUC	Area Under the Curve
ANNs	Artificial neural networks
CMC	Carpometacarpal Joints
CAHAI	Chedoke Arm and Hand Inventory
CSV	Comma-Separated Values
CNNs	Convolutional neural networks
fc	Cutoff frequency
DOF	Degrees of freedom
EMG	Electromyography
E/F	Extension/Flexion
FNT	Finger-to-nose task
FSRs	Force sensing resistors
FMA	Fugl-Meyer assessment
FROM	Functional range of motion
GUI	Graphical User Interface
HB	Hand breadth
HL	Hand length
IMU	Inertial measurement unit
IDE	Integrated Development Environment
IP	Interphalangeal Joints
KNN	K-Nearest Neighbors
LF	Left hemiparesis
ML	Machine learning
MCP	Metacarpophalangeal Joints
9-HPT	Nine Hole Peg Test
Op-amp	Operational amplifier
OMs	Outcome measures
PIP	Proximal interphalangeal joints
RBF	Radial Basis Function
RF	Random Forest
ROM	Range of motion
ROC	Receiver Operating Characteristic
RH	Right hemiparesis
SVM	Support Vector Machine
UE	Upper extremity
WMFT	Wolf Motor Function Test

CHAPTER 1
Introduction

1.1 Motivation

Stroke remains one of the leading causes of death and disability in Europe, and projections show that the burden of stroke will not decrease in the next decade or beyond. An important contributing factor to this is that the number of older persons in Europe is rising, with a projected increase of 35% between 2017 and 2050 [1]. Stroke is caused by the death of brain cells as a result of blockage of a blood vessel supplying the brain (ischemic stroke) or bleeding into or around the brain (hemorrhagic stroke), is a serious medical emergency [2]. According to the World Health Organization, 15 million people suffer stroke worldwide each year. Of these, 5 million die and another 5 million are permanently disabled. Therefore, it is one of the main causes of disability, a large number of people who survive have important sequels that limit the performance of their activities of daily living (ADL). In addition, the need of medical attention translates in a very high economic cost in health services e.g. the expense on both caring and rehabilitation reaches $34 billion per year in the US [3]. One of the main sequels produced by Stroke is the loss of mobility in the upper extremities of the human body (hands). The human hand consists of 27 bones and 27 joints and is one of the most important tools in the human body. The hands allow us to perform a wide variety of actions to interact with the environment, such as touching, reaching, holding, grasping, and manipulating different types of objects. The people who suffer the loss of mobility in this upper extremity of the human body (hand) endure a great negative impact on their living standards, causing problems in their family, work, and social environment. For that reason, the rehabilitation process for hand recovery is vital to post-stroke patients. The rehabilitation process is traditionally carried out by a physiotherapist specializing in treating disabilities related to motor and sensory impairments [4]; hand therapy helps to improve strength and increase the range of motion (ROM) of the finger joints. Therefore, to evaluate and improve the effectiveness of rehabilitation programs, it is important to assessment upper extremity (UE) function, and the use of standardized outcome measures (OMs) can lead to more efficient rehabilitation for the patients [5], [6]. There are several types of OMs used for evaluating patients with UE disability with good psychometric these are: the Fugl-Meyer assessment (FMA), the Action Research Arm Test, the Box and Block test (BBT), the Chedoke Arm and Hand Inventory (CAHAI), the Nine Hole Peg Test (9-HPT), and the Wolf Motor Function Test (WMFT). However, one of the most OMs used by physical therapists and other health care professionals to assess the performance of the upper extremities in people post-stroke is The Action Research Arm Test (ARAT). The ARAT is a measurement tool used to assess UE functional impairments that has shown good reliability and validity [7], [8], [9]. The ARAT evaluates 19 movement

tasks divided into four subtests (Grasp, Grip, Pinch, and Gross arm movement) assess a patient's ability to handle objects differing in size, weight, and shape.

However, the ARAT, like most other OMs, requires a human examiner to transform observations of the patient's movement into a score. Therefore, reliance on a human examiner leaves room for subjective measures, especially in scoring, limited to assessing the quality of performance on each task. The ARAT also presents problems in assessing patterns of movement abnormality that emerge after stroke [7]. In addition, it presents a ceiling effect that prevents detection of improvements produced with rehabilitation treatments in subjects with mild impairments with high scores [10]. In recent years, due to technological development, several investigations have been developed in medical rehabilitation post-stroke, such as using multiple types of sensors to measure human hand motion. However, to the best of our knowledge, few studies integrate sensors during the performance of the ARAT [10],[11],[12],[13] but none of them focused on the assessment of hand function through the analysis of the range of motion (ROM) of the finger joints and the fingertip forces. Therefore, we proposed in this thesis the use of a Hand motion system based on a data glove (CyberGlove II®) and five force-sensing resistors (FSRs) during the performance of the ARAT. The system is a novel alternative for occupational therapists and health care professionals for a more objective, sensitive, and quantitative assessment method with the ARAT in post-stroke patients.

1.2 State of Art

In the last years, due to technological development, several investigations have been developed in robotics, biomechanics, and medical rehabilitation, such as using multiple types of sensors to analyze human hand motion. Sensors for hand motion analysis most commonly used are Data glove, Inertial measurement unit (IMU), Optical markers, vision-based capturing (Ordinary Cameras, Depth Cameras, Leap Motion Controller), electromyography sensor (EMG), and Force sensors (Capacitive, Piezoresistive, Piezoelectric) [14] [15]. The hand motion data obtained from these sensors allow us to know: hand position, finger joint angles, force detection, and angular velocity in real-time.

1.2.1 Data Glove based capturing

Data gloves are the more popular and widely sensor used in research use highly precise sensors to achieve hand dynamic gestures including positions, velocities, and accelerations. The gloves use different types of sensors, such as wire driven mechanism, optical fiber sensors, resistive bend sensors, inertial measurement units (IMUs). Some Gloves are commercial and others was developed for researchers. The first glove prototypes included the Sayre Glove, the Massachusetts Institute of Technology (MIT)- LED glove, and the Digital Entry Data Glove. The Sayre Glove was developed in 1977 by Thomas de Fanti and Daniel Sandin based on the idea of Rich Sayre. This glove used flexible tubes with a light source at one end and a photocell at the other, mounted along with each finger [16]. The first glove-like data system is the Digital Data Entry Glove developed at AT&T Bell Laboratories in 1983. This glove was designed to

measure hand positions, including finger flexure, hand orientation, and wrist position (Grimes G,1983). In the 80s Thomas G. Zimmerman developed research about hand gestures with the VPL Data Glove TM and the Z-Glove TM [17]. These lightweight gloves with flexion sensors measured finger flexion, positioning, and orientation systems, and used tactile feedback vibrators. Moreover, the CyberGlove I model CG1801 has 18 or 22 bend sensors placed at critical points to measure the posture of the hand [18] , which was used in researches [19], [20].

On the other hand, the CyberGlove II uses 18 or 22 bend sensors to capture the hand and finger motion. The CyberGlove II 22-sensor model has three flexion sensors per finger, four abduction sensors, a palm arch sensor, and measures flexion and abduction [21]. The CyberGlove II has been used in various research about: teleoperation [22], human robot interaction [23], [24], rehabilitation [25], [26] [27]. In contrast, the CyberGlove III glove provides 22 bend sensors placed along each MCP, PIP and DIP finger joint. This glove has been used in applications witch touchscreen gestures by Asakawa [28], Hand pose estimation [29]. Other several glove prototypes with bend sensors have been developed by [30] [31] [32] [33] [34]. On the other hand, some Data-glove-based systems for tracking hand motion use sensors of mechanical architecture [35], [36] . In 2014, Park et al. proposed a data glove-based system composed of linear potentiometers, flexible cables, and linear springs to measure finger flexion angles [36]. Another similar glove that used linear potentiometer was developed by Saliba et al. [37]. The most representative data-glove-based system with optical fiber sensors is the 5DT data glove MRI developed by the Fifth Dimension Technologies. The 5DT data glove has been used to capture hand motion in virtual reality [38], for rehabilitation [39][40], for applications in biomechatronics [41], for teleoperation [42] and for hand gesture recognition [43]. Another commercial glove is the Human Glove (manufactured by HumanWare) consists of 22 Hall Effect sensors that measure the flexion-extension and adduction–abduction movements of the fingers and wrist. In addition, we found a review of commercial Data Glove Systems in the study presented by Dipietro [16]. The Gloves based on inertial measurement units (IMUs) can record hand kinematics accurately and provide valuable parameters, such as measures parameters such as angular velocity, acceleration, and range of motion [44]. A sensory glove for hand-object manipulation that employs a network of 15 IMUs to measure the rotations between individual phalanxes was developed by Liu [45]. A data glove system with 6-axis IMU sensors to capture hand kinematics was developed by Shing Lin [46]. Finally, a Novel Smart Glove for measuring the angles of the finger joints was developed by O´Flynn [47].

1.2.2 Force sensing

Haptics/tactile/force information is an important part of the study of human hand motions, especially for object manipulations. In order to measure the force applied by the human hand, there have been implemented several types of research. Some researchers placed force sensors on the object of interaction, and others placed sensors just on the subject's fingertips. However, this thesis focuses on force sensors placed on the hand or the fingertips. A glove equipped with six customized force sensors made from

Velostat for the study of hand-object manipulation was proposed by Liu et al. [45]. Nikonovas et al. developed a system that measures forces over the entire hand using 12 Flexiforce sensors (Tekscan Inc., Boston, MA, USA) in each hand [48]. On the other hand, Qiang et al. developed a Force-sensing glove system for measuring real-time hand forces during motorbike riding, using two gloves with four Flexiforce sensors [49]. While Battaglia et al. proposed the ThimbleSense: a fingertip-wearable tactile sensor for grasp analysis [50]. Ferre et al. developed a thimble with Flexiforce sensors for measuring forces applied during manipulating virtual and real objects [51]. Castro and Cliquet proposed a Low-Cost instrumented glove for monitoring forces during object manipulation with force sensing resistors (FSR) by Interlink Electronics [52]. O'Flynn et al. developed the Tyndall glove composed of a combination of 20 bend sensors, 16 triaxial accelerometers and 11 force sensors to detect joint movement and force [33]. As we can see, many researchers use the Flexiforce sensors; we can find a complete study of this sensor made by Vecchi [53].

1.2.3 Sensors for stroke rehabilitation

Assessment and analysis of upper extremities in post-stroke patients using diverse types of sensors can be found in several studies. Lin et al. proposed a data glove system integrated with six-axis inertial measurement unit sensors for evaluating the hand function in patient post-stroke [54]. A shoe-based sensor with force-sensitive resistors (FSRs) to accurately identify postures in people with stroke was proposed by Fulk and Sazonov [55]. Ambar et al. designed an arm rehabilitation monitoring device utilizing an Arduino based Microcontroller using a flex sensor to detect arm bending movement, an IMU board (InvenSens Inc., San José, CA, USA) and two force-sensitive resistors to detect muscle force [32]. Data from a Microsoft Kinect sensor (kinematic upper limb) and an FSRs glove (strength of muscles) were used to predict muscle forces in stroke patients through the least square regression matrix by Hoda et al. [56]. A data-glove-based system embedded with 9-axis IMUs sensors and FSRs for evaluation of hand function was designed by Hsiao et al.[44]. Kim et al. used a Microsoft Kinect sensor during the Fugl–Meyer assessment (FMA) to predict scores in hemiplegic stroke patients [57]. Schwarz et al. used a wearable inertial sensing system composed of eight IMUs, with triaxial accelerometers and gyroscopes, to assess upper extremity movement impairments after stroke [12]. Ganeson et al. developed a low-cost instrumented glove based on flex sensors and FSRs for post-stroke hand rehabilitation [58].

1.2.4 Incorporation of sensors in the Action Research Arm Test (ARAT)

The use of sensors allows for more quantitative and sensitive assessment methods during clinical rehabilitation of the upper extremities. However, to the best of our knowledge, few studies have integrated sensors during the performance of the ARAT. Carpinella et al. presented an analysis for quantitative assessment of upper limb motor function on healthy subjects and persons with Multiple Sclerosis, using a single inertial sensor on the wrist [10]. Nam et al. quantified the Range of Motion (ROM) of the upper extremities (UE) during the performance of the ARAT and six essential ADL, using 25 Inertial Measurement Unit (IMU) sensors [11]. Ticó Falguera assessed the functional recovery of the upper

extremity and the motion of the finger joints in stroke patients with the CyberGlove II® from week one after stroke to six months after stroke [25]. Held et al. designed a study to evaluate rehabilitation progress with a full-body IMU system (Xsens Technologies, Enschede, Netherlands) in stroke patients, over four weeks [13]. Repnik et al. presented a study in healthy subjects and patients post-stroke to quantify upper limb movement, using a wearable system of seven IMUs for kinematics and electromyography (EMG) sensors for muscle activity analysis [59].

1.2.5 Machine Learning and ARAT test

In recent years, machine learning models have been used to predict outcome measures such as the ARAT and to classify functional motion performance. Dutta et al. evaluated grasp abilities in the ARAT test with Support Vector Machine (SVM) algorithms in healthy subjects and post-stroke patients using an instrumented glove composed of six flex sensors, three force sensors, and a motion processing unit [60]. In contrast, Bochniewicz et al. during the performance of the ARAT used a Random Forest model to classify UE movement into functional and non-functional, using inertial measurement units (IMU) [61]. Lum et al. developed several machine learning algorithms K-Nearest Neighbors (KNN), Random Forest (RF), Linear Support Vector Machine (SVM), and Radial Basis Function SVM (RBF-SVM) to classify functional and nonfunctional activities using a wrist-worn IMU during the performance of the ARAT [62]. Moreover, Kanzler et al. predicted outcomes scores of the ARAT, BBT, and 9-HPT with several machine learning models (decision tree, KNN, linear regression, and RF) using clinical data, and digital health metrics [63].

1.2.6 Machine Learning in Clinical Measures of Upper extremities

Furthermore, the use of machine learning models has been widely used in other clinical assessments of the upper extremity, most notably in the Fugl-Meyer Assessment. Lee et al. proposed a binary logic classification algorithm to automate the evaluation of the FMA using a Kinect v2 and force-sensing resistor (FSR) [64]. In addition, Kim et al. used an artificial neural network learning to predict FMA scores in hemiplegic stroke patients using a Kinect [57]. Formstone et al. proposed a system that combines Inertial measurement and mechanomyography (MMG) sensors to quantify hand and wrist motor function and predict FMA scores with the Light Gradient Boosting Classification Model (LightGBM) (Microsoft Corporation) [65].On the other hand, Yu et al. presented a quantitative FMA framework with two accelerometer and seven flex sensors used to monitoring the movement function of upper limb, wrist and fingers in stroke patients using extreme learning machine (ELM) algorithms to predict FMA scores [66]. Julianjatsono et al. presented a work for predict FMA scores using a sensor data and five regression algorithms: Linear Regression (L-R), Bayesian Linear Regression (BL-R), Neural Network Regression (NN-R), Boosted Decision Tree Regression (BDT- R), and Decision Forest Regression (DF-R) [67]. Otten et al. proposed a framework to predict scores of FMA using SVM and Backpropagation Neural Network (BNN) algorithms using multiple sensors (Kinect, Data glove, FSR sensors and IMU) [68]. Tozlu et al. Predicted FMA scores and clinical improvement of patients with chronic stroke using five machine learning

methods Elastic net (EN), support vector machines (SVM), artificial neural networks (ANNs), classification and regression trees (CART), and random forest (RF) [69]. In contrast, during the Wolf Motor Function Test execution, Del Din et al. used six accelerometers placed on the arm and the trunk to estimate FMA Test scores [70]. Finally, Routhier et al. studied the correlation between finger-to-nose task (FNT) and Upper limb motor function in subacute stroke patients, using an IMU [71].

1.3 Thesis Objectives

The overall objective of this thesis is to improve the assessment of hand function in post-stroke patients with the ARAT through the use of a hand motion system. Towards this general objective, several more specific targets must be pursued, which also represent the main contributions of this research. These objectives are the following:

- Develop a hand motion system capable of measuring finger joint movement and fingertip force with a graphical interface for real time hand simulation.
- Measure the ROM of the finger joints and the fingertip force of healthy subjects during the performance of the Grasp, Grip, and Pinch subtests of the ARAT using the hand motion system.
- Determine the functional range of motion (FROM) and the ROM of the finger joints in post-stroke patients with a global ARAT score ≥ 10.
- Compare the functional range of motion (FROM) and the ROM of finger joints between healthy subjects and poststroke patients.
- Identify alterations in joint movement and compensatory strategies in patients with stroke.
- Develop machine learning models to classify activities between healthy subjects and post-stroke patients with similar ARAT score.

1.4 Outline of the Thesis

This dissertation is divided into seven chapters and references. The chapters are summarized as follows:

Chapter 2: In this chapter, we have introduced a few concepts about the functional anatomy and bio-mechanics of the hand. The objective of these concepts is to know the function and range of motion of the joints of each of the fingers. These concepts are fundamental in this thesis since one of the objectives is to measure and evaluate the movement of the finger joints.

Chapter 3: In this chapter, we presented the development of the Hand motion system proposed. This chapter includes the development of the device to measure finger force, the integration with the Cyberglove

II to measure the angle of the finger joints and the development of the graphical user interface (GUI) for hand simulation and data acquisition.

Chapter 4: This chapter presents a study to assess hand function in healthy subjects using the hand motion system developed in Chapter 3 with the aim of improving the ARAT assessment. Hence, in this chapter, we measured the flexion angles of 11 finger joints and fingertip forces during the performance of three subsets (Grasp, Grip, and Pinch) of the ARAT. Therefore, the results of this study provided an important database of finger joint ROM and fingertip force in ARAT activities of healthy subjects.

Chapter 5: This chapter presents a study where the ROM and the functional range of motion (FROM) were compared between stroke patients and healthy subjects. The data used from healthy patients are those obtained in Chapter 4, while the data from stroke patients were obtained in a previous study [26]. The aim of this chapter is to identify joint impairments and compensatory grasping strategies in stroke patients with left hemiparesis (LH) and right hemiparesis (RH) that are not detected by the ARAT scoring method.

Chapter 6: In this chapter, we present the development of machine learning models to classify whether ARAT activities were performed by a healthy subject or by a post-stroke subject with good upper extremity function, based on the hand motion information obtained with the Cyberglove II in Chapters 4 and 5. The aim of this chapter is to demonstrate that there are differences between the activities of healthy and post-stroke subjects that are not detected by the ARAT scoring method.

Chapter 7: In this chapter, we present a general conclusion and presents future work for this research.

CHAPTER 2
Anatomy of the Hand

This chapter describes the hand's anatomy because it is our main object of study. Although this chapter does not intend to perform a detailed analysis at the clinical level, we consider it essential to have a general knowledge of the hand structure to understand the subsequent chapters better. First, we describe the bones of the hand and the joints of the fingers. Next, we present the types of motion and the normal range of motion proposed by various authors. Finally, we show the methods for measuring the range of motion of the joints and the strength of the hand.

2.1 Basic Hand Anatomy

The hand is one of the most complex parts of the human body to study. The hand's anatomy is efficiently organized to perform simple and complex tasks within the Activities of Daily Living (ADLs). These tasks require a combination of coordinated movements and finely controlled force production [72]. The human hand consists of 27 bones. The wrist, which joins the hand to the forearm, contains eight carpal bones arranged in two rows of four bones each. The metacarpus, or palm, is composed of five long metacarpal bones. Finally, fourteen phalangeal bones constitute the four fingers and thumb. Each finger has 3 phalanges (distal, middle, and proximal) and two phalanges in the thumb (distal, proximal). The finger digits are designated numerically from one to five, or as called the Thumb, Index, Middle, Ring, and Little (or Small).

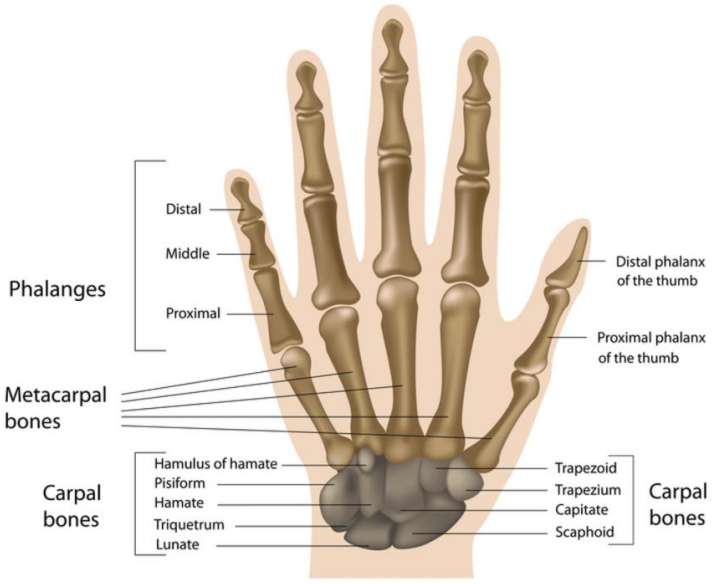

Figure 2.1. Bones of the Human Hand.

2.1.1 Finger Joints

The finger joints of the hand involved in hand motion, beginning with the joints at the connection between the metacarpals and distal row of carpal bones and moving distally to the tips of the phalanges, will be described below and are shown in Fig. 2.2.

Carpometacarpal Joints (CMC)

The carpometacarpal (CMC) joints connect the carpals with each of the five fingers via the metacarpal bones. The CMC is a gliding joint that moves directionally with the carpals and offers very little movement for the four fingers. In contrast, The CMC joint of the thumb is a saddle joint consisting of the articulation between the trapezium and the first metacarpal that provides most of the range of motion for the thumb [73]. Motions at the Thumb CMC joint occur primarily in 2 degrees of freedom. Abduction and adduction occur generally in the sagittal plane, and flexion and extension in the frontal plane [74].

Metacarpophalangeal Joints (MCP)

This joint is located between the metacarpal head and the base of the proximal phalanx [75]. The function of the MCP joints of the four fingers differs from that of the thumb. The MCP joints of the four fingers are condyloid joints that allow flexion-extension and abduction-adduction motions. The joint is well reinforced on the dorsal side by the dorsal hood of the fingers, on the palmar side by the palmar plates that span the joint, and on the sides by the collateral ligaments or deep transverse ligaments [73]. The MCP for the thumb is a hinge joint allowing motion in only one plane flexion and extension. Active abduction and adduction of the thumb MCP joint is limited and therefore these are considered accessory motions [74].

Interphalangeal Joints (IP)

The interphalangeal articulations (IP) are the most distal joints in the upper extremity. Each finger has three phalanges, the proximal, middle, and distal. Therefore, fingers have two IP joints, the proximal interphalangeal (PIP) and the distal interphalangeal joint (DIP). The thumb has only two phalanges, the proximal and distal phalanges; consequently, the thumb has only one IP. The IP joints are hinge joints allowing for motion in one plane flexion and extension, and they are reinforced on the lateral sides of the joints by collateral ligaments that restrict movements other than flexion and extension [73]. From both a structural and a functional perspective, these joints are simpler than the MCP joints [74].

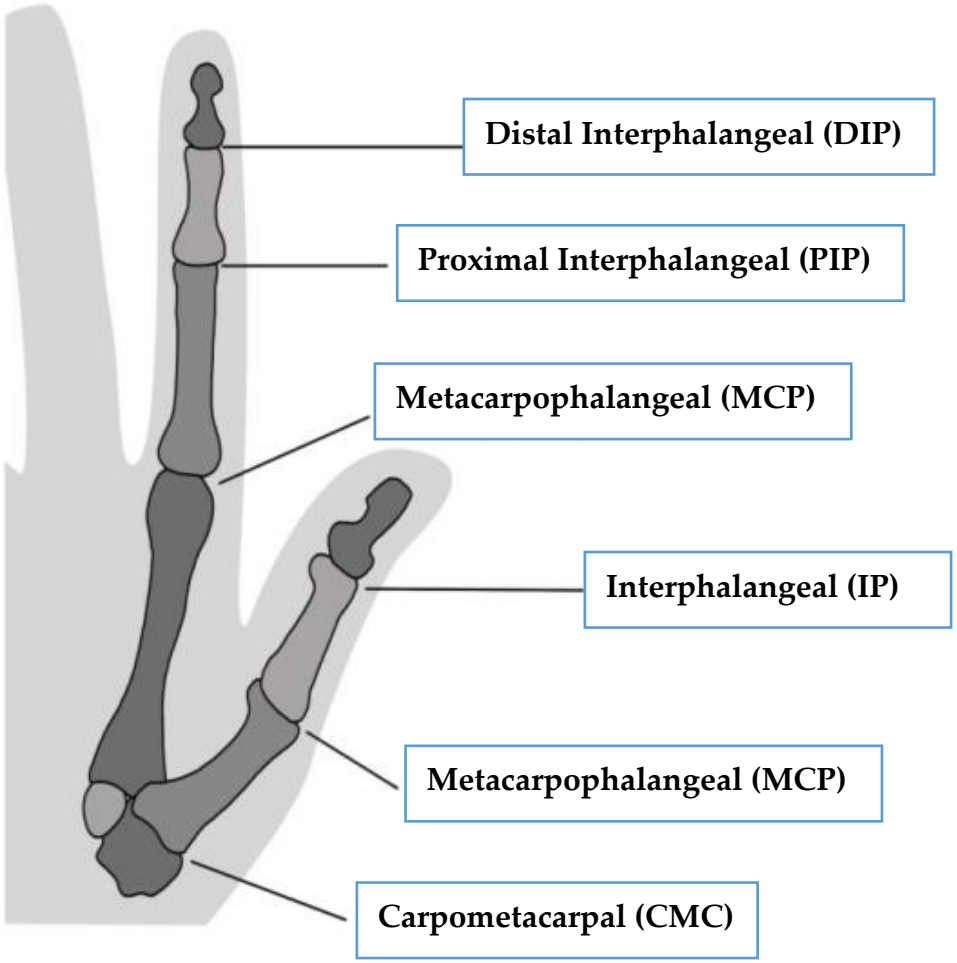

Figure 2.2. Finger Joints of the Index Finger and the Thumb.

2.1.2 Palm Arch

The natural curvature of the hand's palmar surface makes it possible to grasp and manipulate objects of various shapes and sizes. The human hand palm is supported for three arches (see Fig 2.3). Firstly, the proximal transverse arch is formed by the distal row of carpal bones. This static, rigid arch forms the carpal tunnel, permitting passage of the median nerve and many flexor tendons coursing toward the digits. Secondly, the distal transverse arch of the hand passes through the metacarpophalangeal (MCP) joints. In contrast to the rigid proximal arch, the ulnar and radial sides of the distal arch are relatively mobile. Finally, the longitudinal arch of the hand follows the general shape of the index and middle fingers. These relatively rigid articulations provide an important element of longitudinal stability to the hand [74]. Therefore, the index and the middle fingers are constant when the hand arches the palm, but for the ring and small fingers, the metacarpal bones rotate about their respective CMC joints. This movement decomposes into two, one in the direction of extension/flexion (E/F) and the other in the direction of abduction/adduction (Ab/Ad).

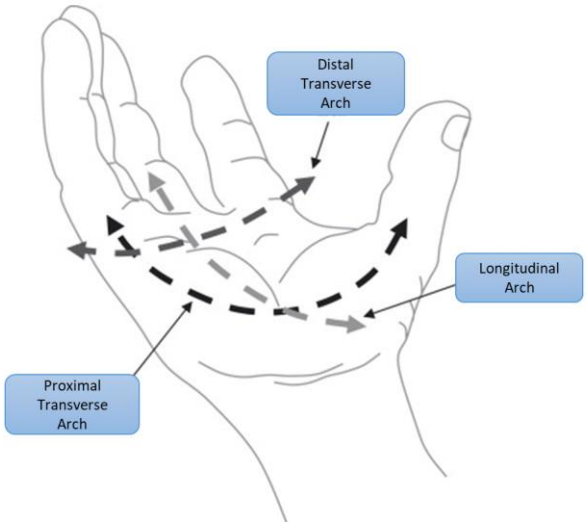

Figure 2.3. The three arches supporting the palm of the hand: one longitudinal and two transverse.

2.1.3 Normal Range of motion

The type of motion that is available at a joint varies according to the structure of the joint. The main types of motion of the finger joints are E/F, and Ab/Ad. Flexion and extension occur in the sagittal plane, while abduction and adduction occur in the frontal plane. Fig 2.4 shows the types of motion of the fingers. On the other hand, the wrist is composed of a complex series of joints. These joints allow three types of movement: flexion/extension, supination/pronation, and ulnar deviation/radial deviation. Fig 2.5 shows the movements of wrist for E/F and the radial/ulnar deviation for the wrist.

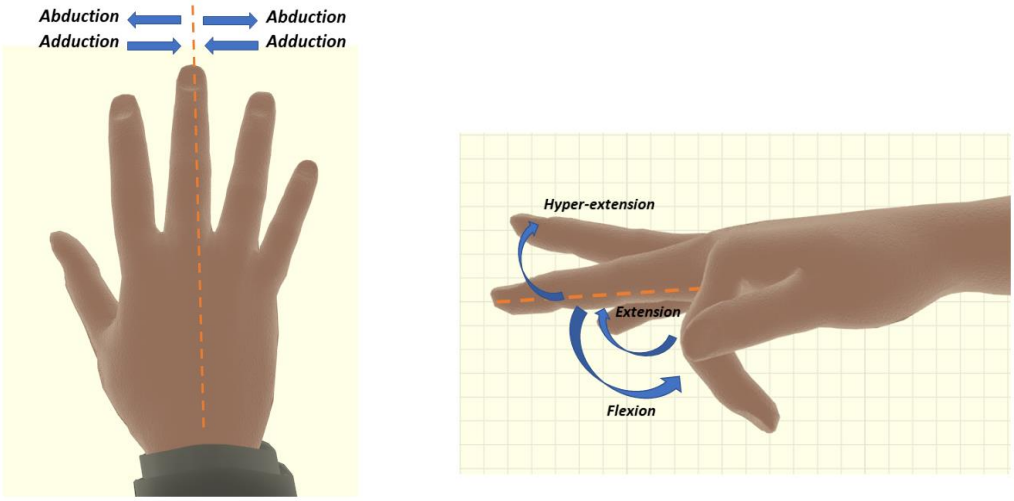

Figure 2.4. Abduction/adduction(Ab/Ad) (left); Flexion/extension (F/E) for one finger(right)

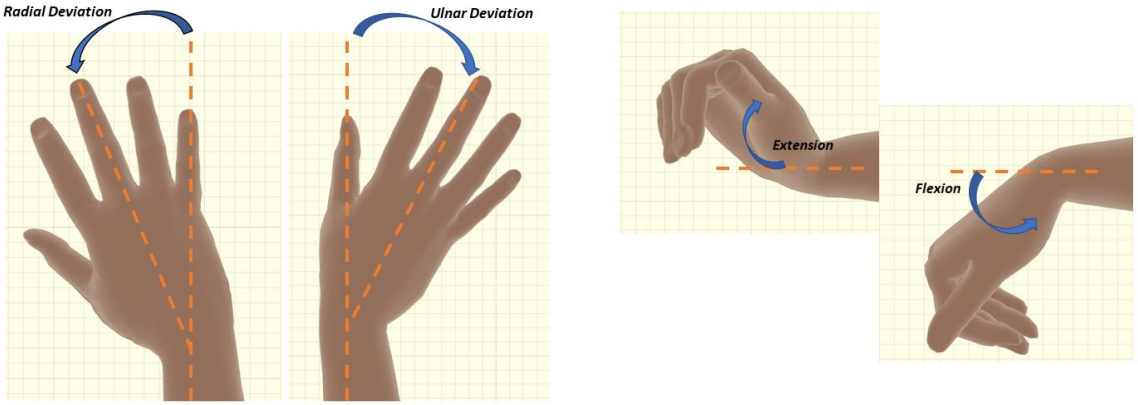

Figure 2.5. Radial/ulnar deviation of the wrist (left); Flexion/extension of the wrist (right)

The Range of motion (ROM) is the arc of motion in degrees between the beginning and the end of a motion in a specific plane [76]. In order for a subject move efficiently and with the minimal effort, full range of motion across the joints is imperative. The measurement of the ROM has been used for physio-therapist and health professionals as an outcome measure to evaluate the functional recovery of a joint after a medical condition, surgical intervention or injury. The most widely system used to define ROM are the 0- to 180-degree system [76]. Thus, neutral extension at each joint is recorded as 0 degrees and proceeds in an arc toward 180 degrees. Table 2.1 summarizes the finger joints of the hand and their associated normal ranges of motion; these values comes from the literature [77], [78]. It's important mention that not all the fingers have these movements, and these tables do not cover all the populations. The term hyperextension is used to describe a greater than normal extension ROM.

Table 2.1. Range of Motion for the joints of the Hand

Finger	Joint	Adduction/Abduction	Extension/Flexion
	CMC	0/60	25/35
Thumb	MCP	0/60	10H/55
	IP	-	15H/80
	MCP	13/42	0/80
Index	PIP	-	0/100
	DIP	-	10H/90
	MCP	8/35	0/80
Middle	PIP	-	0/100
	DIP	-	10H/90
	MCP	14/20	0/80
Ring	PIP	-	0/100
	DIP	-	20H/90
	MCP	19/33	0/80
Little	PIP	-	0/100
	DIP	-	30H/90

CMC= carpometacarpal; MCP = metacarpophalangeal; IP = interphalangeal; PIP = proximal interphalangeal. SD= standard deviation; H= hyperextension.

2.1.4 Muscular Hand Function

The motion and force of the fingers would not be possible without the linked muscles and flexors acting at the hand and wrist and collateral ligaments that restrict motion to certain directions. The muscles that help with finger motion are located in the hand and forearm. The following section describes the basic anatomy and function of extrinsic and intrinsic muscles [74]. The extrinsic muscles are originated in the forearm or arm and entered at the hand as tendons, some tendons are quit long and ended on the tip of the finger. The extrinsic muscles provide considerable strength and dexterity to the fingers. In addition, the intrinsic muscles originated in the hand create motion at the MCP and PIP joints. The Finger flexion is performed primarily by the flexor digitorum profundus and flexor digitorum superficialis. However, the flexion of the middle, ring and little fingers usually is simultaneously because the flexor digitorum profundus tendons derive from a common tendon and muscle. In contrast, the flexor digitorum superficialis allows flexing each finger independently. However, the fingers can be independently flexed at the PIP but not at the DIP joint. The flexion of the MCP joint is produced by two intrinsic muscles, the lumbricales and the interossei [73]. On the other hand, for the extension of the fingers the primary muscle is the extensor digitorum. The extensor digitorum formed an extensor hood that wraps around the dorsal surface of the phalanges. Therefore, the lumbricales and the interossei muscles connected into the hood, assist with extension of the PIP and DIP joints [73].

On the other hand, most of the activities performed with our hands require the use of a small or large amount of wrist flexion, therefore we consider it important to talk a little about the functioning of this muscle group. The wrist flexors and extensors originating in the vicinity of the medial and lateral epicondyle, respectively. Flexor and extensors are paired to produce ulnar and radial flexion [73].

2.2 Methods of ROM Measurement

There are several instruments that are used for physical therapists and other health professionals for the measurement of the ROM: 1) Goniometer 2) Inclinometer 3) Electrogoniometer 4) Radiography and Photography.

2.2.1 Goniometer

The goniometer is the measurement tool most commonly used in clinical practice to measure joints' range of motion (ROM). It can be used to measure joint position and ROM at almost all body joints. Universal Goniometers are constructed of metal or plastic and are produced in different sizes but follow the same design. The design consists of two straight arms, a stationary and a moving arm [76]. The scales on a half-circle goniometer read from 0 to 180 degrees and from 180 to 0 degrees. The universal Goniometer come in two forms; a short arm goniometer used for smaller joints and long arm goniometer which are more accurate for larger joints. The goniometer is still the most economical, and most portable device for assessment of the range of motion.

2.2.2 Inclinometer

The Inclinometer uses gravity's effect on pointers and fluid levels to measure joint position and motion. An inclinometer consists of a circular, fluid-filled disk with a bubble or weighted needle that indicates the number of degrees on the scale of a protractor [76]. There are two types of inclinometers: mechanical and electronic. The electronics are more expensive and require special programs and software.

2.2.3 Electrogoniometers

Electrogoniometers were introduced by Karpovich and Karpovich in 1959, are used primarily to obtain dynamic joint measurements. The electrogoniometer is an electronic device that uses sensors for angle measurement, implemented with potentiometers, strain gauges or accelerometers to record measurements [76] . Mostly devices have two arms, similar to those of the goniometer, which are attached to the proximal and distal segments of the joint being measured. A potentiometer is connected to the two arms. Changes in joint position cause the resistance in the potentiometer to vary. The resulting change in voltage indicate the amount of joint motion.

2.2.4 Radiography and Photography

For many years, radiographs were the gold standard used to verify the range of motion measurements of various joints made with goniometers and inclinometers. Nevertheless, since radiographs were produced by x-ray imaging, they had the major drawback of exposing the subject to radiation. Another problem was the processing time of the film [76]. On the other hand, photography has been another method for measuring joint ROM and has been reported to have excellent reliability. However, this method was considered to be more time-consuming and costly than the use of goniometry and therefore has not been used as much in recent years [76].

2.3 Types of human grip

The manipulative abilities of the human hand are divided in two general classes: prehensile and non-prehensile movements. The prehensile movements are defined as the movements where the hand grasped objects using only the fingers or the fingers and the palm. In contrast, non-prehensile movements include pushing or lifting movements of the whole hand or the fingers [79]. The most commonly classification of prehensile movements have been divided into two grips: Power grip and Precision grip.

2.3.1 Power Grip

The power grip is used when an object needs to be held strongly in order to apply force and is executed between the fingers and the palm of the hand. In addition, the fingers flex more, with flexion at all three finger joints, the MCP, PIP, and DIP ant the Thumb acting as a buttress[73]. Therefore, a Power grip require

maximum force and uses the extrinsic muscles. According to Aielle & Dean Power grip can be subdivided into spherical grip, cylindrical grip and disc grip [79].

2.3.2 Precision Grip

On the other hand, the precision grip is used in order to make fine movements [80]. Therefore, the intrinsic muscles are involved and the major flexion occurs at the PIP and DIP joints. The precision grip is performed between the terminal pads of the thumb and the pads of one or more of the remaining fingers[79]. According to Aielle & Dean precision grip can be subdivided into three-jaw chuck, pinch grip and pad-to-side grip [79].

2.4 Hand force measurement methods

According to Ruth Litchfield, Iowa State University, "Grip strength is a measure of muscular strength or the maximum force/tension generated by one's forearm muscles". There are several instruments for the measurement of both static and dynamic grip forces. However, most of them are used during static tests.

2.4.1 Dynamometer

A hand dynamometer is the most commonly evaluation tool used to measure isometric grip force (hand grip strength). Grip strength measurement devices fall into four basic categories: hydraulic, pneumatic, mechanical and strain gauges [81]. The Hydraulic Hand Dynamometer most widely used for professional clinical and recommended to measure grip strength is the he Jamar dynamometer (Asimow Engineering, Santa Fe Springs, CA, USA)[82]. The Jamar dynamometer can be used to measure isometric force and peak strength with five adjustable positions. Hydraulic instruments record the gripping force in kilograms or pounds of force. The Pneumatic Hand Dynamometer is based in the compression of an air-filled bulb or bag to determine grip strength [82]. They are commonly used with clients who have painful hands or fragile skin because they are softer and more comfortable to grasp [81]. In addition, pneumatic hand-held dynamometers are suitable for quick measurement of grip force in comparative studies. Pneumatic hand dynamometer readings are measured in pounds per square inch (PSI). The Mechanical Hand Dynamometer record grip strength based on the amount of tension produced in a steel spring [82]. Mechanical instruments record the gripping force measured in kilograms or pounds of force. They include the Harpenden(R) dynamometer and the Jamar mechanical dynamometer. The strain-gauge Hand Dynamometer can be used to measure grip strength, pinch strength, and to perform muscle fatigue studies. The use of strain gauges is widely, since mechanical methods of strain measurement are not very reliable. The basic principle of a strain gauge sensor is based on the transformation of the applied force into an electrical signal due to elastic strain. Strain gauges commonly measure grip strength in Newtons of force [82].

CHAPTER 3
Human Hand Motion System

3.1 Overview

The design of the Hand motion system is described in this Chapter. Firstly, we present the system overview diagram. Secondly, we present the CyberGlove II calibration protocol based in a previous study [26]. Thirdly, we show the development of the device for fingertip force measurement, where the following stages were carried out: component selection, signal conditioning, signal filtering, calibration, and circuit design. Finally, the design of the graphical user interface (GUI) in the Unity software is presented. In this GUI, the acquisition of data from the sensors as well as the simulation of a model of the hand were carried out.

3.2 Introduction

The system is composed of a data glove CyberGlove II®, Force Sensing Module, and a Graphical User Interface (GUI) developed in Unity® software; the hand motion system diagram is shown in Figure 3.1. The force sensing module allows measuring individual finger forces and contact points when grasping objects. At the same time, the data glove measures the range of motion of the finger joints. Thus, integrating a force sensing module and a data glove provides a novel hand motion system to assess hand function during the performance of the ARAT activities.

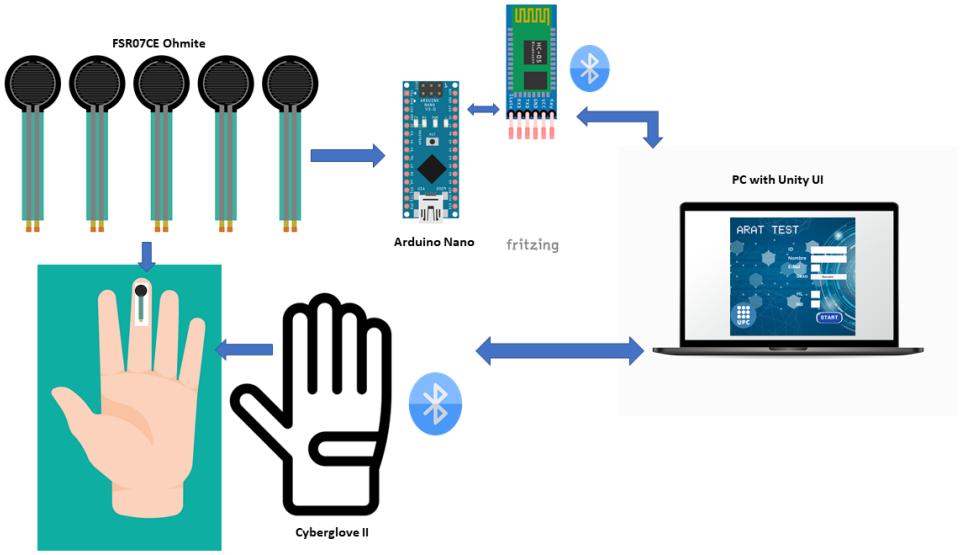

Figure 3.1. Diagram of the Hand motion system.

3.3 Data Glove

The data glove used in this thesis is the CyberGlove II® which provides up to 22 high-accuracy joint angle measurements in real-time (see Figure 3.2). The glove has 18 resistive flex sensors and 8-bit digital signal output; the sensor has a resolution: <1 degree and sensor repeatability: 3 degrees [83].

Figure 3.2. A subject wearing the CyberGlove II.

3.3.1 Calibration

A previously calibrated protocol to convert raw data obtained from the CyberGlove II® in finger joints angles was used in this study [26]. The protocol is based on a 25 degrees of freedom (DOF) model [84]. The hand model of 25 DOF is shown in the Figure 3.3.

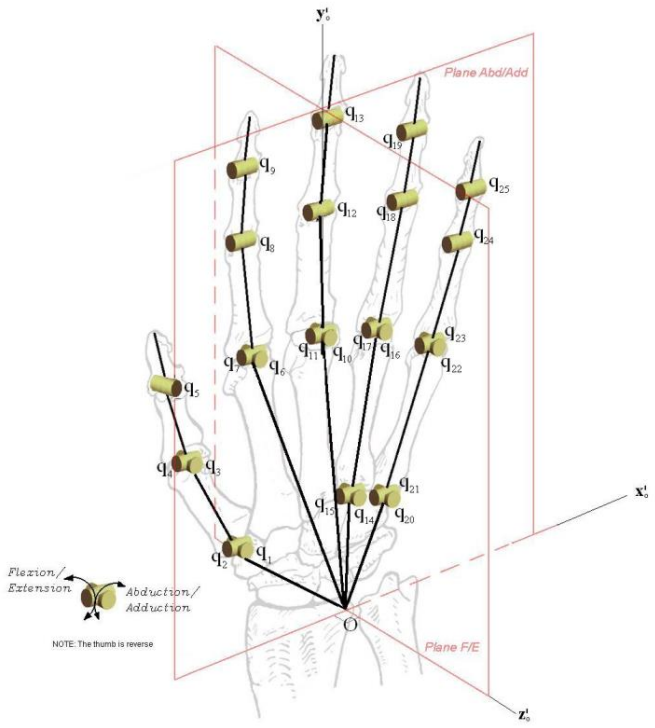

Figure 3.3. Dorsal view of the model of the right hand with 25 degrees of freedom proposed by Peña-Pitarch et al. [84]; *q* value represents a degree of freedom.

The procedure to pass the readings of the 18 sensors of the glove to the 25 DOF model is based on linear interpolation, and it's the same for each joint. Since there are DOF that depend on the readings of one or more sensors, the maximum and minimum reading of each sensor and the range of motion (ROM) of each hand joint are considered to obtain each calibration equation [26]. The eleven sensors used in this Thesis are shown in Figure 3.4.

Consequently, to demonstrate the procedure of calibration used, the Index metacarpophalangeal joint (MCP) of the right hand was used as one example. For other fingers joints, the procedure was similar. The sensor (x_5) of the CyberGlove II® corresponds to the motion (Extension/ Flexion) of this joint. In addition, the range of motion (ROM) of the index MCP is Extension (0°) and Flexion (80°) according Tubiana et al. [85]. Therefore, when the index MCP joint is in extension (0°) the value of the sensor (x_4) was 105 and in flexion (80°) the value was 135°. Finally, the equation of the Index MCP is as follows.

$$Index_{MCP} = \frac{8}{3} \cdot (x_4 - 105)$$

Figure 3.4. Numbering of the sensors used (CyberGlove II®)

The eleven finger joints angles assessed in this thesis were: Thumb carpometacarpal (CMC) joint, Thumb, Index, Middle, Ring, and Little metacarpophalangeal (MCP) joints, Thumb interphalangeal (IP) joint, and Index, Middle, Ring, and Little proximal interphalangeal (PIP) joints. The calibration equations for each finger joint are shown in the Table 3.1. In this thesis we don't include the Abduction and Adduction (Ab/Ad) motion of the finger joints since multiple sensor were involved in the motion of each joint. Therefore, the finger joints angles of Ab/Ad with this calibration method could be variable and unreliable.

In addition, in a previous study of Tico-Falguera with stroke patients, no significative improvements were found in the joints angles of Ab/Ad after six months of rehabilitation [25].

Table 3.1 Calibration equations for finger joints.

Finger	Joint	Calibration equation
Thumb	CMC	$Thumb_{CMC} = \frac{1}{2} \cdot (x_1 - 60) - 25$
	MCP	$Thumb_{MCP} = \frac{65}{35} \cdot (x_2 - 105) - 10$
	IP	$Thumb_{IP} = \frac{95}{10} \cdot (x_3 - 65) - 15$
Index	MCP	$Index_{MCP} = \frac{80}{13} \cdot (x_4 - 120)$
	PIP	$Index_{PIP} = \frac{10}{14} \cdot (x_5 - 36)$
Middle	MCP	$Middle_{MCP} = 0.90 \cdot (x_6 - 58)$
	PIP	$Middle_{PIP} = \frac{100}{115} \cdot (x_7 - 45)$
Ring	MCP	$Ring_{MCP} = \frac{8}{9} \cdot (x_8 - 53)$
	PIP	$Ring_{PIP} = \frac{10}{13} \cdot (x_9 - 15)$
Little	MCP	$Little_{MCP} = \frac{8}{11} \cdot (x_{10} - 85)$
	PIP	$Little_{PIP} = \frac{10}{14} \cdot (x_{11} - 45)$

Note. Adapted from Peña-Pitarch et al. [26]. CMC= carpometacarpal; MCP = metacarpophalangeal; IP = interphalangeal; PIP = proximal interphalangeal.

Finally, the raw data from the CyberGlove II® was transmitted to a PC via Bluetooth connection. To read and record the data, a graphic user interface (GUI) was developed in Unity® software. The GUI description is explained in detail below.

3.4 Force sensing module

3.4.1 Force Sensors

The Force Sensing Resistors (FSR) are a polymer thick film (PTF) devices that show a decrease in resistance to an increase of force applied to the active surface. The FSR sensors allow measuring static and dynamic forces [86]. In recent years, FSR sensors have been used in robotics and biomechanics

applications. Currently, there are several manufacturers of this type of sensor with very similar designs and operating principles. Their main advantages are the wide variety of shapes and sizes, the low cost per unit, the portability, their use in human touch applications (forces less than 10Kg), and their easy integration (thicknesses less than 1.25mm) [87] [88]. The FSR sensor consists of two membranes separated by a thin air gap. The air gap is maintained by an adhesive spacer and due to the stiffness of the two membranes. One of the membranes has two sets of electrically isolated interdigitated tracks and each set is connected to an output terminal. The other membrane is coated with FSR carbon-based ink. When the sensor is pressed, the FSR ink short-circuits the two traces and the resistance value depends on the applied force [86]. The schematic diagram of the FSR sensor and its components are shown in Figure 3.5.

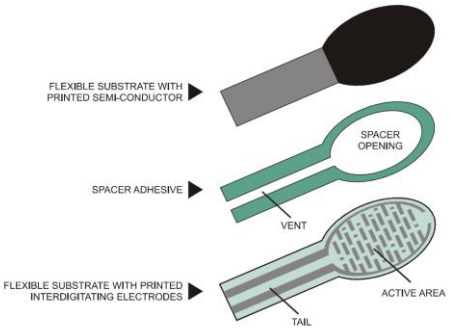

Figure 3.5. Basic schematic of the force sensing resistor (FSR).

Ohmite (Manufacturing Company, USA) has designed different FSR sensors. The sensors comprising the FSR-Series family are shown in Figure 3.6. The sensors have similar characteristics, which will be discussed below but are mainly characterized by being optimized for human-machine interface (HMI) or machine-machine interface (MMI) applications, such as medical, industrial, and robotic applications. However, their shape and size vary, so the most suitable sensor for the required application can be chosen.

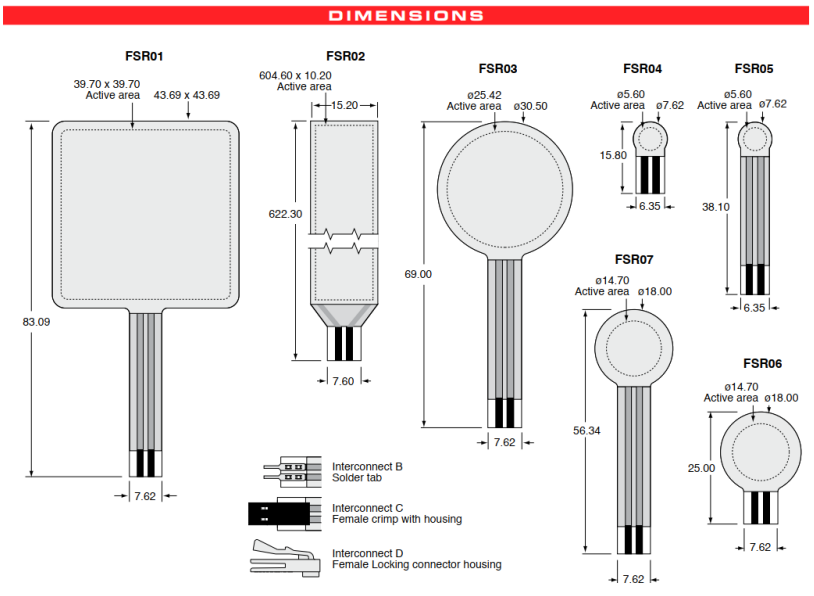

Figure 3.6. The Force sensing resistors family of Ohmite (Manufacturing Company, USA).

The thesis objective was to measure the force applied to the fingertip. The model FSR03 had a larger active area but was too large for the fingertips. On the other hand, model FSR04 had too small an active area. Therefore, the sensor chosen due to its characteristics and size was the model FSR 07 Ohmite. The FSR 07 has the following characteristics: an active area of 14.7 mm, a thickness of 0.375 mm (Inc. 0.05mm adhesive), and a sensor overall length of 56.34 mm and overall width of 18.0 mm as shown in Figure 3.7.

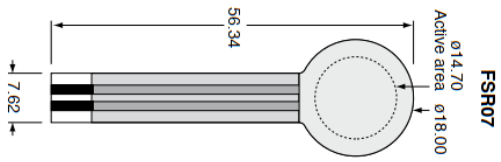

Figure 3.7. Force Sensing Resistor FSR07.

The resistance of an FSR sensor, when there is no pressure applied and the circuit is open, has a value greater than 10MΩ. The response curve of the FSR sensors given by the manufacturers is shown in Figure 3.8. At the curve's start, there is a zone known as the Actuation Force, where there is an abrupt change in resistance and where the sensor's impedance does not show a potential response to the force. The force is influenced by several factors such as the surface, the thickness and the flexibility of the coating, the shape and size of the object acting on the sensor and the space between the conductive elements [86]. Then, the behavior of the response curve is similar to a potential function in which the resistance follows a linear relationship with the force on a logarithmic scale. Therefore, this section is useful for force measurement. Finally, it should be noted that there is a saturation zone where the sensor's resistance has reached its limit and can no longer decrease [89]. On the other hand, Figure 3.9 shows the plot of the conductance vs. force (the inverse of resistance: 1/r). This last plot allows the interpretation of force on a linear scale.

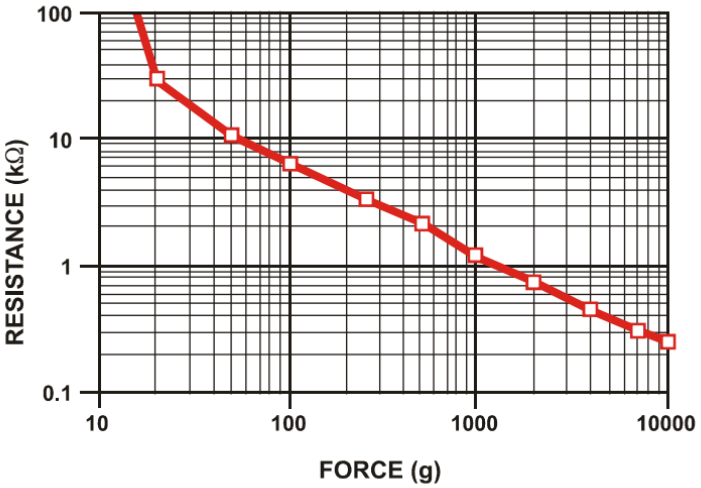

Figure 3.8. Curve of Resistance vs Force.

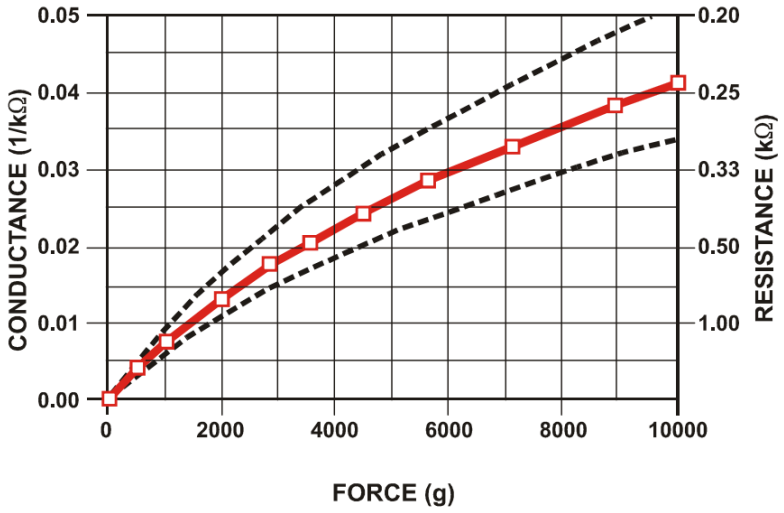

Figure 3.9. Curve of Conductance vs Force.

3.4.2 Signal conditioning

A signal conditioning circuit was designed to provide a variable voltage according to the force exerted on the sensor. The FSR is a resistive sensor and there are several circuits for resistive sensors to convert this signal to voltage. The most common conditioning methods are:

- The voltage divider.
- The Wheatstone bridge.
- Amplifier circuits.

Voltage Divider

The voltage divider circuit is the simplest and most commonly used circuit for FSRs. In fact, the manufacturers propose a voltage divider as a conversion circuit. The circuit is shown in the Figure 3.10.

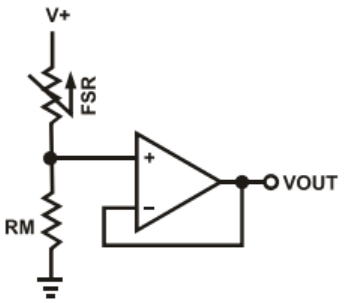

Figure 3.10. Circuit of a voltage divider for a force sensing resistor (FSR).

The voltage divider uses two resistors; the FSR resistor (which is variable and depends on the force applied) and the bottom R_M resistor, which is a measuring resistor. The R_M resistor is chosen to maximize the desired force sensitivity range and to limit current. In this configuration, the output voltage (V_{OUT}) increases as the applied pressure increases until a value is reached where the voltage no longer grows and becomes constant [86], [89]. The equation (1) describes the output of the voltage divider, while the Figure 3.11 shows the characteristic curves for a standard Interlink FSR sensor with different RM resistor values.

$$Vout = \frac{R_M}{R_M + R_{FSR}} \cdot V^+$$

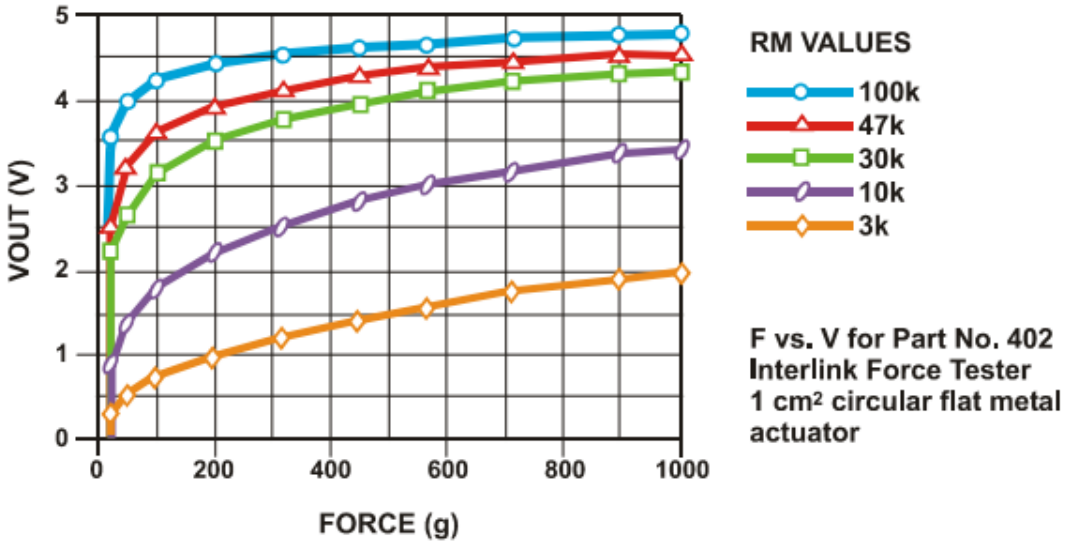

Figure 3.11. Characteristic curves for a FSR Voltage Divider with different RG resistor values.

Inverting operational amplifier

Another alternative was to use an inverting operational amplifier (op-amp) circuit. In this circuit, the output voltage is inverse to the reference voltage (V_{REF}) in polarity and inversely proportional to the FSR value R_{FSR}. Therefore, the output voltage (V_{OUT}) will be inversely proportional to the pressure. The circuit diagram is shown in Figure 3.12. In this configuration, when there is no pressure, the circuit will have an output voltage of zero due to the high impedance of the resistor R_{FSR} [86], [89]. However, the output voltage will increase as pressure is applied, in major or minor proportion, depending on the value of R_G chosen. The equation (2) describes the output of this amplifier, while the Figure 3.13 shows the characteristic curves for a standard Interlink FSR sensor with different RG resistor values for an input voltage of -5V.

$$Vout = -\frac{R_G}{R_{FSR}} \cdot V_{REF}$$

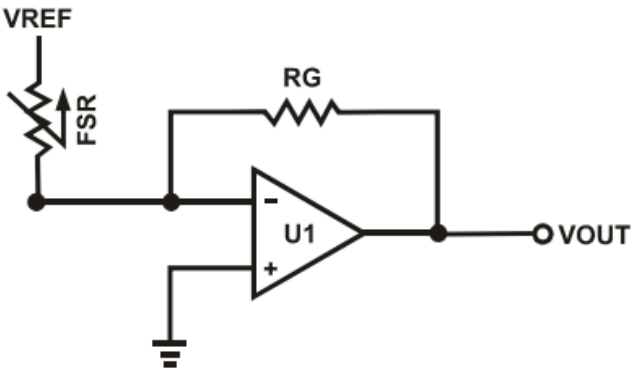

Figure 3.12. Inverting operational amplifier circuit diagram for an FSR.

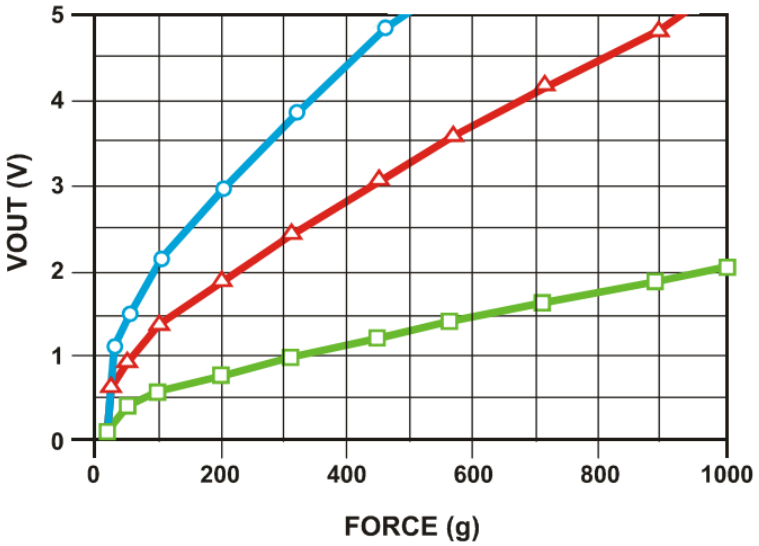

Figure 3.13. Characteristic curves for a FSR Inverting Operational Amplifier with different RG resistor values.

Selection of the components for signal conditioning

The objective of this thesis is to measure the fingertip forces when grasping different objects while performing various activities. Therefore, the sensors presented a wide range of pressures for each finger in each test. The equations of the voltage divider and the inverting op-amp circuits showed a linear behavior, as was observed previously. This linearity was seen in the voltage divider at low-pressure values, while it became more constant at higher values. In contrast, the inverter always presented a linear behavior between the output voltage and pressure. Therefore, the best alternative for our objective was the inverting op-amp since using the voltage divider for high pressures would not be reliable. In addition, the linearity of the inverting op-amp allowed us to operate in a smaller range and extrapolate to higher values.

The inverting op-amp circuit was integrated by a Fixed Regulator, an Operational amplifier (op-amp) and a Resistor. The selected op-amp was the LM324 model based on its characteristics. The advantages of

the LM324 are its low cost and it does not require a large voltage power. The LM324 needs two voltage sources, one negative and one positive. However, the op-amp has a voltage swing of 0v ± 1.5v. Therefore, a fixed 7806CT regulator was used for feed the op-amp with 6v and have an output close to 5v. For the FSR sensor, a -5v power supply was used, so we used a 7905CT regulator. Next, the adequate resistor value for the circuit was chosen based on the following considerations. An Arduino board processes the data from the FSR sensors. The microcontroller inputs allow an input power of 5 v, so if it had a higher output voltage, it would saturate and would not be useful. In addition, the maximum finger force applied to the FSR sensor was measured with a voltmeter and the R_{FSR} value reached was 100 ohms. Therefore, we decided to use a resistor value close to that value to provide an output near to 5 volts. For these reasons, a commercial resistor value (R_G) of 150 ohms was chosen. It is important to mention that since the inverse op-amp only has four inputs, it would be necessary to use two LM324 amplifiers for the five sensors required.

3.4.3 Signal filtering

In this section, a low pass filter was designed to eliminate high-frequency noise. We decided to use a filter before the analog to digital conversion to limit high frequencies and prevent aliasing. Therefore, a first-order active low pass filter was selected; this filter permits only the low frequencies and attenuates the high frequencies. The filter is composed of an active element which is the operational amplifier (Op-amp), and is first order because it contains only one reactive element (a capacitor). The passband begins from 0Hz and continues at -3dB to the designated cut-off point. In addition, the active filter is simple, low cost, and practical. We considered that a cut-off frequency (*fc*) of 60 Hz was adequate to reduce the signal noise caused by the electronic circuit. Therefore, it was necessary to calculate the value of the capacitor using the design equation shown below.

$$C = \frac{1}{2\pi f_c R_f}$$

Where: *C* = Capacitor value; *fc* = cut-off frequency; *Rf*= resistor value

Finally, taking into consideration that the value of R_f = 150 ohms and *fc=60Hz;* the obtained value of the capacitor was 17.69 μF. However, the value obtained is not commercial, so we used the closest value which was 22 μF. The circuit diagram of the force sensing device is shown in Figure 3.14.

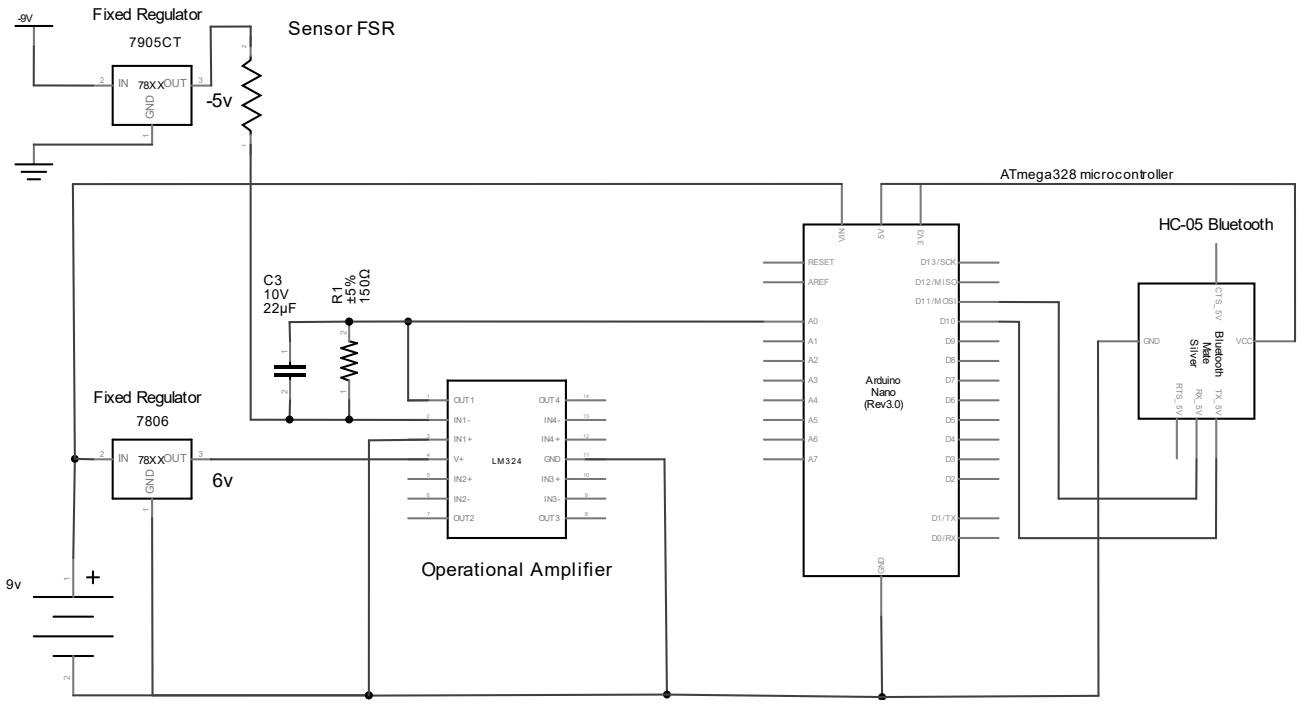

Figure 3.14. Circuit diagram of the force sensing module; configuration for a single FSR is shown.

The five FSR sensors were calibrated under static conditions before application to reduce inaccuracies. Calibrated weights were statically placed over each sensor to obtain a graph with the relation between the force applied and the output voltage, thus obtaining the equations of the calibration curve. During the whole test, the output voltage was measured. For this purpose, we used the Arduino board and the data was stored in a .xlsx file using the PLX DAQ application. The analog-to-digital conversion is explained in more detail below. Similar procedures to calibrate FSRs have been proposed in several studies [49], [87], [90].

The calibration curve of one FSR sensor is shown in Figure 3.15. Generally, a coefficient of correlation $R^2 \geq 0.990$ is considered acceptable. Therefore, the coefficients of the equations show that the output voltage is proportional to the applied force and equivalent to that exerted by the calibrated weights. In addition, this equation allows the possibility of extrapolating the results to higher pressures if necessary. The calibration equations for the five FSRs are shown below.

$$Sensor\ 1 = 3.6915x - 0.2895 \quad \mathcal{R}^2 = 0.994$$

$$Sensor\ 2 = 3.6497x - 0.3745 \quad \mathcal{R}^2 = 0.991$$

$$Sensor\ 3 = 3.7318x - 0.6047 \quad \mathcal{R}^2 = 0.992$$

$$Sensor\ 4 = 3.7741x - 0.6082 \quad \mathcal{R}^2 = 0.994$$

$$Sensor\ 5 = 3.7543x - 0.3652 \quad \mathcal{R}^2 = 0.990$$

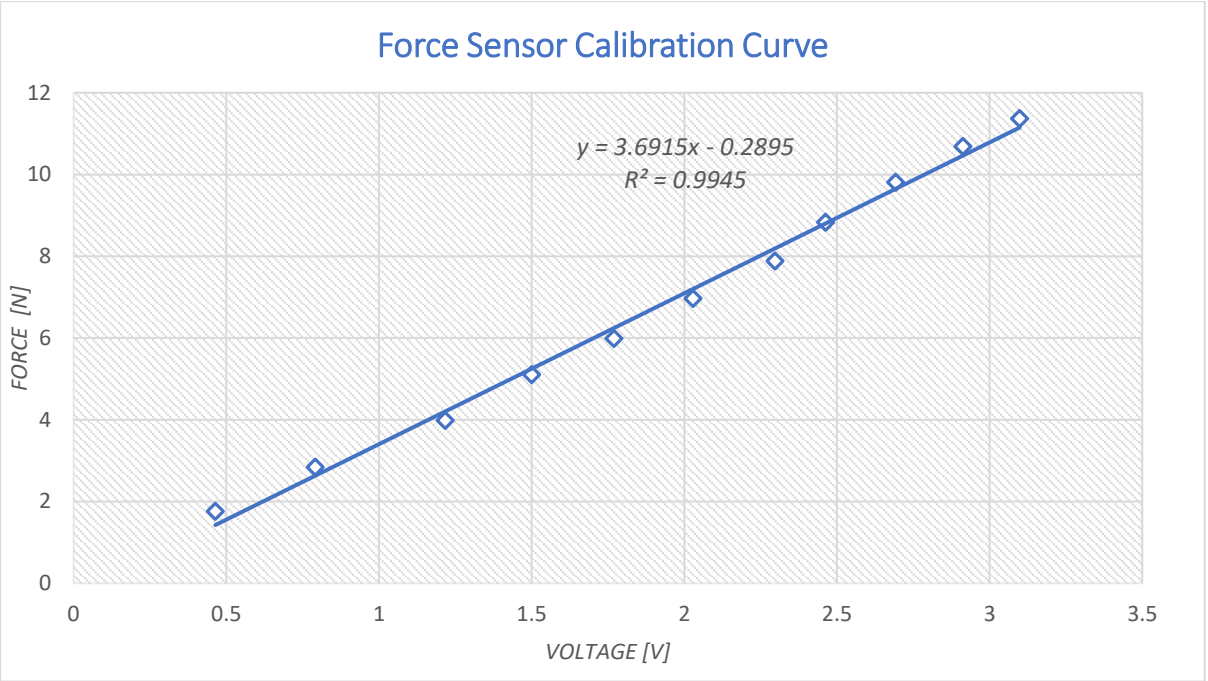

Figure 3.15. Calibration curve of a single FSR.

3.4.4 Data Acquisition

Once we conditioned the force sensor signal, we proceeded to the data acquisition phase to digitally process and visualize the fingertip force and the hand kinematics data on the PC. The data acquisition system was implemented in Arduino and Unity®. The board selected was the Arduino Nano shown in Figure 3.16. This board was selected due to its small size and the following characteristics:

- Microcontroller: ATmega328
- Analog Input Pins: 8 (A_0 – A_7)
- PCB Size: 18 x 45 mm
- Weight: 7 grams.
- Input Voltage: 7 – 12v
- Analog to digital converter (ADC): 10 bits
- Frequency (Clock Speed): 16 MHz

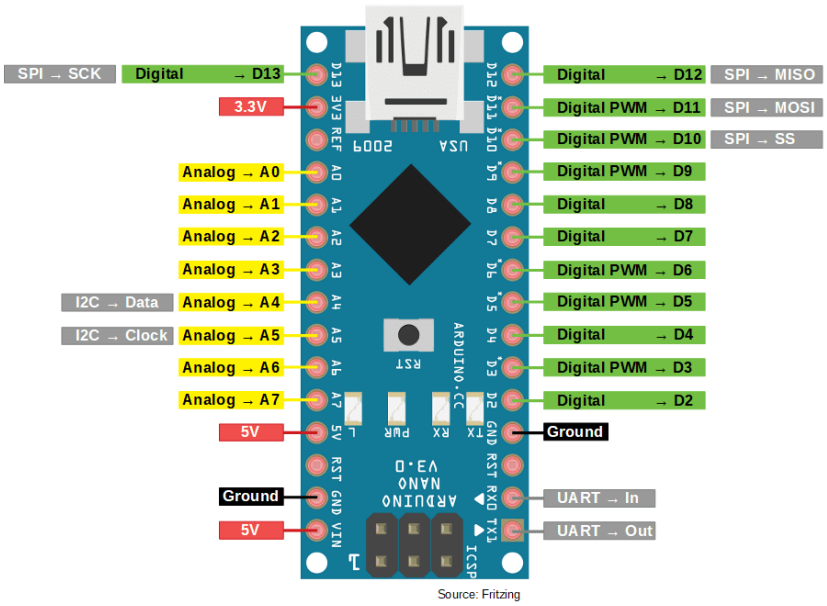

Figure 3.16. Schematic circuit of the Arduino Nano.

The software used for the Arduino boards is the Arduino IDE (Integrated Development Environment), a free software used as a programming platform. In addition, Arduino code is written in C++ with an addition of special methods and functions so it is easy to use.

The process to perform the analog conversion to force values after obtaining the calibration equations is as follows. First, the output terminals of the inverting op-amp were connected to the analogic inputs of the Arduino Nano to convert raw data into force. Next, we program an Arduino sketch to read the analog inputs voltages corresponding to the amount of pressure on each sensor and converted into digital voltage. Then, the digital voltage was transformed into a force using the linear equations derived during the calibration process for each sensor. Finally, the force data from Arduino were transmitted via wireless to the Graphical User Interface (GUI); for this purpose, we used the HC-05 module Bluetooth SPP (Serial Port Protocol) because of its compatibility and size. The HC-05 module has six pins and can easily be interfaced with the Arduino Nano board; the logic voltage level of the data pin is 3.3 V to 5 V [91]. The Arduino Nano and HC-05 module were powered by 9 volts Li-Ion battery.

3.4.5 Graphical User Interface

A user-friendly Graphical User Interface (GUI) was developed using the software Unity® version 2020.2.2f1.Unity® is a game-development environment used to create games and applications [92]. We chose Unity software because of the following features: high-quality 2d and 3d graphics, based on object-oriented programming, compatible with various platforms, and the integrated development editor supports JavaScript and C# for scripting. In addition, Unity is compatible with Augmented reality (AR) and Virtual reality (VR) applications so we will seek to migrate the hand motion system to these technologies in future

work. We decided to make a simple and intuitive interface design that anyone could handle without any problem. Three scenes were designed for the GUI.

The first scene shown in Figure 3.17 contains the main menu with the basic information of patients (Id, name, gender, age, hand length (HL), hand breadth (HB). The data was subsequently stored in the next scene. When the button START is clicked, the following scene is accessed.

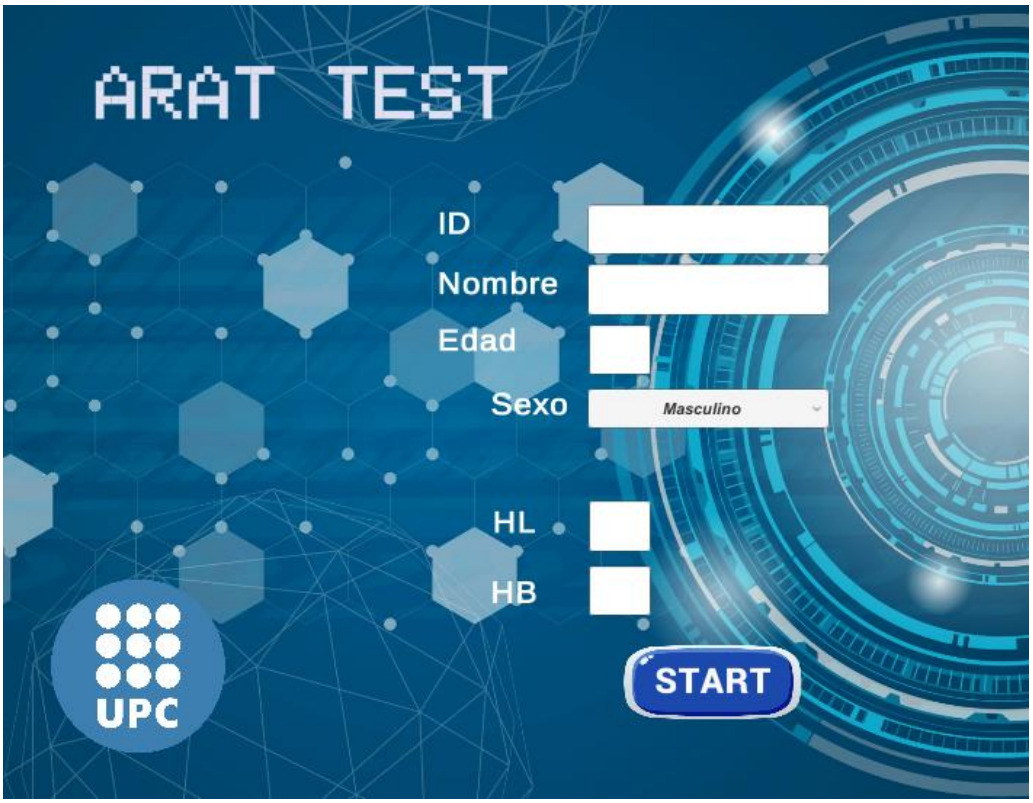

Figure 3.17. Main menu scene of the Graphical User Interface (GUI).

The second scene was dedicated to the ARAT menu and is shown in Figure 3.18. This is the main scene for the assessment of each patient with the ARAT. In this scene, the information from the sensors is displayed and recorded during the performance of each of the ARAT tests. A script was written in C# using JetBrains Rider 2019.2.3 and attached to the ARAT scene for reading raw data from the CyberGlove II® and converted in the angles of the finger joints based in the calibration equations obtained previously. Another script was created using an Arduino Bluetooth Plugin to connect the Arduino board and obtain the force data of each fingertip. Sensor information is displayed in real-time at the top of the screen. In addition, the user can time and score each task. Data obtained from the sensors in each activity were recorded at a rate of 50 Hz into a Comma-Separated Values (CSV) file. The third scene dedicated to the simulation of the hand is explained below.

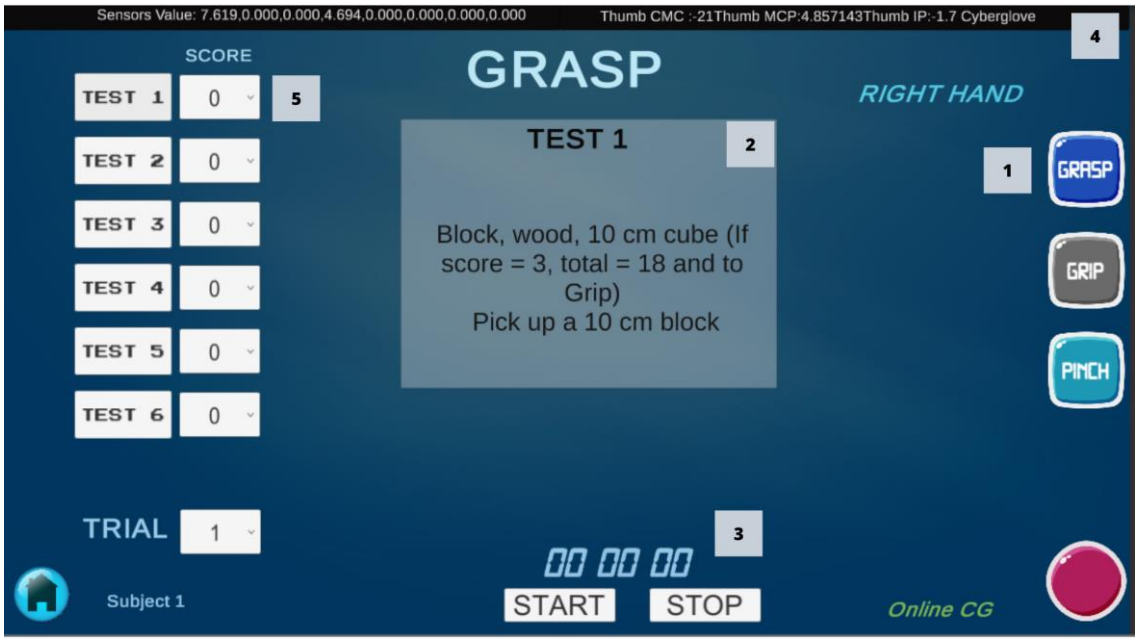

Figure 3.18. ARAT menu scene of the Graphical User Interface; (1) Buttons to select each subtest; (2) Description of the Test; (3) Buttons to record each test with timer; (4) Sensors information in real-time (angle finger joints and forces); (5) Dropdown list to score each test.

3.4.6 Digital Filter

The Butterworth filters are one of the most commonly used digital filters in biomechanics for human motion analysis [93][94][10]. In addition, this type of digital filter is fast and simple to use. In 1974, Winter et al. used an analogue TV camera to record motion in the sagittal plane and proposed to filter data with a second-order low-pass Butterworth filter with a cutoff frequency (*fc*) of 6 Hz with zero-lag. The zero-lag (or zero-phase) involves applied the filter two times to the signal, obtaining a frequency response of 4th order. In addition, the results of Winter et al. showed that the cut-off at the 7th harmonic reduces the high frequency noise of the data [95][96]. Similar results were presented in [97]. In human hand motion analysis several studies have been used a second order zero-lag Butterworth low-pass filter with a fixed *fc* = 5 Hz [98][99][100][101]. Therefore, Data recorded from the CyberGlove II® and the Force sensor FSRs were filtered with a 5-Hz lowpass second-order Butterworth filter in MATLAB® software for statistical analysis. The gain and the normalized response of the Butterworth filter for different orders are given in Figure 3.19.

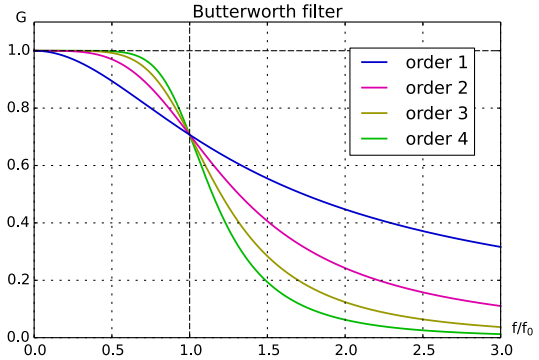

Figure 3.19. Butterworth filter gain at distinct orders.

3.5 Hand Model and Simulation

The following section describes the process performed for the creation of the hand model, and the simulation in Unity.

3.5.1 Hand model

We made the model of the hand from the design of each of the finger bones, using Blender v2.80 software. Blender is a cross-platform computer software, especially dedicated to modeling, rendering, animation and the creation of three-dimensional graphics. In addition, Blender has the following features: is an open-source software, is compatible with Unity, and include the FBX and OBJ formats. In order to create a realistic hand model of the hand we used parametric lengths. Therefore, the parameters hand length (HL) and hand breath (HB) were used to determine the bone lengths (see Figure 3.20). The equations for determine the parametric lengths of each finger bone were based on the work of [102]. The equations for calculating the lengths of the metacarpal bones and the phalangeal bones of the fingers are shown in Table 3.2. In other hand, the Figure 3.21 shows the dimensions used in the equations for the fingers (Index, Middle, Ring, Little, while Figure 3.22 shows the dimension used for the thumb.

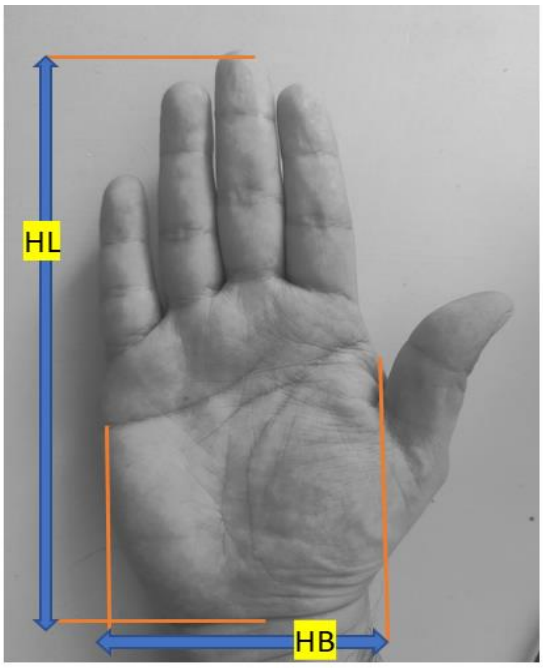

Figure 3.20. Parametric length for a hand; HL= Hand length (measured from the tip of the longest finger to the crease under the palm); HB= Hand breadth (measured across the widest area where the fingers join the palm). Adapted from Peña-Pitarch et al. [102].

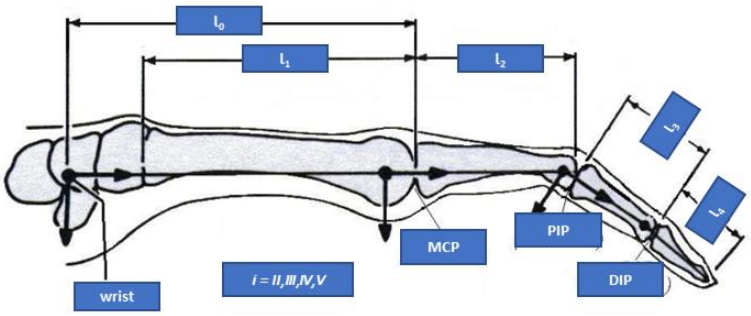

Figure 3.21. Parametric length for a finger; fingers(*i*) II=Index, III=Middle; IV=Ring; V= Little. Adapted from Peña-Pitarch et al. [102].

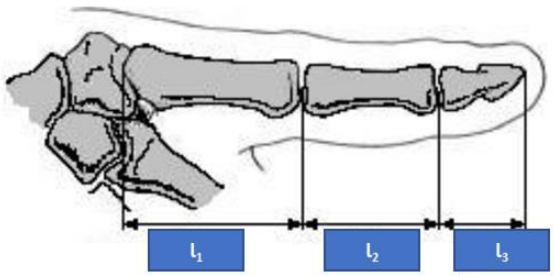

Figure 3.22. Parametric length for the Thumb. Adapted from Peña-Pitarch et al. [102].

Table 3.2. Formulas for determining metacarpal and phalangeal bone lengths

Finger	Metacarpal (l1)	Proximal (l2)	Middle (l3)	Distal (l4)
Thumb	$0.251 * HL$	$0.196 * HL$	----	$0.158 * HL$
Index	$\sqrt{(0.374 * HL)^2 + (0.126 * HB)^2}$	$0.265 * HL$	$0.143 * HL$	$0.097 * HL$
Middle	$0.373 * HL$	$0.277 * HL$	$0.170 * HL$	$0.108 * HL$
Ring	$\sqrt{(0.336 * HL)^2 + (0.077 * HB)^2}$	$0.259 * HL$	$0.165 * HL$	$0.107 * HL$
Little	$\sqrt{(0.295 * HL)^2 + (0.179 * HB)^2}$	$0.206 * HL$	$0.117 * HL$	$0.093 * HL$

Note. Adapted from Buchcholz et al. [77] and Sancho-Bru [78]. HL= Hand length; HB= Hand breadth

According to the National Aeronautics and Space Administration (NASA), the average hand sizes of biological adult males are 7.6 in for HL and 3.5 in for HB and for females are 6.8 in for HL and 3.1 in for HB [103]. We used the average hand size of males and females for the hand model. Therefore, we used 19.5 cm for Hand length and 8.5 cm for Hand breadth to calculate the parameters of each finger bone. The Table 3.3 shown the parametric lengths calculated for each finger bone.

Table 3.3. Lengths for the metacarpal and phalangeal bones of the hand model

Finger	Metacarpal (l1)	Proximal (l2)	Middle (l3)	Distal (l4)
Thumb	4.89 cm	3.82 cm	—	3.08 cm
Index	7.37 cm	5.17 cm	2.79 cm	1.89 cm
Middle	7.27 cm	5.40 cm	3.32 cm	2.11 cm
Ring	6.58 cm	5.05 cm	3.22 cm	2.09 cm
Little	5.95 cm	4.02 cm	2.28 cm	1.81 cm

cm=centimeters

For the design of the hand bones in Blender, first the hand armature was created. An armature in Blender is similar to a human skeleton, and can consist in several bones. The bones are associated with each other to have movement and deform similarly to the human hand. During this stage the parametric measurements of each bone were not taken into consideration. However, is important to use the correct hand bones structure [104]. Next, the bones length was adjusted with the parametric measurements obtained previously shown in table. The bones can be rotated around the X, Y and Z axes, so the rotation of each bone was limited according to the corresponding range of motion. In addition, the axes of rotation were constrained according to the type of motion that each finger joint can perform (extension/flexion and abduction/adduction) with the objective of having a more accurate simulation. Finally, the armature was attached to a hand mesh; this process is known as rigging [105]. Therefore, we can realistically control and move the hand mesh without seeing the armature. It is important to mention that each bone has an identifier that allows it to move independently according to the sensor values during the simulation. The hand model (see Fig 3.23) was exported and saved as a .fbx file for further simulation in Unity.

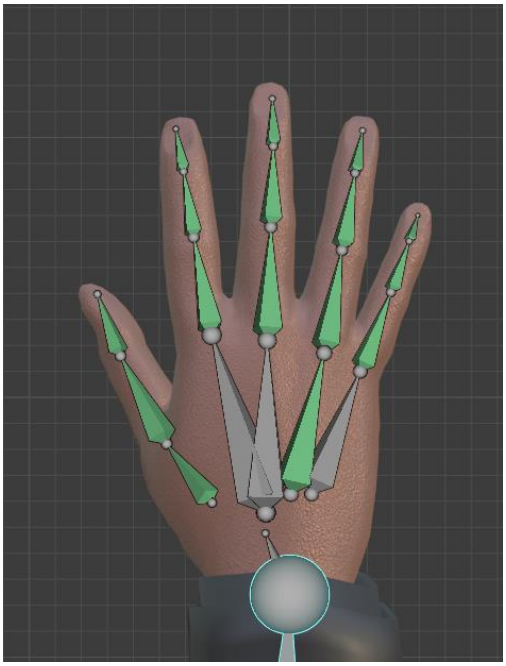

Figure 3.23. Hand model created in Blender with parametric lengths.

3.5.2 Simulation

The third scene was dedicated to the hand simulation. First, the Hand model was imported to Unity for perform the hand simulation in real-time. We used the same script developed for the ARAT menu scene, where we acquire the CyberGlove II® data and convert them into angles with the calibration equations. The fundamental objects in Unity are called GameObjects. In this case, the object is the armature of the hand, and to access each bone, we need a Unity function. For this, we use the function Gameobject.transform.Find for each bone and we assign the value to a variable [92].

Then, we assign the rotation angles obtained with the CyberGlove II® to each variable using the function transform.localEulerAngles [92]. The previous function is used to set de rotation of a game object relative to the parent transform's rotation, in this case the parent is the previous bone. Therefore, at the time of each ARAT test the hand movement is simulated in this scene. Importantly, to access this scene the ARAT scene button must be pressed and scenes can be alternated without stopping the assessment process since this scene works as a secondary display. The model of the hand in the Unity scene is shown in the Figure 3.24.

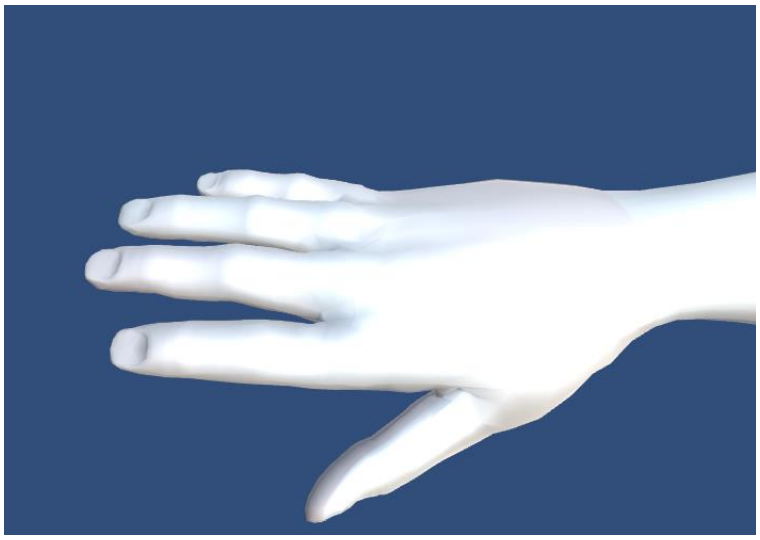

Figure 3.24. Hand model in the Unity Scene.

3.6. Conclusions

In this chapter, we present the calibration protocol used in the CyberGlove II®. In addition, a force sensing module based on five force sensing resistors (FSR) was developed using an inverting operational amplifier. The calibration process was performed on each sensor and showed an output voltage linearly proportional to the exerted pressure. In addition, we developed a user-friendly graphical user interface (GUI) that allows real-time monitoring of the sensor data and its storage in a CSV file for further analysis. Finally, we developed a hand model with parametric lengths with 25 degrees of freedom, which provides a realistic simulation of the hand in the GUI.

CHAPTER 4
Hand Motion Analysis in Healthy Subjects during the performance of the Action Research Arm Test

4.1. Overview

In this chapter, we conducted a study with 25 healthy subjects (age 40.2 ± 18 years) to measure the flexion angle of the finger joints and fingertip forces during the performance of three subtests (Grasp, Grip, and Pinch) of the ARAT using the hand motion system described in Chapter 3. The joints evaluated in this study were the proximal interphalangeal (PIP), and metacarpophalangeal (MCP) joints of the (index, middle, ring and little fingers) and the interphalangeal (IP), carpometacarpal (CMC) and MCP joints of the thumb. The results showed that the mean flexion angles of the finger joints required to perform the 16 ARAT activities were Thumb (CMC 28.56°, MCP 26.84°, and IP 13.23°), Index (MCP 46.18° and PIP 38.89°), Middle (MCP 47.5° and PIP 42.62°), Ring (MCP 44.09° and PIP 39.22°), and Little (MCP 31.50° and PIP 22.10°). The averaged fingertip force exerted in the Grasp Subtest was 8.2 N, in Grip subtest 6.61 N and Pinch subtest 3.89 N. These results suggest that the integration of multiple sensors during the performance of the ARAT has clinical relevance, allowing therapists and other health professionals to perform a more sensitive, objective, and quantitative assessment of the hand function.

4.2. Introduction

The human hand is one of the most complex and fascinating structures in the human body consisting of 27 bones, including eight carpal bones, five metacarpals, and 14 phalanges, making it difficult to study [107]. Human hand function allows object manipulation and physical interaction with the environment. Deficits in hand function severely affect their quality of life by preventing them from performing activities of daily living (ADLs). Stroke is the number one cause of severe adult disability in the U.S. and worldwide [108], [109]. One of the main sequels after a stroke is the loss of mobility in the upper extremities, often affecting hand dexterity. Therefore, the rehabilitation process for hand recovery is vital to post-stroke

patients. The rehabilitation process is traditionally carried out by a physical therapist specializing in treating disabilities related to motor and sensory impairments [4]; hand therapy helps to improve strength and increase the range of motion (ROM) extension/flexion. Therefore, to evaluate and improve the efficacy of rehabilitation programs, it is crucial to measure upper limb function with standardized outcome measures (OMs). The use of OMs in physical therapy can lead to more efficient rehabilitation programs for the patients and more significant insights into the clinical condition [5], [6]. Hence, the selection of OMs with good psychometric properties is highly recommended. One of the most commonly OMs used by physical therapists and other health care professionals to assess the performance of the upper extremities in people who have suffered a stroke is The Action Research Arm Test (ARAT). The ARAT is a standardized and validated test that consists of 19 movement tasks divided into four subtests (grasp, grip, pinch, and gross arm movement). The ARAT has demonstrated excellent reliability, and it's a relatively short and simple measure of upper limb function, and testing can be completed quickly on higher functioning patients [110]. ARAT, like most other tests, requires a human examiner to transform observations of a patient's movement into a score; reliance on a human examiner leaves room for subjective measures, particularly in scoring, especially patterns of motor test abnormality that emerge after stroke [7]. In the last years, due to technological development, several investigations have been developed in medical rehabilitation, such as using multiple types of sensors to analyze human hand motion. Sensors for hand motion analysis most commonly used are Data glove, Inertial measurement unit (IMU), Optical markers, vision-based capturing (Ordinary Cameras, Depth Cameras, Leap Motion Controller), electromyography sensor (EMG)-based capturing, and Force sensors (Capacitive, Piezoresistive, Piezoelectric) [14]. The Hand motion data obtained from these sensors allow us to know: hand position, finger joint angles, force detection, and angular velocity in real-time. Assessment and analysis of upper extremities in post-stroke patients using diverse types of sensors can be found in several investigations. Lin et al. [54] proposed a data glove system integrated with six-axis inertial measurement unit sensors for evaluating the hand function. A shoe-based sensor with force-sensitive resistors (FSRs) to accurately identify postures in people with stroke was proposed by Fulk and Sazonov [55]. Ambar et al. [32] designed an arm rehabilitation monitoring device utilizing an Arduino-based Microcontroller using a flex sensor to detect arm bending movement, an IMU board InvenSens Inc., and two force-sensitive resistors to detect muscle force. Data from a Microsoft Kinect sensor (kinematic upper limb) and an FSRs glove (strength of muscles) to predict muscle forces in stroke patients through the least square regression matrix were used by Hoda et al. [56]. A data-glove-based system embedded with 9-axis IMUs sensors and FSRs for evaluation of hand function was designed by Hsiao et al. [44]. Kim et al. [57] proposed a Microsoft Kinect sensor tool during the Fugl-Meyer Assessment (FMA) and validated it for hemiplegic stroke patients. Schwarz et al. [12] used a wearable inertial sensing system composed of eight IMUs, with triaxial accelerometers and gyroscopes, to assess upper extremity movement impairments after stroke. However, to the best of our knowledge, few studies integrate sensors during the execution of the ARAT. Carpinella et al. [10] presented an analysis for quantitative assessment of upper limb motor function on healthy subjects and persons with Multiple Sclerosis, using a single inertial sensor

on the wrist. Nam et al. [11] quantified the Range of Motion (ROM) of the upper extremities during the performance of the ARAT and six essential ADL, using 25 Inertial Measurement Unit (IMU) sensors. Ticó Falguera [111] published a study to assess the ROM of finger joints and hand simulation using an instrumented glove (CyberGlove II®) in post-stroke patients during the first six months of recovery. Held et al. [13] designed a study to evaluate rehabilitation progress with a full-body IMU system composed of 14 IMUs, over four weeks. Repnik et al. [59] presented a study in healthy subjects and patients after stroke to quantify upper limb movement, using a wearable system of 7 IMUs for kinematics and electromyography (EMG) sensors for muscle activity analysis. Nevertheless, only one research incorporates multiple sensors and focuses on hand finger joints, but not on finger forces.

Multisensory information of human hand motion with wearable sensors during a standardized OMs performance as is the ARAT test is an alternative for a more objective, accurate, and quantitative measurement method. The purpose of this study is to measure the flexion angle of the finger joints and the finger forces during the performance of the three subtests (Grasp, Grip, and Pinch) of the ARAT test in healthy subjects. In the next stage of the project, the data obtained will be used for clinical purposes as a dataset for machine learning classification algorithms in post-stroke patients.

4.3 Materials and Methods

4.3.1. Action Research Arm Test

The ARAT evaluates 19 tests of arm motor function, both distally and proximally. The tests are distributed across four subtests (Grasp, Grip, Pinch, Gross movement), with four to six tasks each. The first three subtests assess the patient’s ability to perform functional tasks, including lifting and moving objects of various shapes and sizes (e.g., blocks, balls, and marbles) [7], [112]. The last subtest is the gross arm movement which assesses the movement of the entire upper limb. The required materials are a chair without armrests, a table, a 37-cm high shelf, and specific materials.

The description of each test and material specifications are shown in Table 4.1. In each subtest, task performance is scored on a 4-point scale and ordered hierarchically by difficulty to improve testing efficiency. The ARAT is scored from 0 to 3 [112]; A score of 3 is given when the task is performed normally, A score of 2 is given when the subject completes the test but takes a long time or have a difficult, A score of 1 is given when the subject performs the test partially, A score of 0 is given when the subject cannot perform any part of the test [7], [112]. Sometimes the assessment can be complex and subjective, based on the examiner's observation and criteria alone.

Table 4.1. Materials and test description of the Action Research Arm Test

Subtest	Test	Item (size)	Description
Grasp	1	Block, 10 cm^3	Grasp, lift vertically, place, and release the item onto the top of the shelf.
	2	Block, 2.5 cm^3	
	3	Block, 5 cm^3	
	4	Block, 7.5 cm^3	
	5	Cricket ball (Diameter, 7cm)	
	6	Sharpening stone (10.0 x 2.5 x 1 cm)	
Grip	7	Two plastic tumblers (Upper diameter, 7 cm; lower diameter, 6 cm; height, 12 cm)	Pour water from one glass into another.
	8	Displace alloy tube (Diameter,2.25cm)	Displace from one side of the table to the other.
	9	Displace alloy tube (Diameter,1 cm)	Displace from one side of the table to the other.
	10	Put washer over bolt (Diameter, 0.5 cm)	Put washer over the bolt.
Pinch	11	Ball-bearing (Diameter, 6 mm)	Held the ball-bearing between ring and thumb finger.
	12	Marble (Diameter, 1.6 cm)	Held the marble between index and thumb finger.
	13	Ball-bearing (Diameter, 6 mm)	Held the ball-bearing between middle and thumb finger.
	14	Ball-bearing (Diameter, 6 mm)	Held the ball-bearing between index and thumb finger.
	15	Marble (Diameter, 1.6 cm)	Held the marble between ring and thumb finger.
	16	Marble (Diameter, 1.6 cm)	Held the marble between middle and thumb finger.

4.3.2. Participants

This study included 25 healthy subjects, 14 women and 11 men, whose descriptive data are shown in Table 4.2. The subjects were selected under the criteria of being right-handed, over 18 years old, and not having suffered any hand disorders or injury. The study was approved by the Ethics Committee of the Polytechnic University of Uruapan (UPU) Michoacán, Mexico. All participants provided written consent after being informed of the aims and procedures of the experiments.

Table 4.2. Descriptive data of the subjects.

Subject Data	Descriptive Statistics			
	Mean	SD	Min	Max
Age (years)	40.2	18.1	18.0	72.0
HL (mm)	176.6	4.4	167.0	184.0
HB (mm)	75.4	3.8	70.0	84.0

HL= Hand length (measured from the tip of the longest finger to the crease under the palm); HB= Hand breadth (measured across the widest area where the fingers join the palm); Standard Deviation (SD); Minimum (Min); Maximum (Max).

4.3.3. Experimental Setup

The study was performed in the facilities of the UPU. The ARAT equipment for the test performance was prepared according to the instructions and measures obtained from the model described by Lyle [31]. All subjects received verbal and written descriptions for all procedures before the test. Hand length and Hand breadth were measured in each subject with a tape measure. The subjects were equipped with the hand motion system in the right hand; five FSRs were attached to the fingertip of the fingers (thumb, index, middle, ring, little) with a double-sided tape, the force sensing module was placed at one side of the table. Then, a silk glove was placed taking care that the FSRs wires pass through the dorsal part of the hand. Next, the CyberGlove II® was put on in the hand, and the connection Bluetooth with the GUI was tested. Finally, the subjects performed the 16 tests part of the subtests: Grasp, Grip, and Pinch, the description of each test are shown in Table 4.1. Each subject performed the 16 tests three times each (Figure 4.1). The data were measured and recorded in a CSV file from the start to the end of each activity.

Figure 4.1. A participant is wearing the hand motion system, performing the Action Research Arm test (ARAT).

During the beginning of each test, the hand is in a neutral position placed horizontally on the table, so we assumed that this would be the maximum extension angle of the finger joints in many tasks and was not considered in the analysis. Next, at the time of pre-grasp the object, the angle of flexion increases, but no force is exerted. During the grasping event, the maximum flexion angle and maximum force are reached. Finally, when the subject releases the object, the force starts to decrease and the hand back to the start position (extension). Therefore, the maximum values of the three measurements obtained for each subject during each test were averaged. These values were defined as the flexion angle and fingertip force of a subject for a given test. Next, the respective flexion angles and force among the 25 participants were

averaged. The finger joints evaluated in this study were as follows: MCP and PIP joints of the fingers (index, middle, ring, and little) and CMC, MCP, and IP for the thumb.

On the other hand, the distal interphalangeal (DIP) joint was not considered in the analysis because a linear relationship with the proximal PIP joint was assumed, it was considered as $DIP = 2/3 * PIP$ adopted from [32]. However, the information of the DIP joint is in the database. The gross movement subtest is excluded in the study because it assesses the entire arm, and the objective of this study is to assess finger joints.

4.3.4. Statistical Analysis

Statistical analysis was conducted using the Software R 4.1.0 and IBM SPSS Statistics Version 28.0. Armonk, NY: IBM Corp. First, the flexion angles of the finger joints were compared among the three subtests (Grasp, Grip, and Pinch), an ANOVA Welch's test for unequal variances was used to determine whether the differences between group means were statistically significant. In the Pinch subtest, an independent-samples t-test was conducted to compare the flexion angle of the finger joints between similar tests using specific fingers but with different objects (ball-bearing, marble). Finally, the mean flexion angles during the 16 tests were compared among the finger joints using a Welch's ANOVA. Subjects' age and hand length (HL) were tested for significant differences with respect to the flexion angles using a Mann–Whitney U test. Differences in fingertip force between age groups were analyzed using a Mann–Whitney U test. A Games–Howell post hoc test was conducted for significant differences with a Bonferroni p-adjust correction. The level of significance was set at $\alpha = 0.05$ for statistical tests.

4.4. Results

4.4.1. Finger Joints Flexion Angles

The flexion angles of the finger joints required to perform each test are shown in Table 4.3. In the grasp subtest, maximum flexion angles were found during the performance of Test 2 (index MCP 49.9°, middle MCP 50.1°, and ring MCP 39.2°), and Test 6 (thumb CMC 31°, index MCP 52.6°, middle MCP 49.2°, ring MCP 42.2°, index PIP 40.6°, middle PIP 49.5°, and ring PIP 45.2°). In the grip subtest, maximum flexion angles were found in Test 10 (index MCP 58.6°, index PIP 54.7°, middle MCP 57.4°, middle PIP 58.6°, ring MCP 63.5°, ring IP 54.3°, little MCP 52.9°, and PIP 33.6°), Test 8 and Test 9 presented similar flexion angles. In the pinch subtest, flexion angles were similar in the six tests, considering that specific fingers were used in each test.

Table 4.3. Descriptive statistics of flexion angles required to perform ARAT test.

Test	Thumb (deg)			Index (deg)		Middle (deg)		Ring (deg)		Little (deg)	
	CMC	**MCP**	**IP**	**MCP**	**PIP**	**MCP**	**PIP**	**MCP**	**PIP**	**MCP**	**PIP**
	Mean (SD)	*Mean (SD)*	*Mean (SD)*	*Mean (SD)*	*Mean (SD)*	*Mean (SD)*	*Mean (SD)*	*Mean (SD)*	*Mean (SD)*	*Mean (SD)*	*Mean (SD)*
1	15.9	27.6	20.3	36.1	33.2	37	46.5	28.4	45.6	22.3	29.3
	(6.0)	(9.0)	(12.0)	(9.4)	(11.9)	(10.3)	(6.7)	(9.0)	(6.4)	(6.4)	(14.3)
2	27.3	23.8	9.6	49.9	32	50.1	35.7	39.2	31.6	27.6	19.3
	(6.5)	(8.4)	(6.8)	(7.6)	(9.8)	(6.6)	(7.7)	(7.6)	(10.1)	(8.2)	(12.1)
3	24.4	22.2	9.9	40.4	34.6	44.4	37.8	36.2	34.9	27.7	19.6
	(6.4)	(9.5)	(8.0)	(9.4)	(9.6)	(7.7)	(6.5)	(5.3)	(6.8)	(7.5)	(12.4)
4	21.2	23.2	11.3	37.8	36.8	37.6	44.1	32.2	39.9	27.8	22.8
	(6.6)	(9.6)	(10.8)	(9.5)	(12.8)	(9.6)	(7.2)	(8.2)	(8.8)	(6.0)	(13.2)
5	24.3	22.3	13.1	39.4	34.1	41.4	36.7	36	33.7	34.1	23.5
	(5.8)	(8.3)	(10.2)	(10)	(7.9)	(8.9)	(5.5)	(6.0)	(6.1)	(8.7)	(10.5)
6	31.0	27.0	15.8	52.6	40.6	49.2	49.5	42.2	45.2	33.3	23.1
	(4.9)	(7.2)	(17.9)	(9.4)	(9.7)	(7.5)	(10.1)	(9.5)	(10.8)	(11.7)	(12.4)
7	25.7	21.5	15.5	34.1	41.1	35.8	44.5	35.2	36.6	30	20.2
	(5.4)	(8.3)	(12.6)	(10.1)	(9.3)	(7.8)	(6.7)	(9.7)	(7.8)	(5.0)	(11.7)
8	32.1	29.8	15.2	48.1	49.5	50.5	50.5	50.6	45.6	41.8	23.6
	(4.9)	(8.3)	(15.4)	(9.2)	(10.2)	(6.5)	(8.6)	(12.1)	(8.5)	(10.4)	(12.6)
9	32.5	30.4	23.1	50.5	54.2	51.3	53.8	53.4	47.6	42.3	23.2
	(5.5)	(8.9)	(21.4)	(10.3)	(11.1)	(7.1)	(8.8)	(12.3)	(9.1)	(11.2)	(13.4)
10	32.5	32	20.5	58.6	54.7	57.4	58.6	63.5	54.3	52.9	33.6
	(5.5)	(9.2)	(20.6)	(12.4)	(13.8)	(12.6)	(10.5)	(12.1)	(11)	(12.2)	(16.4)
11	34.4	33.5	9.2	36.9	28.4	44.7	41.6	60.1	43.5	37.5	28.9
	(6.0)	(7.4)	(14.9)	(12.7)	(12.1)	(9.7)	(10.9)	(11.5)	(11.2)	(8.5)	(15.7)
12	29.3	24.6	12.6	61.1	43.8	44.8	34.9	39.6	28.7	24.0	17.6
	(5.2)	(6.9)	(16.8)	(8.9)	(10.1)	(7.1)	(10)	(8.6)	(11.2)	(9.9)	(11.7)
13	32	28.7	8.9	45.4	30.9	64.3	44.8	59.5	43	25.7	16.9
	(5.8)	(8.6)	(14.2)	(11.2)	(11.3)	(9.2)	(11)	(9.3)	(11.8)	(9.1)	(11.8)
14	31.9	27.4	11.0	64.4	52	46.9	34.5	37.2	28	21.4	15.7
	(4.4)	(8.3)	(13.5)	(9.6)	(13.2)	(7.0)	(8.9)	(8.1)	(10.5)	(7.3)	(11.5)
15	32.3	29.5	8.2	40.1	27.7	44.6	31	54.7	35.0	31.3	20.9
	(5.4)	(7.2)	(13.5)	(11.5)	(9.8)	(8.2)	(9.1)	(8.8)	(9.8)	(8.7)	(12.5)
16	30.2	25.8	7.4	43.4	28.6	60.1	37.4	47.3	34.1	24.4	15.3
	(5.2)	(7.1)	(14.3)	(10.2)	(9.7)	(8.4)	(8.7)	(8.3)	(9.1)	(8.5)	(10.1)

Test 1–6 corresponds to grasp subtest, Test 7–10 corresponds to grip subtest, Test 11–16 corresponds to Pinch Subtest. CMC= carpometacarpal; MCP = metacarpophalangeal; IP = interphalangeal; PIP = proximal interphalangeal. SD= standard deviation; deg= degrees.

4.4.2. Pinch Subtest t-Test

An independent-samples t-test showed that flexion angle of the Index PIP in Test 12 (M = 43.8, SD = 10.1) was significantly smaller than Test 14 (M = 52, SD = 13.15) conditions; t (48) = −2.46, p = 0.017 see Table 4.4. The flexion angle of the Middle PIP in Test 13 (M = 44.8, SD = 11) was significantly larger than Test 16 (M = 37.3, SD = 8.72) conditions; t (48) = 2.64, p = 0.011 see Table 4.5. Lastly, flexion angle of the Ring PIP in Test 11 (M = 43.5, SD = 11.1) was significantly larger than Test 15 (M = 34.9, SD = 9.82) conditions; t (48) = 2.87, p = 0.006 see Table 4.6.

Table 4.4. Independent samples t-test for comparison flexion angles with respect to Test 12 and Test 14.

Finger Joints	Levene's Test		*t*-Test for Equality of Means		
	F	Sig.	t	df	*p*-Value
Thumb CMC	0.78	0.383	−1.95	48	0.58
Thumb MCP	1.14	0.291	−1.27	48	0.21
Thumb IP	0.74	0.394	0.38	48	0.71
Index MCP	0.13	0.719	−1.26	48	0.21
Index PIP	0.96	0.333	−2.46	48	0.017 **

** $p < 0.05$, considered statistically significant.

Table 4.5. Independent samples t-test for comparison flexion angles with respect to Test 13 and Test 16.

Finger Joints	Levene's Test		*t*-Test for Equality of Means		
	F	Sig.	t	df	*p*-Value
Thumb CMC	0.175	0.678	1.135	48	0.26
Thumb MCP	1.315	0.257	1.319	48	0.19
Thumb IP	0.08	0.929	0.353	48	0.73
Middle MCP	0.872	0.355	1.658	48	0.10
Middle PIP	2.062	0.157	2.647	48	0.011 **

** $p < 0.05$, considered statistically significant.

Table 4.6. Independent samples t-test for comparison flexion angles with respect to Test 11 and Test 15.

Finger Joints	Levene's Test		*t*-Test for Equality of Means		
	F	Sig.	t	df	*p*-Value
Thumb CMC	0.27	0.60	1.29	48	0.20
Thumb MCP	0.08	0.78	1.95	48	0.06
Thumb IP	0.26	0.61	0.24	48	0.81
Ring MCP	1.61	0.21	1.87	48	0.07
Ring PIP	0.73	0.40	2.87	48	0.006 **

** $p < 0.05$, considered statistically significant.

4.4.3. Grasp, Grip, and Pinch Subtests

A Welch's ANOVA was conducted to determine whether the flexion angle of the finger joints differed based on the different subtests (Grasp, Grip, and Pinch). The results showed that mean flexion angles of the Thumb (CMC 31.68°, MCP 28.27°), Index MCP 48.54°, Middle MCP 50.91°, and Ring MCP 48.08° obtained in the Pinch subtest were significantly larger than flexion angles of the Thumb (CMC 24.02°, MCP 24.34°), Index MCP 42.70°, Middle MCP 43.27°, and Ring MCP 35.71° obtained in the Grasp subtest. In contrast, flexion angles in the Index PIP 49.87°, Middle PIP 51.88°, and Ring PIP 46.03° obtained in the Grip subtest were significantly larger than flexion angles obtained in the Grasp and Pinch subtest. The full results are shown in Figures 4.2-4.4.

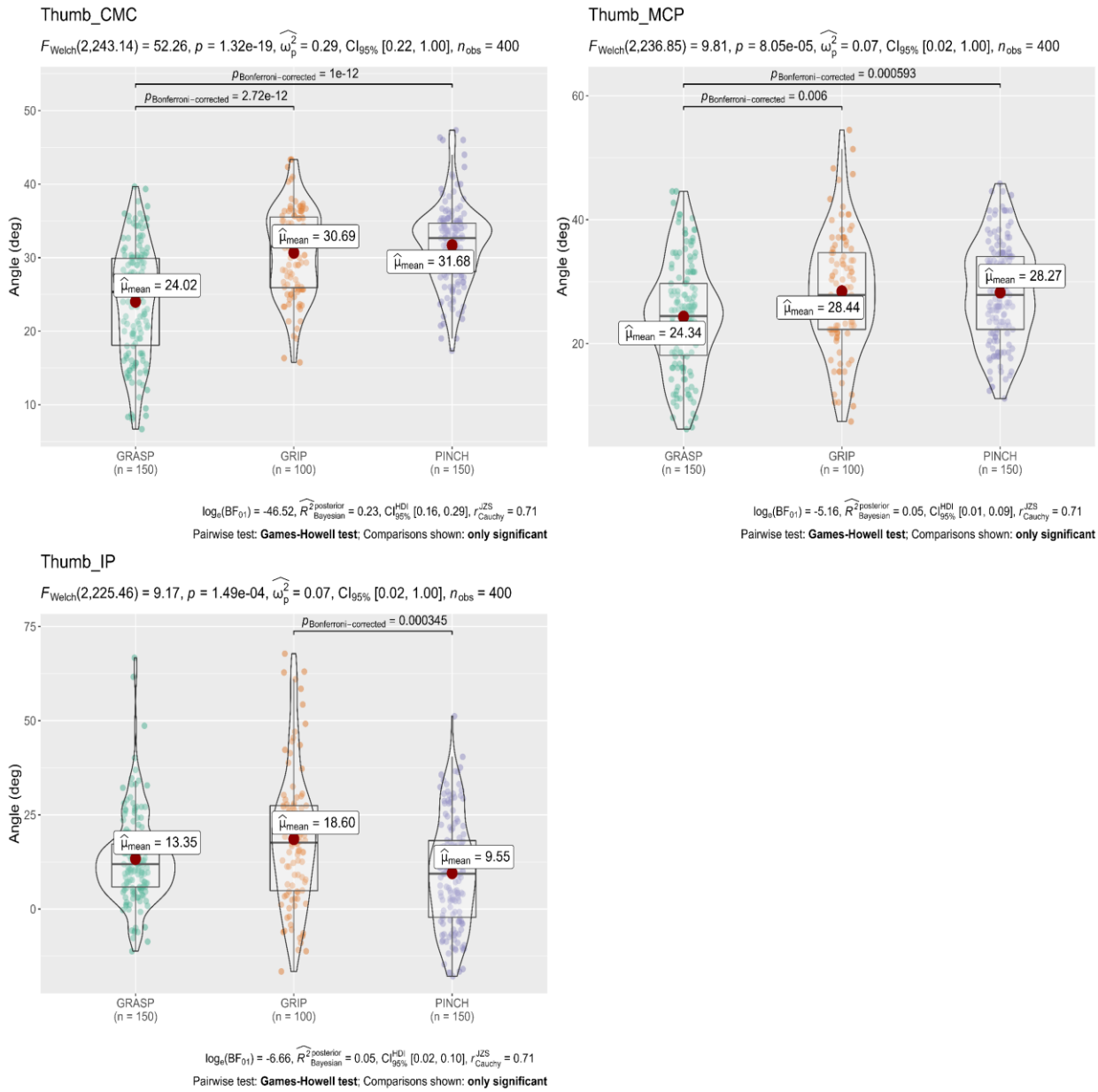

Figure 4.2. Welch's ANOVA and post hoc results; Comparison of flexion angles of the Thumb joints concerning the three Subtests of the ARAT. The flexion angles of the carpometacarpal (CMC) and metacarpophalangeal (MCP) joints of the Thumb finger were significantly larger ($p < 0.05$ each) in the Pinch and Grip subtest than in the Grasp subtest. Likewise, the flexion angles of the interphalangeal (IP) were significantly larger ($p < 0.05$ each) in the grip subtest than in the grasp subtest. Horizontal lines indicate significant differences ($p < 0.05$, Games–Howell test post hoc comparison); deg= degrees.

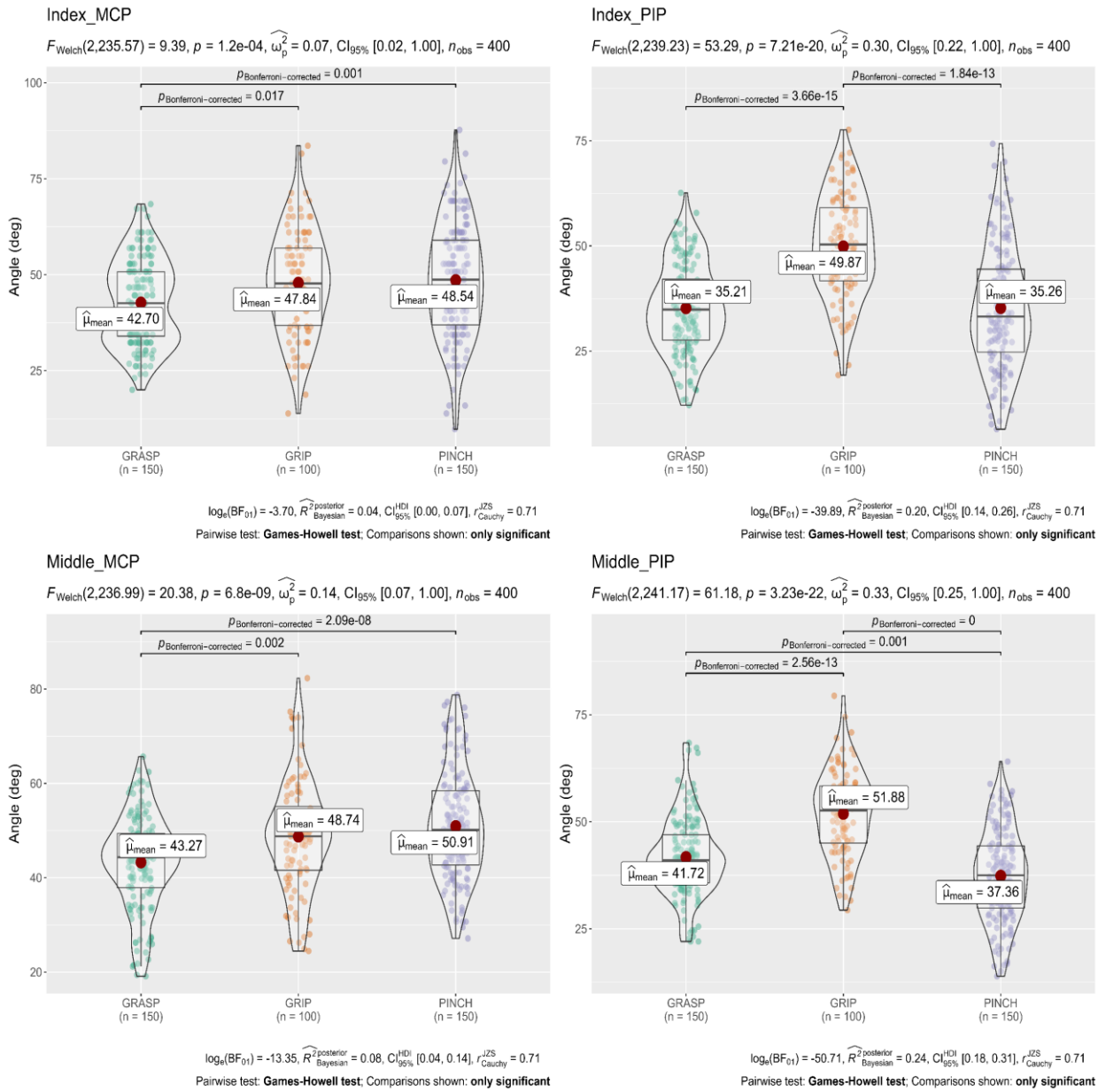

Figure 4.3. Welch's ANOVA and post hoc results; Comparison of flexion angles of the Index and Middle joints concerning the three subtests of the ARAT. The flexion angles of the proximal interphalangeal (PIP) joints of the Index and Middle fingers were significantly larger ($p < 0.05$ each) in the grip subtest than in the grasp and pinch subtest. In contrast, the flexion angles of the metacarpophalangeal (MCP) joints were significantly larger ($p < 0.05$ each) in the pinch subtest than in the grasp subtest. Horizontal lines indicate significant differences ($p < 0.05$, Games–Howell test post hoc comparison); deg = degrees.

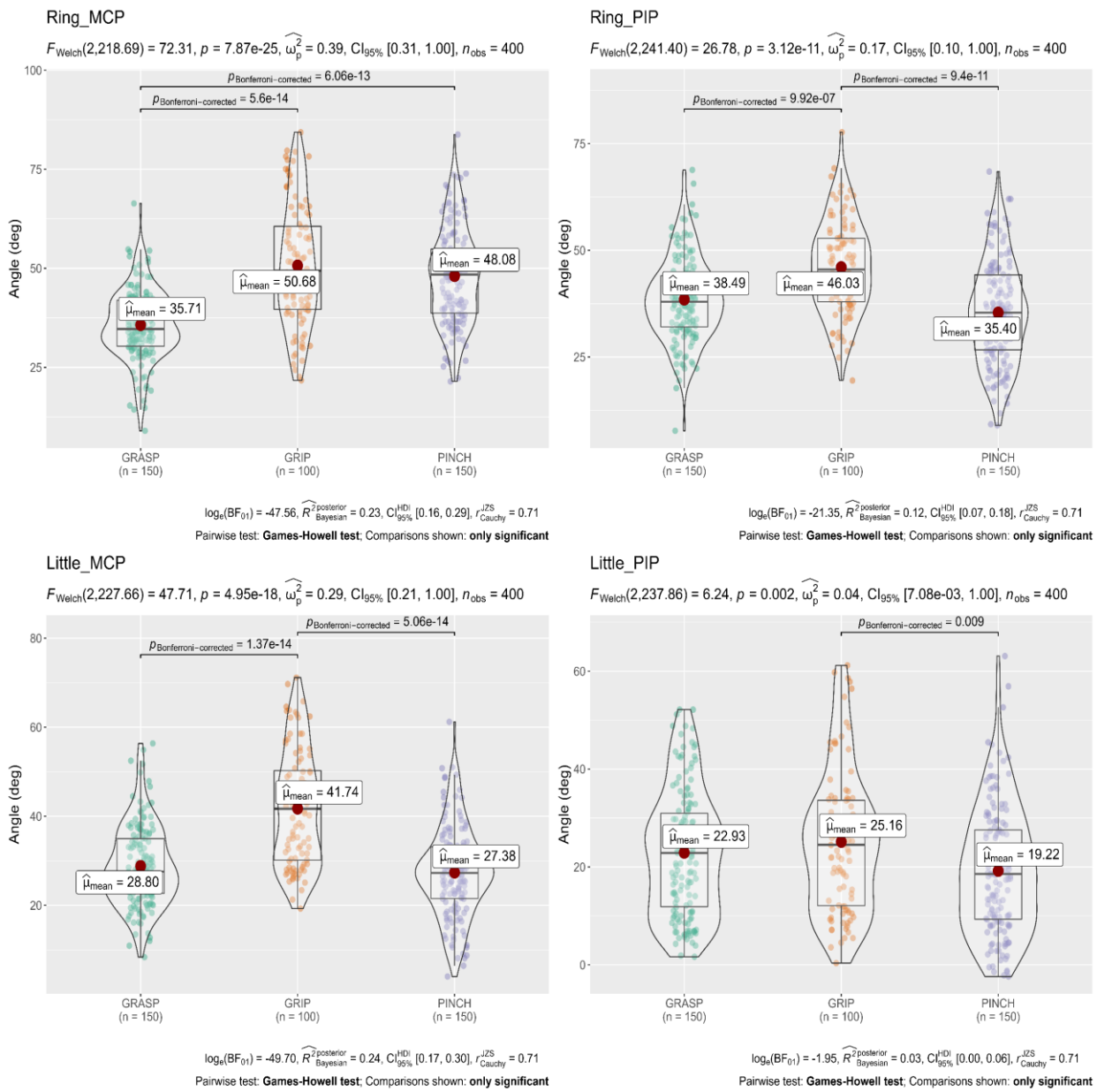

Figure 4.4. Welch's ANOVA and Post hoc results; Comparison of flexion angles of the Ring and Little joints concerning the three Subtests of the ARAT. The flexion angles of the metacarpophalangeal (MCP) and proximal interphalangeal (PIP) joints of the Ring finger were significantly larger ($p < 0.05$ each) in the grip subtest than in the grasp subtest. On the other hand, the flexion angles of the metacarpophalangeal (MCP) and proximal interphalangeal (PIP) joints of the Little finger were significantly larger ($p < 0.05$ each) in the grip subtest than in the pinch subtest. Horizontal lines indicate significant differences ($p < 0.05$, Games–Howell test post hoc comparison); deg = degrees.

4.4.4. Flexion Angle of Each Finger Joint during the 16 Tests

A Welch's ANOVA was conducted to determine whether the mean flexion angle during the 16 ARAT tests differed based on the different finger joints. The results showed no significant differences between the mean flexion angle of the Index MCP 46.18°, Index PIP 38.89°, Middle MCP 47.5°, Middle PIP 42.62°, Ring MCP 44.09°, Ring PIP 39.22° finger joints, while mean flexion angles of the Thumb (CMC 28.56°, MCP

26.84°, IP 13.23°) and Little PIP 22.10° were significantly smaller than the other finger joints. The full results are shown in Figure 4.5.

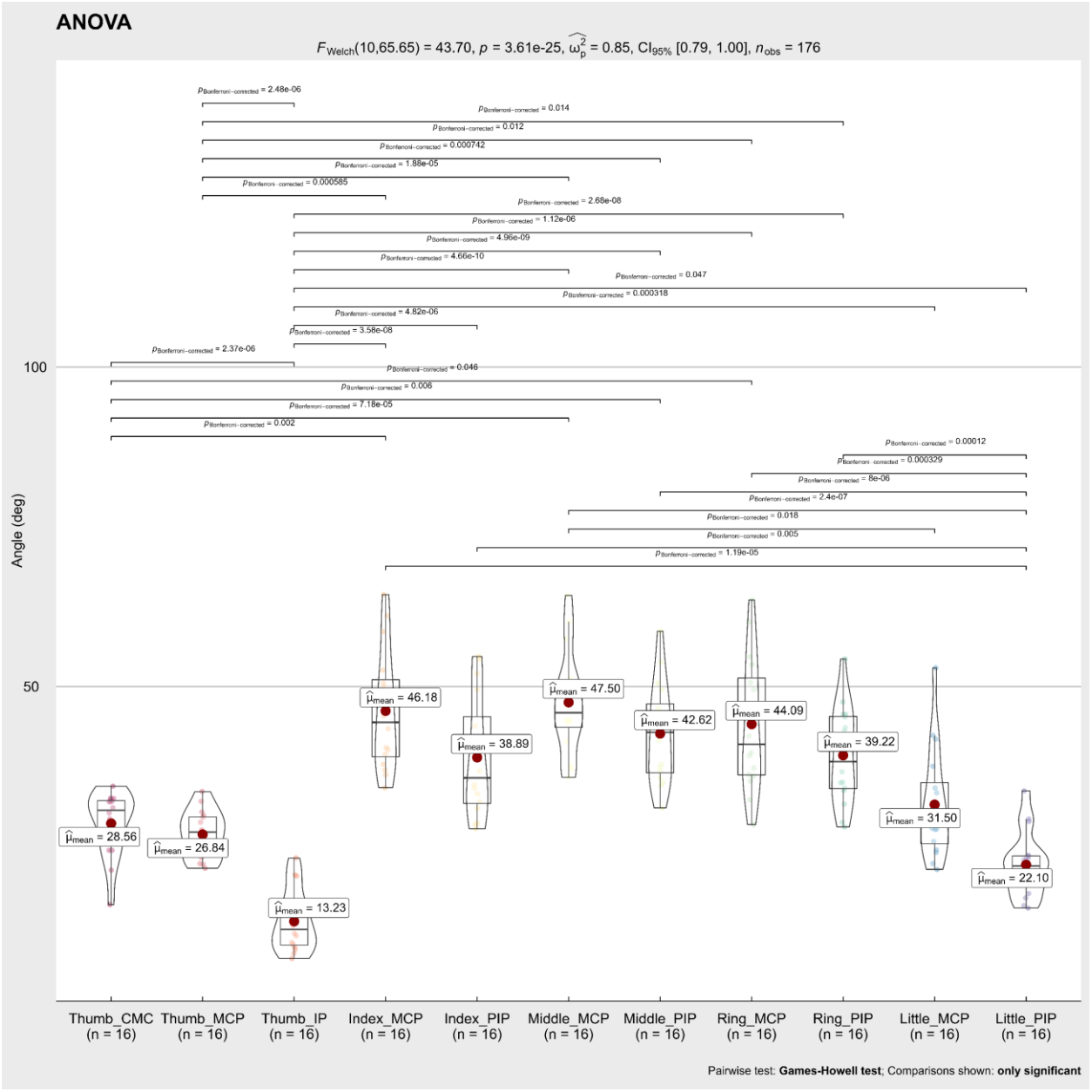

Figure 4.5. Welch's ANOVA and Post hoc results; Comparison flexion angles concerning the finger joints, during the 16 tests of the ARAT; Horizontal lines indicate significant differences ($p < 0.05$, Games–Howell test post hoc comparison). The flexion angles of the carpometacarpal (CMC), metacarpophalangeal (MCP), and interphalangeal (IP) joints of the Thumb finger were significantly smaller ($p > 0.05$ each) than the flexion angles of the MCP joints of the Index, Middle, Ring. Similarly, the flexion angles of the proximal interphalangeal (PIP) joint of the Little finger were significantly smaller ($p > 0.05$ each) than the flexion angles of the MCP and PIP joints of the Index, Middle, and Ring fingers. deg= degrees.

4.4.5. Differences in the Flexion Angles Respect to Age and Hand Length Groups

A Mann–Whitney U test was used to compare the flexion angles of the finger joints between different age groups, and between hand length groups, during the performance of the 16 activities. Results showed that subjects (18–32 years) had a significantly higher flexion angle in the finger joints (Thumb MCP, Index MCP, Index PIP, and Middle MCP) than subjects (45–72 years), as shown in Figure 4.6. On the other hand, the Mann–Whitney tests in Figures 4.7 and 4.8 showed that flexion angles in the Thumb IP, Index PIP, Middle PIP, and Ring PIP in subjects with a hand length of 190–230 mm were larger and statically significant than in subjects with a hand length of 167–178 mm. In contrast, the flexion angles in Middle MCP and Ring MCP were significantly larger in subjects with a hand length of 167–178 mm than subjects with a hand length of 190–230 mm.

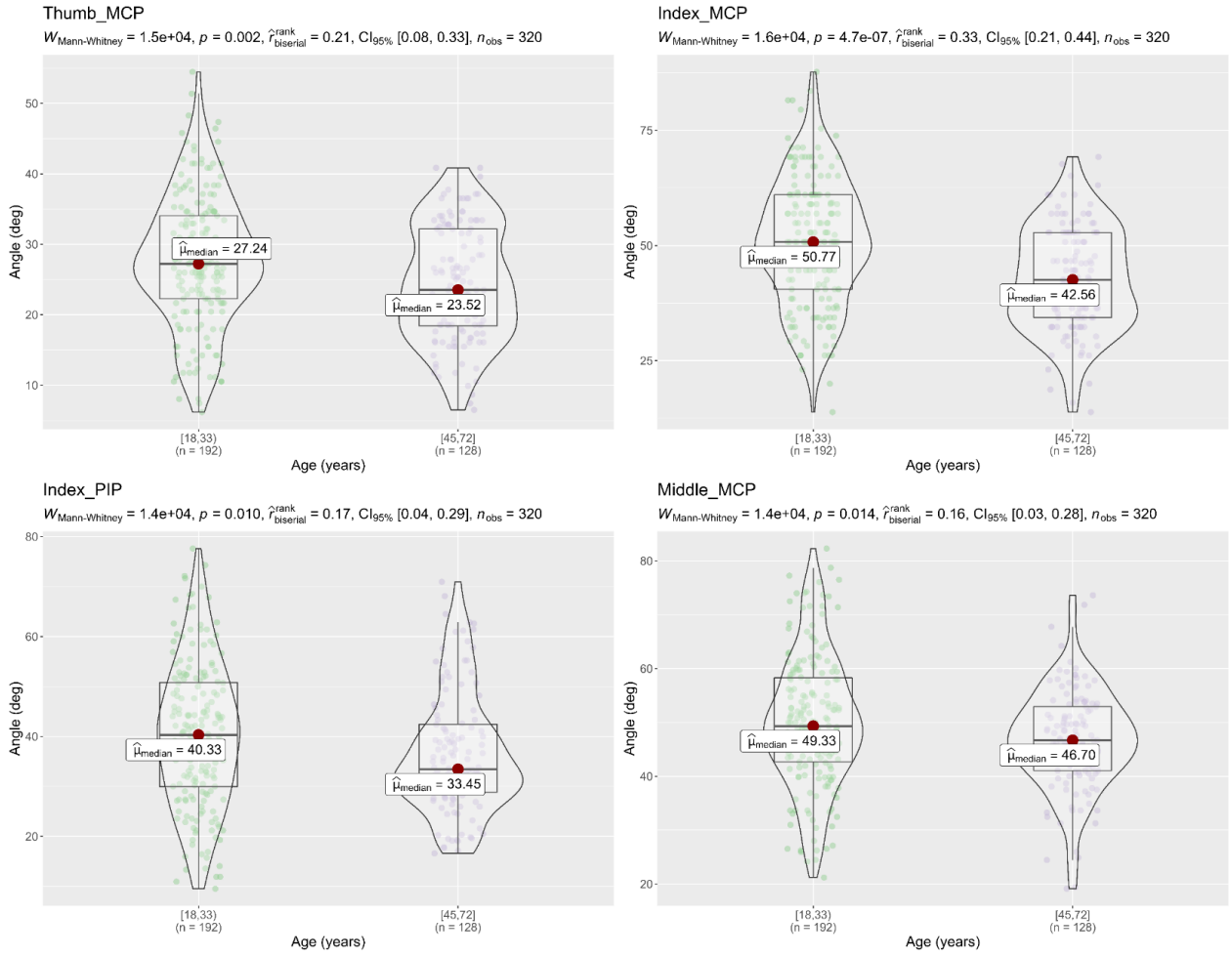

Figure 4.6. Mann–Whitney U test flexion angle of the finger joints with respect to different age groups. The figure only shows the finger joints in which significant differences were found (Thumb MCP, Index MCP, Index PIP, Middle MCP); $p < 0.05$, significantly different; deg= degrees.

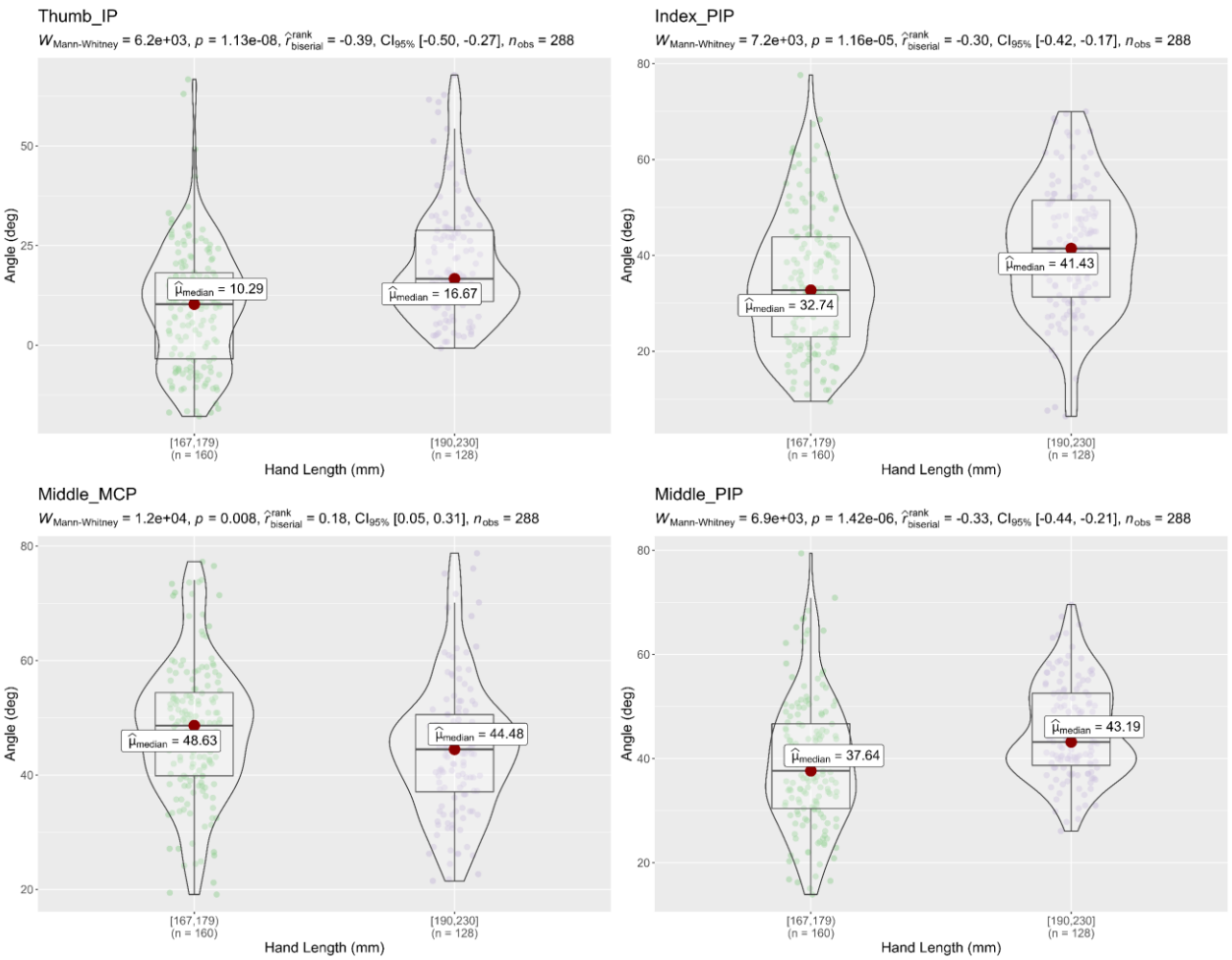

Figure 4.7. Mann–Whitney U test of flexion angle in finger joints with respect to different hand length groups; The figure only shows the finger joints in which significant differences were found (Thumb IP, Index PIP, Middle MCP, Middle PIP); $p < 0.05$, significantly different; deg= degrees.

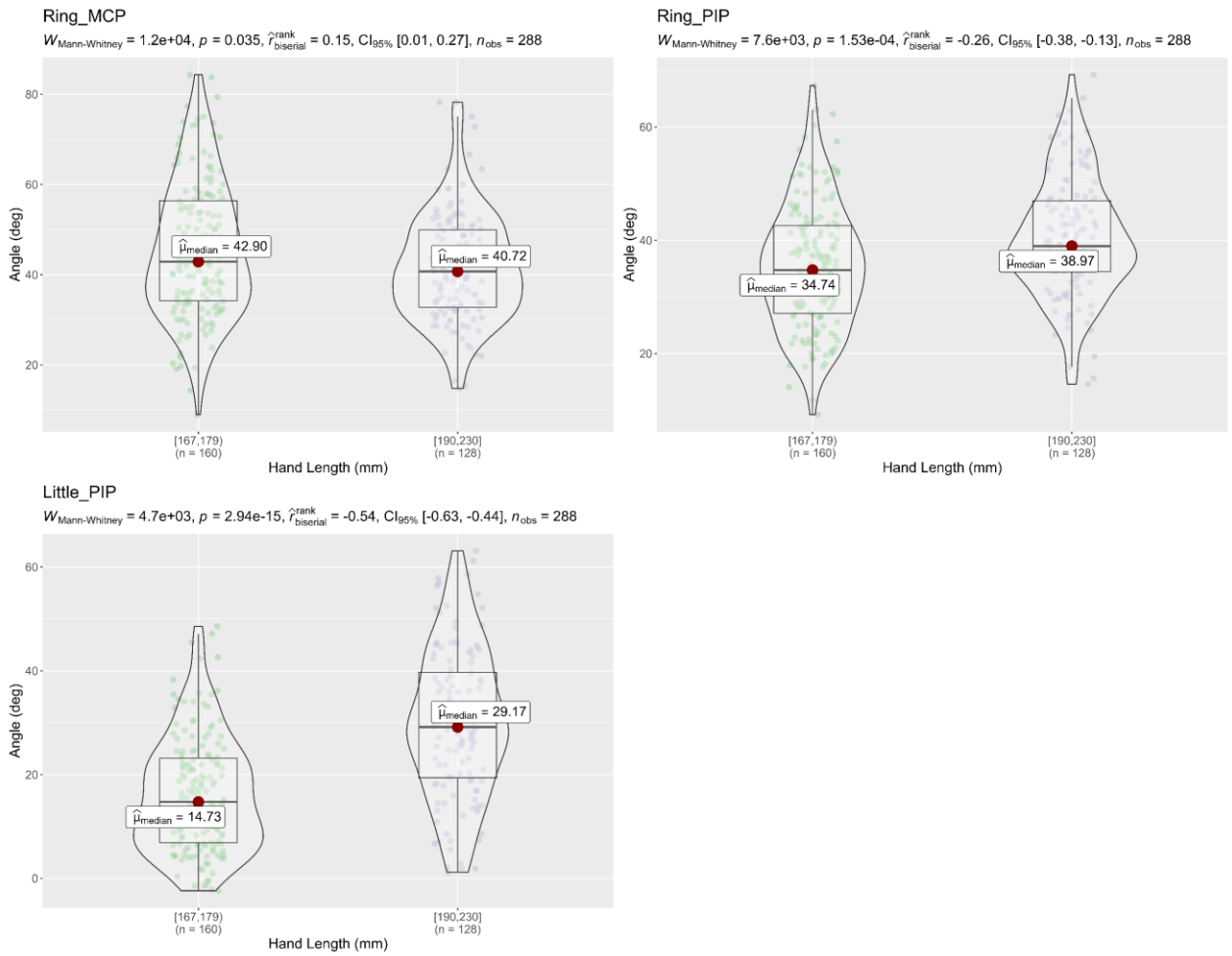

Figure 4.8. Mann–Whitney U test of flexion angle in finger joints with respect to different hand length groups; The figure only shows the finger joints in which significant differences were found (Ring MCP, Ring PIP, Little PIP); $p <$ 0.05, significantly different; deg= degrees.

4.4.6. Fingertip Forces

The force exerted for the fingertips (thumb, index, middle, ring, and little) during the performance of the 16 tests of the grasp, grip, and pinch subtest are shown in Table 4.7. During Test 1 of the grasp subtest, the thumb exerts a mean force of 4.5 N, the index exerts a mean force of 2.9 N, the middle exerts a mean force of 3.5 N, the ring exerts a mean force of 2.1 N, and the little exerts a mean force of 1.1 N, with a total force of 14.1 N, these values were the highest of all the tests. In grip subtest maximum total force of 8.1 N was applied in Test 7. Additionally, in the pinch subtest, maximum total forces of 4.5 N and 4.4 N were applied in Test 16 and Test 12, respectively.

The mean force of the fingertips thumb, index, middle, ring, and little fingers required to perform the tests in the Grasp subtest were thumb 2.8 N (1.52), index 2.08 N (1.13), middle 2.16 N (1.2), ring 0.74 N (0.9), and little 0.24 N (0.73). Mean force required to perform grip subtest were thumb 2.39 N (1.5), index 1.95 N (0.94), middle 1.89 N (0.96), and ring 0.39 N (0.63). Finally, the mean forces required to perform the pinch subtest were thumb 2.06 N (0.68), index 2.13 N (0.81), middle 2.02 N (0.69), and ring 1.35 N (0.84).

Table 4.7. Descriptive statistics of fingertip forces during the performance of the ARAT test.

Test	Thumb Force (N)		Index Force (N)		Middle Force (N)		Ring Force (N)		Little Force (N)		Total Force (N)
	Mean	SD	Mean	SD	Mean	SD	Mean	SD	Mean	SD	
1	4.5	2.1	2.9	1.5	3.5	1.7	2.1	1.1	1.1	1.3	14.1
2	2.3	0.7	2.2	1.1	1.8	0.7	-	-	-	-	6.3
3	2.4	1.1	1.7	0.6	1.5	0.6	0.5	0.7	-	-	6.1
4	2.6	0.9	1.9	1.0	1.8	0.7	1.1	0.8	-	-	7.7
5	2.6	1.2	1.6	0.8	1.9	0.6	0.4	0.6	-	-	6.6
6	2.2	0.9	2.2	1.1	2.5	0.7	-	-	-	-	6.9
7	3.0	1.8	2.0	0.7	2.3	1.1	0.8	0.8	-	-	8.1
8	2.3	1.1	2.1	1.0	1.9	0.8	-	-	-	-	6.4
9	2.1	1.0	1.9	1.1	1.8	0.8	-	-	-	-	6.1
10	2.1	1.0	1.9	0.9	1.7	1.0	-	-	-	-	5.8
11	1.8	0.2	-	–	-	-	1.2	1.0	-	-	3.0
12	2.1	0.7	2.4	0.9	-	-	-	-	-	-	4.4
13	1.8	0.2	-	-	1.8	0.5	-	-	-	-	3.5
14	2.2	0.5	1.9	0.6	-	-	-	-	-	-	4.1
15	2.3	1.0	-	-	-	-	1.5	0.9	-	-	3.8
16	2.2	0.9	-	-	2.3	0.8	-	-	-	-	4.5

Test 1–6 corresponds to grasp subtest; Test 7–10 corresponds to grip subtest; Test 11–16 corresponds to pinch subtest; Force N = Newton.

4.4.7. Differences in Fingertip Force with Respect to Age Groups

An independent-samples t-test was conducted to compare the fingertip force exerted for different age groups of subjects during the performance of the tests in grasp subtest. Table 8 shows there was a significant difference in the index finger force of subjects (18–32 years) (M = 1.35, SD = 1.4) and subjects (45–72 years). (M = 0.76, SD = 1.24) conditions; t (118) = 2.38, p = 0.019. There was a significant difference in the middle finger force of subjects (18–32 years) (M = 1.77, SD = 1.14) and subjects (45–72 years). (M = 1.14, SD = 1.34) conditions; t (118) = 2.47, p = 0.015 see Table 4.8. Although in the grip subtest there was a significant difference in middle finger force of subjects (18–32 years) (M = 1.28, SD = 1.17) and subjects (45–72 years); (M = 1.14, SD = 1.34) conditions; t (78) = 2.43, p = 0.017 see Table 4.9.

Table 4.8. Independent samples t-test for comparison finger forces in grasp subtest, with respect to different groups of age (18–32 years) and (45–72 years).

Fingertip	Levene's Test		*t*-Test for Equality of Means		
	F	Sig.	t	df	*p*-Value
Thumb	1.715	0.193	0.807	118	0.421
Index	1.314	0.254	2.385	118	0.019 **
Middle	0.038	0.846	2.477	118	0.015 **
Ring	1.421	0.236	0.662	117	0.510
Little	0.013	0.908	0.051	118	0.959

** $p < 0.05$, significant difference.

Table 4.9. Independent samples t-test for comparison finger force in grip subtest, with respect to different groups of age (18–32 years) and (45–72 years).

Fingertip	Levene's Test		*t*-Test for Equality of Means		
	F	Sig.	t	df	*p*-Value
Thumb	3.152	0.080	1.628	78	0.108
Index	0.247	0.621	0.534	78	0.595
Middle	2.913	0.092	2.429	78	0.017 **
Ring	0.339	0.562	0.618	78	0.538

** $p < 0.05$, significant difference.

4.5. Discussion

There are only a few studies about the integration of sensors in upper limb measurement methods, but there is a need for more quantitative tests [5], [6]. In this paper, we used a hand motion system to determine the flexion angles of the finger joints and fingertip force required to perform the 16 tests of the ARAT in healthy subjects. Traditionally the ARAT is scored on an ordinal four point-scale, that is, from 0 to 3 [112]. A score of 3 is given when the task is performed normally, a score of 2 is given when the subject completes the test but takes a long time or has a difficulty, a score of 1 is given when the subject performs the test partially, a score of 0 is given when the subject cannot perform any part of the test [7], [112]. Nevertheless, sometimes the ARAT assessment can be complex and subjective, based on the examiner's observation and criteria alone. The data obtained indicates that the integration of multiple sensors during the performance of the ARAT allows therapists and other health professionals to perform a more objective, sensitive, and accurate evaluation with a validated clinical test.

To analyze and evaluate the data obtained by the hand motion system, we studied the behavior of each finger joint, from particular to general, during the performance of the 16 tests of the ARAT. The flexion angles were determined for each test presented in Table 3. The flexion angles of the finger joints were compared in each subtest to carry out a more in-depth analysis. In the grasp subtest, flexion angles of finger joints were larger when grasping a small object (Test 2 and Test 6) in comparison to when grasping a larger object (Test 1 and Test 4). In the grip subtest, significant differences were found in Test 7 with respect to the other tests of the subtest. These differences were because the object's size is larger in this test than in the others. In the pinch subtest, the results showed that in similar tests using specific fingers but different objects, no significant differences were found in the flexion angle of the thumb joints (CMC, MCP, IP) despite grasping objects of various sizes (Tables 4–6). The angle adjustment to make the pinch grip was made by the PIP joint of the other finger involved (index, middle, ring). Similar results where thumb joints did not show significant changes in the flexion angle but index finger joints changed significantly with respect to the object's width were presented by [113], [114]. Next, the subtests of the ARAT were grouped for statistical analysis. Although the subtests are similar, each of them involves different types of grasp, and, therefore, different flexion angles of the finger joints are required. In our study, we observed that flexion angles of the joints MCP in the fingers (index, middle, ring) were larger in tests involving the grasping of small objects, and the pinch subtest involved many of them.

Similar results were presented for Lee et al. [115], who found that MCP and PIP joints increased as cylinder diameter decreased, but flexion angles were fairly constant in the DIP joint. Shimawaki et al. [116] found the same correlation using a three-dimensional bone model during the grasping of a cylinder of three different diameters (10, 60, and 120 mm). Finally, the mean flexion angles obtained during the performing of the 16 activities were as follows: Thumb CMC: 28.56°; Thumb MCP: 26.84°; Thumb IP: 13.23°; Index MCP: 46.18°; Index PIP: 38.89°; Middle MCP: 47.5°; Middle PIP: 42.62°; Ring MCP: 44.09°; Ring PIP: 39.22°; Little MCP: 31.50°; Little PIP: 22.10°. The mean flexion angles of the thumb joints (CMC, MCP, and IP) were significantly smaller than the flexion angles of the index, middle, ring, and little finger (MCP, IP) joints. A similar result was obtained during the performance of 16 activities of daily living (ADL) in the MCP joints of the hand by Murai et al. [117]. On the other hand, no significant differences were found in the mean flexion angle of the index, middle, and ring (MC, PIP) joints, but statistically significant differences were found in the flexion angle of the Little (MCP, PIP) with respect to the other finger joints. Excluding the pinch test in our research, no statistically significant differences between all the MCP fingers joints were found. Hume et al. [118] reported similar results, that there were no significant differences between the flexion angles of the finger joints during 11 ADL, while Bain et al. [119] found during the performance of the Sollerman hand grip function test, statistically significant differences between the mean values for the active ROM of the finger joints. The differences found in these studies with our study is that grip and pinch subtests of ARAT involved the radial side of the hand, radial activities include the precision grip between (thumb, index, and middle fingers) and precision pinch between the thumb and the (index or middle or ring) finger. As far as we know, there is little research studying the range of motion of the thumb joints. Hume et al. Measured a mean angle of 21 degrees of flexion in the Thumb MCP and 18 degrees in the IP joint during grip postures, and Murai et al. [117] measured 35.3 degrees of flexion in his research. Our study obtained similar results than Hume et al. [118], the flexion angles of the thumb were MCP 26.84° and IP 13.3°. The flexion angles were smaller than Murai et al. Because many of the tests in ARAT involves precision grip and pinch. Regarding to the relationship of the flexion angle of finger joints with respect to different age groups, the results showed that young subjects (18–32 years) had a greater flexion angle in the finger joints (Thumb MCP, Index MCP, Index PIP, and Middle MCP) than elderly subjects (45–72 years) during the performance of the 16 activities. Similar results were presented for Smahel and Klímová [120]. They found that university students had a statistically significantly wider range of motion in the finger joints MCP, PIP, and DIP than Seniors citizens, while DeSmet et al. [121] found a significant correlation between increasing the age and decreasing MCP and IP flexion of the thumb in a study with 101 subjects. Regarding the flexion angles of the finger joints compared to different hand sizes, the result showed that subjects with a longer hand length performed greater flexion in Thumb IP, Index PIP, Middle PIP, and Ring PIP, but had a smaller flexion in Middle MCP and Ring MCP. Similar results were found during an experiment with cylinders of different radius, subjects with the largest HL, close the hand around the object with a slightly larger joint angle by Peña-Pitarch et al. [122]. The fingertip forces for each test are presented in Table 7. Maximum total finger forces were exerted during the performance of Test 1 (14.1

N), Test 4 (7.7 N), and Test 7 (8.1 N). In these tests, a power grip was executed between the fingers and the palm, power grip uses high force but low precision movements and involves the radial and ulnar sides of the hand [43]. Moreover, the results showed that the youngest subjects applied greater strength than the oldest subjects in the index and middle fingertip when performing the six tests part of the grasp subtest and in the middle fingertip during the four tests of the grip subtest. The mean total force in the six tests of the grasp subtest was 8.2 N, grip subtest 6.61 N, and pinch subtest 3.89 N. On the other hand, the force sensor data allows us to know the contact points used to grasp an object. Peña-Pitarch et al. (Peña-Pitarch et al., 2020) found that the number of fingers used to grasp a cylindrical object depends on the radius (ρ) of the object, e.g., for $5 \leq \rho \leq 12.5$ mm used two fingers, $12.5 \leq \rho \leq 20$ mm used three fingers, $20 \leq \rho \leq 35$ mm used four fingers, and $35 \leq \rho \leq 70$ mm used five fingers. In our study, we found similar results, e.g., when we used objects with a length (l) ≤ 100 mm subjects used five fingers, in objects $50 \leq l \leq 75$ mm subjects used four fingers and in objects $10 \leq l \leq 25$ mm were used three fingers. The differences found in our study were due to the object orientation, while in Peña-Pitarch et al., subjects performed a cylindrical grip since the cylinder was in a horizontal position and in this research, the subjects performed a three jaw-chuck grip due to the vertical position of the object.

4.6. Limitations

The limitation in the study was that using a data glove and sensors attached to the fingertips makes it difficult for some subjects to grasp small objects accurately; despite this, all subjects completed the tests. Another limitation is that the test of gross movement was not performed. Therefore, it would be suitable to use a motion capture system based on inertial measurement units (IMU), as were found in other studies [11], [59] for measuring flexion angles of the entire arm. In our research, the abduction and adduction angles of the finger joints were not analyzed; these data may be important for evaluating the ARAT and should be considered for future studies.

4.7. Conclusions

The results showed that flexion angles in Thumb (CMC, MCP), Index MCP, Middle MCP, and Ring MCP finger joints obtained in the pinch subscale were significantly larger than flexion angles in the grasp subtest. We determined that the flexion angles depend on the object size and the type of grasp used (power, precision, or pinch). In contrast, the mean total fingertip force exerted on the fingers was significantly greater in the grasp subtest (8.2 N) than in the grip (6.61 N) and the pinch (3.89 N) subtests. The data obtained showed that the integration of multiple sensors during the performance of 16 tests of the ARAT allows therapists and other health professionals to perform a more sensitive, objective, and quantitative assessment of the hand function. In the chapter 6, we will use the data as a dataset for machine learning algorithms with stroke patients.

CHAPTER 5
Quantitative Assessment of Hand Function in Healthy Subjects and Post-Stroke Patients with the Action Research Arm Test

5.1. Overview

The aim of this chapter was to identify joint impairments and compensatory grasping strategies in stroke patients with left (LH) and right (RH) hemiparesis. For this purpose, an experimental study was carried out with 12 patients six months after a stroke (three women and nine men, mean age: 65.2 ± 9.3 years), and 25 healthy subjects (14 women and 11 men, mean age: 40.2 ± 18.1 years). The subjects were evaluated during the performance of the ARAT using a data glove. Stroke patients with LH and RH showed significantly lower flexion angles in the MCP joints of the Index and Middle fingers than the Control group. However, RH patients showed larger flexion angles in the proximal interphalangeal (PIP) joints of the Index, Middle, Ring, and Little fingers. In contrast, LH patients showed larger flexion angles in the PIP joints of the Middle and Little fingers. Therefore, the results showed that RH and LH patients used compensatory strategies involving increased flexion at the PIP joints for decreased flexion in the MCP joints. The integration of a data glove during the performance of the ARAT allows the detection of finger joint impairments in stroke patients that are not visible from ARAT scores. Therefore, the results presented are of clinical relevance.

5.2. Introduction

Stroke remains the second-leading cause of death and the third-leading cause of death and disability combined globally. Projections show that the burden of stroke will not decrease in the next decade or beyond [1]. An important contributing factor is that the number of older persons in Europe is rising, with a projected increase of 35% between 2017 and 2050 [2]. Stroke is caused by the death of brain cells as a result of blockage of a blood vessel supplying the brain (ischemic stroke) or bleeding into or around the

brain (hemorrhagic stroke) [3]; the disability and the rehabilitation that is needed post-stroke depends on the size of the brain injury and the particular brain circuits that are damaged [4]. The most common sequelae caused by stroke is motor impairment, which impairs function in muscle movement or mobility [5]. One of the most affected parts are the upper extremities (UE) of the human body; movement problems in these parts limit the quality of life by limiting the ability to perform activities of daily living (ADL). The hand is one of the essential tools of the human body, allowing us to perform a wide variety of actions to interact with the environment, such as touching, reaching, holding, grasping, and manipulating different types of objects. People who suffer the loss of mobility in the hand endure a tremendous negative impact on their living standards, causing problems in their family, work, and social environment. Therefore, the rehabilitation process after a stroke is fundamental to prevent deterioration of function, reduce motor disability and reintegrate patients into their ADL [6]. Stroke rehabilitation is divided into three phases: acute phase (first month), subacute phase (one–six months), and chronic phase (after six months)[124]. In order to evaluate the patient's progress during the rehabilitation program, it is highly recommended the use of standardized outcome measures (OMs) with good psychometric properties. There is a wide range of upper extremity rehabilitation OMs (e.g., motor function, muscle strength, dexterity, global stroke severity, and others) [110]. Many physical therapists have assessed the upper limb function in post-stroke patients with The Action Research Arm Test (ARAT). The ARAT is a measurement tool to assess UE functional limitations. The test described by Lyle [112] evaluates 19 tests of arm motor function that assess a patient’s ability to handle objects differing in size, weight, and shape. Each test is given an ordinal score of 0, 1, 2, or 3, with higher values indicating better arm motor status[7]. The test has been shown good reliability and validity [7]–[9].

The ARAT, like other OMs, is evaluated by an examiner who determines the score of each test. The scoring process can lead to subjective results due to the difficulty of assessing abnormal patterns in patients after stroke. Therefore, with the technological advances, wearable sensors have been incorporated during the performance of various OMs in several clinical investigations. The use of sensors allows having more quantitative and sensitive assessment methods during clinical rehabilitation of the UE. Most research studies have used inertial measurement units (IMU) while performing the ARAT. Carpinella et al. proposed a method to discriminate between healthy subjects and Multiple Sclerosis patients wearing a single inertial sensor on the wrist [10]. Nam et al. obtained a database of the workspace and ROM of the major joints of the UE in healthy subjects using a wearable motion capture system based on an (IMU) [11]. Repnik et al. proposed a system of IMUs for kinematic quantification and electromyography (EMG) sensors for muscle activity analysis in stroke patients [59]. Held et al. measured arm kinematics in stroke patients during different stages of the rehabilitation process using Xsens full-body motion capture suit (Xsens Technologies, Enschede, Netherlands) [13]. In contrast, Dutta et al. Evaluated grasp abilities deploying intelligent algorithms with healthy subjects and post-stroke patients using an instrumented glove composed of six flex sensors, three force sensors, and a motion processing unit [60]. During the Wolf Motor Function

Test execution, Del Din et al. used six accelerometers placed on the arm and the trunk to estimate FMA scores [70]. Finally, Routhier et al. studied the correlation between finger-to-nose task (FNT) and Upper limb motor function in subacute stroke patients, using an IMU [71]. Although many of these studies evaluate the UE with sensory information during OMs, none of them focus on the assessment of hand function by studying the ROM of the finger joints. Nevertheless, there are several studies about the functional range of motion (FROM) of the finger joints during the performance of ADL in healthy subjects [98], [117], [118]. Despite this, only Bain et al., who used the Sollerman hand grip function test [119] and Hayashi et al., who used 19 activities of the Disabilities of the Arm, Shoulder, and Hand (DASH) [125], used rehabilitation OMs. To the best of our knowledge, no study has determined the FROM and the ROM of the finger joints in stroke patients during the performance of the ARAT using a data glove. This study aimed to determine whether differences in the FROM and the ROM of finger joints between healthy subjects and post-stroke patients allow the identification of joint motion impairments and compensatory strategies in stroke patients that are not detected with the ARAT. The data obtained are of clinical importance for occupational therapists, as they allow a more quantitative and objective evaluation method.

5.3. Methods

5.3.1. Subjects

Twelve patients (3 women and 9 men, mean age: 65.2 ± 9.3 years; right-handed) were evaluated six months after a stroke at Sant Joan de Deu Hospital. Ten patients suffered an ischemic stroke, and two patients a hemorrhagic stroke. Inclusion criteria for this study included the following: patients who had a stroke for the first time with motor deficits in the UEs; patients older than 18 years; patients who, before the stroke, were independent in their ADLs; patients with a global ARAT score ≥ 10. Exclusion criteria: patients with UE deficits and sequelae of any etiology before the stroke. Data from the control group used in this study was obtained in Chapter 5. The dataset includes information from 25 healthy subjects (14 women and 11 men, mean age: 40.2 ± 18.1 years). Inclusion criteria were being right-handed, over 18 years old, and not having suffered any hand disorders or injury. Healthy subjects performed sixteen activities of the ARAT corresponding to the subtests (Grasp, Grip, and Pinch) using an instrumented glove (Cyberglove Systems LLC; San Jose, CA, USA). All subjects signed informed consent to the protocol, which was conformed following the Declaration of Helsinki and was approved by the Ethics and Clinical Research Committee of the Fundacio Unió Catalana d'Hospitals ID 13/71. The stroke patients were divided into two groups to evaluate and detect impairments of the finger joints. Therefore, we formed one group of patients with hemiparesis on the right side and the other with hemiparesis on the left side. The information of the two stroke groups and the control group is shown in Table 5.1.

Table 5.1. Characteristics of the groups.

Variable	Groups		
	RH	**LH**	**C**
Age (Mean ± SD)	62 ± 10.3	69.6 ± 5.3	40.2 ± 18.1
Hemisphere Affected	L	R	-
Subjects (N)	7	5	25
S. Grasp (tests)	31	24	150
S. Grip tests (tests)	19	16	100
S. Pinch tests (tests)	30	24	150
Total (tests)	80	64	400
TSS	6	6	-
ARAT score (Mean ± SD)	39.2 ± 14.3	45.4 ± 13.7	-

RH= right hemiparesis; LH= left hemiparesis; C= control group; SD= standard deviation; L= left; R= right; N= Number of participants; tests= complete test (ARAT score ≥ 2); S= Subtest; TS= Time since stroke (months)

5.3.2. Experimental Protocol

In the present study, post-stroke patients performed sixteen tests of the ARAT. These tests correspond to the Grasp, Grip, and Pinch subtests. The ARAT is an evaluative measure used to assess the arm motor status after a stroke, consisting of 19 tests categorized into four subtests: Grasp, Grip, Pinch, and Gross movements. Within each subtest, the first test is the most difficult and the second the easiest to facilitate the application of the test [112]. The Gross movement subtest was excluded because it involves the assessment of large muscle movements and, in this study, we focused on measuring the finger joints. Stroke patients sat upright in a standard chair with a firm back and no armrests. The assessments were performed in the hospital by a trained therapist. Subjects were seated in front of a table; the table was set at a distance of 15 cm and at the abdomen level. The physical therapist ensured that the subjects back remained in contact with the back of the chair and that the legs were positioned in front of the chair with the feet in contact with the floor throughout the test. The subject was asked to grasp, lift vertically, place, and then release each object (block, cricket ball, or marble) onto the top of the shelf. The objects used in each activity were placed one at a time on the table. The ARAT performance score is rated on a 4-point scale, ranging from 0 (no movement) to 3 (movement performed normally). A full description of all ARAT tasks was presented in [7]. In this study, only the ARAT activities that the patient was able to complete, which obtained a score of 2 (complete task that takes a little longer) and 3 (complete task), were analyzed and compared with the control group.

5.3.3. Experimental Equipment

Subjects performed the sixteen activities of the ARAT wearing the CyberGlove II® data glove on the affected hand of subjects with hemiparesis and on the right hand (dominant) of healthy subjects (Figure 1). The data glove is composed of 18 flexion sensors: two bend sensors on each finger, four abduction sensors, and sensors measuring thumb crossover, palm arch, wrist flexion, and wrist abduction. The data glove has a resolution <1 degree and weighs only 70 g [83]. The procedure for converting the readings of the 18 sensors into finger joint angles was based on linear interpolation, according to a previously validated

calibration protocol [26], [84]. The eleven finger joints angles recorded in this study were: Thumb carpometacarpal (CMC) joint, Thumb, Index, Middle, Ring, and Little metacarpophalangeal (MCP) joints, Thumb interphalangeal (IP) joint, and Index, Middle, Ring, and Little proximal interphalangeal (PIP) joints. Data from the CyberGlove II® were transmitted to a PC via Bluetooth connection. The data was read and recorded in a .raw file using the CyberGlove graphical user interface (GUI). A script in the software R 4.1.0 was created in order to convert the raw data of the CyberGlove II® into the finger joints angles according to the equations obtained in the calibration process.

5.3.4. Data Analysis

The data obtained were filtered with a 2nd-order two-way low pass Butterworth filter with a cut-off frequency of 5 Hz in MATLAB® software (MathWorks, Inc., Natick, MA, USA). The following protocol was applied separately to the control group and the stroke groups. At the start of each test, the subject placed the hand tested pronated, immediately lateral to the testing object. Therefore, the initial instants of each record, in which the hand were static, were trimmed. The minimum and maximum values for each activity were calculated for each finger joint of each subject. The respective values were averaged across all subjects during each activity; these values became known as the extension and flexion angles (E/F). Then, the functional range of motion (FROM) was calculated as the 5th and 95th percentiles of the (E/F) angles of each finger joint in the sixteen activities, thus representing the maximum and minimum angles covering 90% of the activities at each specific finger joint. The FROM was used based on 90% of activities because considering 100% of activities may result in excessive values [119]. Alternatively, the range of motion (ROM) was defined as the average of the E/F angles of the finger joints during the sixteen activities of the ARAT. Similarly, the total arc of motion (aROM) was defined as the range of flexion and extension angles that compose the ROM. Finally, the range of motion for each finger joint in each subtest (sROM) was calculated. The sROM was defined as the average of the extension and flexion angles corresponding to the activities of the subtest considered.

Statistical analysis was conducted using IBM SPSS Statistics, Version 28.0. Armonk, NY, USA: IBM Corp. The respective extension and flexion angles (ROM) of each finger joint were compared between control and each stroke group using a non-parametric test, the Mann–Whitney U test. In each subtest (Grasp, Grip, and Pinch), the Mann–Whitney U test was used to compare whether there was a statistical difference in the sROM of the finger joints between the control group and each stroke group. Additionally, the flexion angles of the FROM in each finger joint were compared between the right hemiparesis, left hemiparesis, and control groups. For this purpose, a Welch's ANOVA and a Games–Howell post hoc test was used to detect significant differences. Lastly, the ROM and aROM of each finger joint were compared between the right hemiparesis and the left hemiparesis groups using the Mann–Whitney U test. A *p-value* of less than 0.05 was considered statistically significant for all statistical analyses.

5.4. Results

5.4.1. Functional Range of Motion of the Finger Joints

The functional range of motion (FROM) of the finger joints required to perform 90% of the activities for each group is shown in Figure 5.1. In this study we decided to analyze the mean flexion angles of the 14 tasks that integrate the FROM. Mean and standard deviation values of the mean flexion angles (FROM) of each finger joint in the control, right hemiparesis (RH), and left hemiparesis (LH) groups are shown in Table 5.2. A Welch's ANOVA revealed that there was a statistically significant difference in the flexion angle of the Thumb IP, Index MCP, Index PIP, Middle MCP, Middle PIP, Ring PIP, and Little PIP finger joints between the control, right hemiparesis (RH), and left hemiparesis (LH) groups. The results of the post hoc test (see Table 5.2) showed that the mean flexion angles of the Index MCP and Middle MCP in the control group were significantly larger than those in the RH group. In contrast, the mean flexion angles of the Thumb IP, Middle PIP, Ring PIP, Little MCP, and Little PIP in the RH group were significantly larger than those in the control group. The mean flexion angles of the Thumb IP, Middle PIP, and Little PIP in the LH group were significantly higher than those in the control group. However, the mean flexion angles in the Middle MCP joint in the control group were significantly larger than those in the RH group. Moreover, the mean flexion angles of the Thumb IP and Middle MCP in the LH group were significantly higher than those in the RH group. Lastly, the mean flexion angles of the PIP joints (Index, Middle, and Ring) in the RH group were significantly larger than those in the LH group.

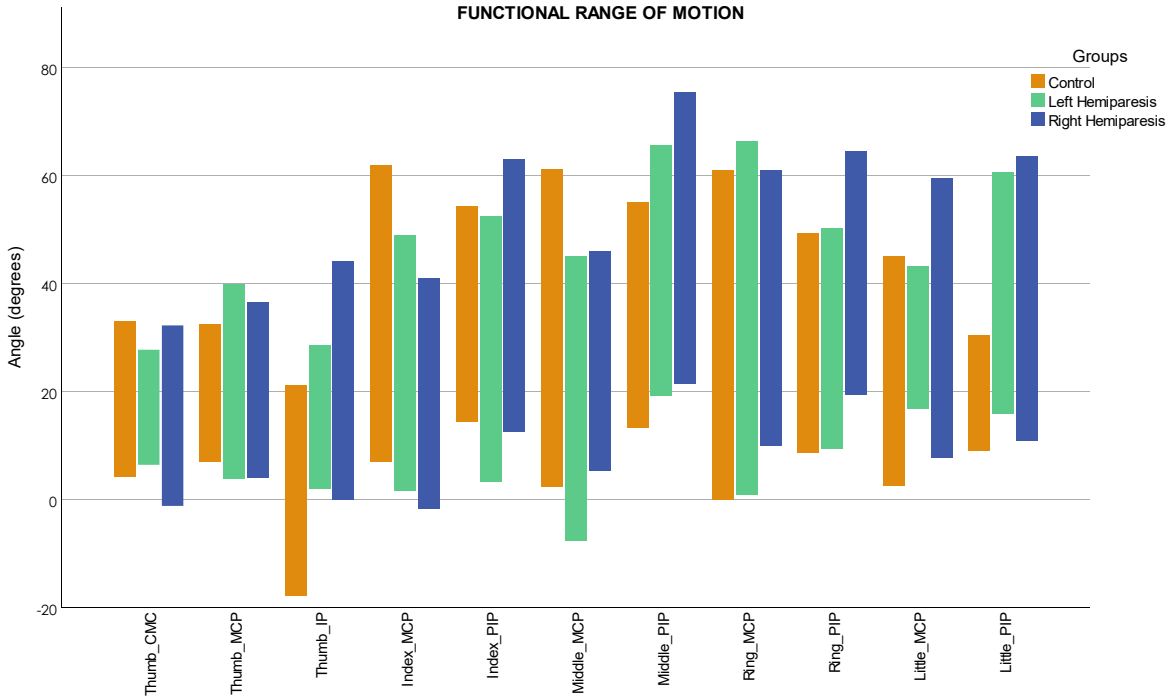

Figure 5.1. Functional range of motion in each finger joint; CMC = carpometacarpal; MCP = metacarpophalangeal; IP = interphalangeal; PIP = proximal interphalangeal; negative values represent hyperextension; maximum = flexion; minimum = extension.

Table 5.2. Flexion angles of the functional range of motion (FROM) during 14 tests.

Finger Joints	C		RH		LH		M(C-RH)		M(C-LH)		M(RH-LH)	
	F	SD	F	SD	F	SD	M	p	M	p	M	p
Thumb CMC	28.2	5.0	26.5	4.8	26.6	0.7	1.65	0.629	1.55	0.474	-0.10	0.996
Thumb MCP	26.4	3.3	29.1	4.2	29.9	5.0	-2.70	0.143	-3.48	0.084	-0.78	0.887
Thumb IP	12.6	4.1	26.8	5.1	21.7	4.1	-14.21	0.000***	-9.16	0.000***	5.04	0.016**
Index MCP	45.0	8.3	35.8	3.4	40.4	6.2	9.18	0.002**	4.53	0.224	-4.64	0.047*
Index PIP	37.8	8.7	43.7	11.3	30.6	11.4	-5.84	0.269	7.24	0.143	13.09	0.010*
Middle MCP	46.4	7.0	34.9	4.6	34.8	7.0	11.46	0.000***	11.54	0.000***	0.083	0.999
Middle PIP	41.6	6.8	59.6	9.9	51.3	8.1	-17.99	0.000***	-9.77	0.003**	8.22	0.048*
Ring MCP	42.8	9.3	49.6	7.3	48.8	10.7	-6.78	0.085	-5.99	0.246	0.79	0.970
Ring PIP	38.2	6.5	54.2	7.3	39.2	6.9	-16.00	0.000***	-1.02	0.909	14.97	0.000***
Little MCP	30.1	6.6	38.9	9.9	33.4	5.1	-8.80	0.023*	-3.34	0.284	5.45	0.166
Little PIP	21.3	4.2	47.2	11.5	48.1	8.8	-25.87	0.000***	-26.73	0.000***	-0.86	0.971

Games–Howell post-hoc comparison; C = control group; RH = right hemiparesis; LH = left hemiparesis; F = flexion; SD = standard deviation; CMC = carpometacarpal; MCP = metacarpophalangeal; IP = interphalangeal; PIP = proximal interphalangeal; * $p < 0.05$; ** $p < 0.01$; *** $p < 0.001$; M = mean differences between groups; p = significance level.

5.4.2. Range of Motion of the Finger Joints in the Stroke Group with Right Hemiparesis

Mean and standard deviation values of the range of motion (ROM) and the total arc of motion (aROM) of each finger joint in the control and the stroke group with right hemiparesis (RH) are shown in Table 5.3. As reported in Table 5.4, the extension angles of the Thumb CMC, Index MCP, Middle MCP joints in the control group were significantly lower than those in the RH group. In contrast, the RH group showed significantly lower extension angles in the Thumb IP, Middle PIP, Ring MCP, Ring PIP, Little MCP, and Little PIP joints. The flexion angles of the Index MCP and Middle MCP joints in the control group were significantly higher than those in the RH group, while flexion angles of the Thumb MCP, Thumb IP, Index PIP, Middle PIP, Ring MCP, Ring PIP, Little MCP, and Little PIP joints in the RH group were significantly higher (see Table 5.4).

On the other hand, the aROM in the control group was significantly larger than that in the RH group in the Middle MCP joint. By comparison, the aROM of the Thumb MCP, Index PIP, Middle PIP, Ring PIP, and Little PIP joints in the RH group was significantly larger (see Table A1.1).

Table 5.3. Range of motion (ROM) during the sixteen activities (control and right hemiparesis).

	Extension (Degree)				Flexion (Degree)				aROM (Degree)			
	C		RH		C		RH		C		RH	
Finger Joints	Mean	SD	Mean	SD	Mean	SD	Mean	SD	Mean	SD	Mean	SD
Thumb CMC	9.7	7.5	5.6	7.5	28.6	7.4	26.8	10.0	18.9	6.4	21.2	9.6
Thumb MCP	12.6	9.3	11.3	10.5	26.8	8.9	29.7	11.4	14.3	7.3	18.4	10.6
Thumb IP	−7.5	16.2	6.4	16.4	13.2	14.9	28.3	16.9	20.7	13.7	21.9	15.6
Index MCP	22.2	13.1	11.2	15.3	46.2	13.5	36.5	12.4	24.0	12.1	25.4	13.3
Index PIP	16.4	9.2	15.8	10.3	38.9	14.0	44.2	16.5	22.4	11.1	28.4	16.8
Middle MCP	17.8	11.9	14.0	12.8	47.5	11.5	36.0	12.6	29.7	10.9	22.0	10.2
Middle PIP	16.3	8.5	27.3	14.5	42.6	11.4	60.0	15.4	26.3	9.3	32.7	15.5
Ring MCP	15.6	11.8	20.6	14.7	44.1	13.6	49.8	13.0	28.5	11.4	29.3	15.7
Ring PIP	12.3	8.1	23.9	13.6	39.2	11.8	54.3	14.1	26.9	9.8	30.5	12.2

Table 5.3. Cont.

	Extension (Degree)				Flexion (Degree)				aROM (Degree)			
	C		RH		C		RH		C		RH	
Finger Joints	**Mean**	**SD**	**Mean**	**SD**	**Mean**	**SD**	**Mean**	**SD**	**Mean**	**SD**	**Mean**	**SD**
Little MCP	9.1	8.8	13.2	8.0	31.5	12.1	39.3	15.1	22.4	8.9	26.2	14.9
Little PIP	11.3	9.5	15.4	11.0	22.1	13.4	47.5	21.6	10.8	8.3	32.1	19.6

C = control group; RH = right hemiparesis group; CMC = carpometacarpal; MCP = metacarpophalangeal; IP = interphalangeal; PIP = proximal interphalangeal; SD = standard deviation; deg = degrees; aROM = arc of motion; negative values represent hyperextension.

Table 5.4. Results of Mann–Whitney test of the ROM with respect to the control and right hemiparesis groups.

			Extension				Flexion			
Finger Joint	**Group**	**N**	**Mean Rank**	**U**	**Z**	***p***	**Mean Rank**	**U**	**Z**	***p***
Thumb CMC	C	400	252.9	11,023.0	−4.39	0.000 ***	245.6	13,959.5	−1.80	0.072
	RH	80	178.3				215.0			
Thumb MCP	C	400	243.1	14,949.0	−0.93	0.353	234.2	13,489.0	−2.22	0.027 *
	RH	80	227.4				271.9			
Thumb IP	C	400	222.4	8764.5	−6.39	0.000 ***	219.1	7435.0	−7.56	0.000 ***
	RH	80	330.9				347.6			
Index MCP	C	400	257.7	9136.0	−6.06	0.000 ***	256.6	9555.5	−5.69	0.000 ***
	RH	80	154.7				159.9			
Index PIP	C	400	242.9	15,058.0	−0.83	0.406	232.7	12,877.5	−2.76	0.006 **
	RH	80	228.7				279.5			
Middle MCP	C	400	248.6	12,758.0	−2.86	0.004 **	259.7	8302.5	−6.80	0.000 ***
	RH	80	200.0				144.3			
Middle PIP	C	400	223.0	9002.0	−6.18	0.000 ***	215.7	6092.5	−8.75	0.000 ***
	RH	80	328.0				364.3			
Ring MCP	C	400	231.6	12,459.0	−3.13	0.002 **	229.8	11,706.0	−3.79	0.000 ***
	RH	80	284.8				294.2			
Ring PIP	C	400	220.7	8085.0	−6.99	0.000 ***	217.0	6593.5	−8.31	0.000 ***
	RH	80	339.4				358.1			
Little MCP	C	400	230.4	11,941.0	−3.58	0.000 ***	228.0	11,012.0	−4.40	0.000 ***
	RH	80	291.2				302.9			
Little PIP	C	400	231.4	12,372.0	−3.20	0.001 **	213.5	5192.0	−9.54	0.000 ***
	RH	80	285.9				375.6			

C = control group; RH = right hemiparesis group; * $p < 0.05$; ** $p < 0.01$; *** $p < 0.001$; control vs. stroke Mann–Whitney U test.; N = number of tests per group.

5.4.3. Range of Motion of the Finger Joints in the Stroke Group with Left Hemiparesis

The range of motion (ROM) and the total arc of motion (aROM) of each finger joint in the control and the stroke group with left hemiparesis (LH) are shown in Table 5.5. As shown in Table 5.6, the extension angles of the Thumb CMC, Index MCP and PIP, Middle MCP joints in the control group were significantly lower than those in the LH group. In contrast, the LH group showed significantly lower extension angles in the Thumb IP, Middle PIP, Little MCP, and Little PIP joints. The flexion angles of the Index (MCP, PIP) and Middle MCP joints in the control group were significantly larger than those in the LH group, while flexion angles in the LH group were significantly larger in the Thumb MCP, Thumb IP, Middle PIP, Ring MCP, Little MCP, and Little PIP joints (see Table 5.6). The aROM of the Thumb IP and Little MCP joints

in the control group was significantly larger than that in the LH group. In addition, aROM in the LH group was significantly larger in the Thumb MCP and Little PIP joints (see Table A1.2).

Table 5.5. Range of motion (ROM) during the sixteen activities (control and left hemiparesis).

Finger Joints	Extension (Deg)				Flexion (Deg)				aROM (Deg)			
	C		LH		C		LH		C		LH	
	Mean	SD	Mean	SD	Mean	SD	Mean	SD	Mean	SD	Mean	SD
Thumb CMC	9.7	7.5	8.1	1.8	28.6	7.4	26.7	1.5	18.9	6.4	18.6	1.6
Thumb MCP	12.6	9.3	11.1	6.5	26.8	8.9	30.4	10.0	14.3	7.3	19.2	10.9
Thumb IP	−7.5	16.2	7.2	8.7	13.2	14.9	22.7	8.5	20.7	13.7	15.5	9.4
Index MCP	22.2	13.1	14.0	18.9	46.2	13.5	41.8	13.0	24.0	12.1	27.9	21.9
Index PIP	16.4	9.2	8.4	11.9	38.9	14.0	32.5	19.3	22.4	11.1	24.1	15.2
Middle MCP	17.8	11.9	7.1	13.1	47.5	11.5	36.4	15.5	29.7	10.9	29.3	18.6
Middle PIP	16.3	8.5	25.8	11.4	42.6	11.4	52.2	13.1	26.3	9.3	26.3	11.8
Ring MCP	15.6	11.8	17.4	13.4	44.1	13.6	50.9	17.3	28.5	11.4	33.5	16.7
Ring PIP	12.3	8.1	15.8	10.0	39.2	11.8	40.1	13.2	26.9	9.8	24.4	11.8
Little MCP	9.1	8.8	21.1	4.6	31.5	12.1	34.5	7.3	22.4	8.9	13.4	7.3
Little PIP	11.3	9.5	21.7	10.4	22.1	13.4	49.6	16.9	10.8	8.3	27.8	15.9

C = control group; LH = left hemiparesis group; CMC = carpometacarpal; MCP = metacarpophalangeal; IP = interphalangeal; PIP = proximal interphalangeal; SD = standard deviation; deg = degrees; aROM = arc of motion; negative values represent hyperextension.

Table 5.6. Results of Mann–Whitney test of the ROM with respect to the control and left hemiparesis groups.

			Extension				Flexion			
Finger Joint	Group	N	Mean Rank	U	Z	*p*	Mean Rank	U	Z	*p*
Thumb CMC	C	400	239.04	10,184	−2.63	0.009 **	241.31	9276.5	−3.54	0.000 ***
	LH	64	191.63				177.45			
Thumb MCP	C	400	236.86	11,055	−1.75	0.080	225.95	10,181	−2.63	0.009 **
	LH	64	205.23				273.42			
Thumb IP	C	400	214.15	5459	−7.37	0.000 ***	216.74	6494.5	−6.33	0.000 ***
	LH	64	347.20				331.02			
Index MCP	C	400	239.85	9862	−2.95	0.003 **	237.69	10,724	−2.08	0.037 *
	LH	64	186.59				200.06			
Index PIP	C	400	246.80	7081	−5.74	0.000 ***	240.10	9761	−3.05	0.002 **
	LH	64	143.14				185.02			
Middle MCP	C	400	248.15	6540	−6.29	0.000 ***	244.94	7825	−5.00	0.000 ***
	LH	64	134.69				154.77			
Middle PIP	C	400	216.99	6595	−6.23	0.000 ***	219.62	7649	−5.17	0.000 ***
	LH	64	329.45				312.98			
Ring MCP	C	400	229.43	11,573	−1.23	0.218	224.78	9712.5	−3.10	0.002 **
	LH	64	251.67				280.74			
Ring PIP	C	400	227.95	10,981	−1.83	0.068	230.32	11,926	−0.88	0.380
	LH	64	260.92				246.16			
Little MCP	C	400	207.59	2836	−10.00	0.000 ***	224.78	9712	−3.10	0.002 **
	LH	64	388.19				280.75			
Little PIP	C	400	216.00	6198	−6.63	0.000 ***	207.51	2805	−10.04	0.000 ***
	LH	64	335.66				388.67			

C = control group; LH = left hemiparesis group; * $p < 0.05$; ** $p < 0.01$; *** $p < 0.001$; control vs. LH Mann–Whitney U test.; N = number of tests per group.

5.4.4. Comparison of the Range of Motion between the Stroke Groups

The results of the comparison between the stroke groups are shown in Table 5.7. The results showed than the extension angles of the Thumb CMC and Little (MCP, PIP) joints in the left hemiparesis (LH) group were significantly lower than those in the right hemiparesis (RH) group. In contrast, the extension angles of the Index PIP and Middle MCP joints in the RH group were significantly lower. The flexion angles of the PIP joints of the Index, Middle and Ring fingers in the RH group were significantly larger than those in the LH group, while, in the LH group, the flexion angle of the Index MCP joint was significantly larger. Lastly, the aROM of the Thumb IP, Middle PIP, Ring PIP and Little MCP in the LH group was significantly larger (see Table A1.3).

Table 5.7. Results of Mann–Whitney test of the ROM with respect to the stroke groups (left hemiparesis vs. right hemiparesis).

			Extension				Flexion			
Finger Joint	**Group**	**N**	**Mean Rank**	**U**	**Z**	***p***	**Mean Rank**	**U**	**Z**	***p***
Thumb CMC	LH	64	82.45	1923.5	−2.56	0.010 **	72.65	2550.5	−0.04	0.970
	RH	80	64.54				72.38			
Thumb MCP	LH	64	70.77	2449.5	−0.44	0.657	73.89	2471	−0.36	0.720
	RH	80	73.88				71.39			
Thumb IP	LH	64	74.30	2445	−0.46	0.644	66.08	2149	−1.65	0.098
	RH	80	71.06				77.64			
Index MCP	LH	64	76.67	2293	−1.08	0.282	82.09	1946	−2.47	0.013 **
	RH	80	69.16				64.83			
Index PIP	LH	64	55.27	1457	−4.44	0.000 ***	57.24	1583.5	−3.93	0.000 ***
	RH	80	86.29				84.71			
Middle MCP	LH	64	60.95	1820.5	−2.97	0.003 **	73.53	2494	−0.27	0.791
	RH	80	81.74				71.68			
Middle PIP	LH	64	70.84	2454	−0.43	0.670	59.94	1756	−3.23	0.001 **
	RH	80	73.83				82.55			
Ring MCP	LH	64	66.91	2202.5	−1.44	0.151	73.13	2519.5	−0.16	0.871
	RH	80	76.97				71.99			
Ring PIP	LH	64	57.68	1611.5	−3.81	0.000	51.55	1219.5	−5.39	0.000 ***
	RH	80	84.36				89.26			
Little MCP	LH	64	96.03	1054	−6.06	0.000 ***	66.45	2173	−1.56	0.120
	RH	80	53.68				77.34			
Little PIP	LH	64	85.30	1741	−3.29	0.001 **	76.23	2321	−0.96	0.337
	RH	80	62.26				69.51			

RH = right hemiparesis group; LH = left hemiparesis group; * $p < 0.05$; ** $p < 0.01$; ***; $p < 0.001$; control vs. stroke Mann–Whitney U test.; N = number of tests per group.

5.5 Discussion

To the best of our knowledge, there are no previous studies that measured and evaluated the finger joint motions during a standardized outcome measure such as the ARAT test. In this study, we determined the functional range of motion (FROM) and the range of motion (ROM) of the finger joints of the right hand, with the exception of distal interphalangeal (DIP) joints, using a data glove (CyberGlove II®) while

performing the Grasp, Grip, and Pinch subtests of the ARAT. The study was conducted in healthy subjects and post-stroke subjects with a global ARAT score ≥ 10. In this study, both the FROM and ROM were analyzed. The FROM is the amplitude of motion necessary for each finger joint to perform 90% of the activities of the ARAT (14 activities). The FROM has been used in several studies to determine the minimum range of motion needed to comfortably and effectively perform activities of daily living [117], [118], [125], [126]. A table with the functional range of motion (FROM) for each finger joint is included in the Supplementary Material (Table A1.4). Determining the FROM allowed us to detect if there is a decrease in the arc of motion in some of the finger joints, and thus to establish rehabilitation therapy goals. To the best of our knowledge, there are no previous studies regarding the FROM in stroke patients. However, the FROM is highly dependent on the activities performed and is normally used with activities of daily living (ADLs) [118],[98][98],[125]. Therefore, we also decided to determine the ROM for a more in-depth evaluation since the ROM analyses relate to flexion and extension angles during the sixteen tests of the ARAT. The results of the flexion angles in the FROM (see Table 5.2) showed that the control group performed significantly greater flexion with the Index MCP and Middle MCP joints than the stroke groups, whereas no significant differences were found in the flexion angles at the Ring MCP joint. In contrast, the right hemiparesis (RH) group performed larger flexion angles in PIP joints of the Index, Middle, Ring, and Little fingers, whereas the left hemiparesis (LH) group performed larger flexion angles in the PIP joints of the Middle finger. The results in the RH stroke group suggest that they use a compensatory grasping strategy for the deficit of flexion in the Index MCP and Middle MCP joints. By comparison, the LH stroke group used a similar strategy for the deficit of flexion in the Middle MCP joint. In the ARAT, most of the activities are radial activities that include precision grip and pinch (Grip and Pinch subtests); as a result, the Index and Middle joints are essential in most of the tests.

In addition, the results of the ROM in the RH and LH stroke groups showed significantly larger extension angles (closer to 0 deg) in the Index MCP and Middle MCP joints than those in the control group. Finger joint extension problems may occur because, after stroke, the ability to extend the fingers during grip is highly variable due to issues with the active extensor muscles of the fingers and the coordination of muscle activity between the flexor and extensor muscles of the fingers [127]. In Carpinella et al., patients with hemiplegic stroke showed significantly lower extension and flexion angles than healthy subjects in all the finger joints (MCP, IP) during hand open and closing movements [94]. By comparison, in our study, the LH and RH stroke groups showed significantly lower flexion angles in the Index MCP and Middle MCP joints than healthy subjects. However, the RH stroke group showed significantly larger flexion in the Index, Middle, Ring, and Little PIP joints. Moreover, the LH stroke group showed significantly larger flexion in the Middle and Little PIP joints than in the control group. The difference with Carpinella et al. is that their study only evaluated hand movement (open and close). In contrast, our study assessed ROM of the finger joints during the performance of sixteen activities with different objects (shape and size). A previous study found a relationship between the size of the object and the fingers used when grasping an object [122].

According to Peña-Pitarch et al., in the Grasp subtest, healthy subjects used five, four, or three fingers. In contrast, the subjects used a three-jaw chuck pinch, involving the pads of the thumb as opposed to the pads of the Index and Middle fingers in the Grip subtest. Activities in the Grasp subset involve power grasping. Power grasping is usually used when the object needs to be held firmly and involves the ulnar side of the hand. In contrast, in the Grip subtest, most activities include precision grasping, which is used to perform fine-grained actions that require accuracy [80]. In addition, the Grasp activities involve global activities where the radial and ulnar sides of the hand are employed. In our study, the RH patients showed significantly larger flexion angles in the Ring MCP, Little MCP, and the PIP joints than the control group in the Grasp and Grip subset (see Tables S5 and S6), but significantly lower flexion in the Index and Middle MCP joints. Nevertheless, RH patients in the Grip subset, which involves radial activities (precision grip and pinch), used greater flexion in the ulnar side of the hand. Furthermore, RH patients showed increased PIP joint flexion angles, indicating a compensatory strategy involving increased Index PIP and Middle PIP flexion as compensation for reduced flexion angles in the Index MCP and middle MCP joints. Furthermore, the LH patients showed significantly lower flexion angles in the Middle MCP in the Grasp and Grip subtest but significantly larger flexion angles in the Middle PIP in the grip subtests (see Tables A1.5 and A1.6). Therefore, the LH patients showed a PIP compensation strategy similar to the RH patients in the Middle joints. In addition, LH patients showed reduced flexion angles in the Index MCP and Index PIP joints. On the other hand, several studies [113] showed that, in a precision pinch, the Index finger worked actively and the Thumb worked passively, i.e., the Index joints performed a more significant flexion movement than the Thumb joints. Similar results were observed in the control group during the Pinch subset in our study. At the same time, RH patients showed impairment at the MCP joints of the Index and Middle fingers, compensating with increased flexion of the Thumb MCP and IP joints, and the PIP joints of the Index, Middle, and Ring fingers (see Table A1.7). Furthermore, the LH group in the Pinch subtest showed reduced flexion angles in the Index MCP, Index PIP, and Middle MCP, compensating with increased flexion of the Thumb CMC, Thumb MCP, Middle PIP, and Ring PIP joints. Therefore, during the Pinch subtest, the LH and RH stroke patients also used the PIP strategy to compensate for the flexion deficit in the MCP joints. In addition, we found the same compensation strategy during the FROM analysis (see Figure 5.1), showing that this metric performed reliably with the ARAT tasks.

On the other hand, Raghavan et al. found that stroke patients with right hemiparesis used a compensatory strategy that involved increased MCP flexion rather than the PIP flexion seen in controls [128]. The stroke patients showed reduced flexion angles at the PIP joints and extension angles at the MCP joints when grasping three objects of different shapes (rectangular, concave, and convex) wearing an instrumented glove. The difference with our study is that Raghavan et al. found the compensatory strategy in stroke patients with significant impairments, as were noted in their scores on the Fugl–Meyer Scale (FMS). In contrast, our study found the compensatory strategy in LH and RH stroke patients with moderate and good recovery, who obtained an ARAT global score greater than ten before the study. Furthermore, in

Raghavan et al., stroke patients were evaluated during the grasping of only three objects, and in our study, stroke patients were assessed using 12 different objects. In addition, we found the compensatory strategy in the assessment of patients with left and right hemiparesis.

Finally, we evaluated patients with right and left hemiparesis separately in this study. Although patients with right-sided hemiparesis had the dominant hand affected, the results showed similar behavior in both groups. However, the results showed that, in the LH group, the flexion angle of the Index MCP joint was significantly higher than that in the RH group. In contrast, the index PIP joint flexion angle was larger in the RH group. Therefore, we determined that the LH group presented the compensatory strategy (PIP) in the Middle finger, whereas the RH group presented the PIP strategy in the Index and Middle fingers. Movement deficits in finger joints in patients with right hemiparesis found in our study suggested that patients with RH suffered a more severe stroke. Moreover, Hedna et al. found that left hemispheric ischemic strokes appear to be more frequent and have a worse outcome [129]. In our study, seven patients presented stroke in the left hemisphere and five in the right hemisphere. In addition, patients having suffered a stroke in the right hemisphere showed a higher ARAT score, consistent with that presented by Hedna et al. However, given the small and selected sample in this study, we are unable to generalize these compensatory strategies to post-stroke patients overall.

Importantly, the results presented in this study showed that the integration of the CyberGlove II® during the performance of the ARAT allows for a more quantitative and sensitive assessment of post-stroke patients. In addition, analyzing and measuring the FROM and ROM of the finger joints revealed the compensatory strategies used for impairments in the finger joints of stroke patients.

5.6. Limitations

This research, however, is subject to several limitations. Firstly, the subjects in this study had a moderate and good recovery; futures studies should evaluate subjects with more severe impairments for more complete results. Secondly, it was impossible to obtain consent from the hospital's ethics committee to have access to more stroke patients due to the restrictions of COVID-19 and the risk of SARS-CoV-2 infection among patients with a history of stroke. Thirdly, the method proposed in this study to evaluate the finger joints is not compatible with the Gross movement subtest of the ARAT because this test evaluates the movement of the arm. Finally, abduction and adduction angles of the finger joints were not obtained and not assessed in this study.

5.7. Conclusions

The results presented in this study demonstrated that the integration of a data glove (CyberGlove II®) during the performance of a validated clinical test such as the ARAT can be used to determine the range of motion (ROM) and the functional range of motion (FROM) of the finger joints. Therefore, the assessment of the FROM and ROM allowed us to detected finger joint impairments and compensatory grasp strategies

in stroke patients that were not detected using clinical scores. The present study is of clinical relevance and allows for a more accurate and sensitive evaluation of a validated test, which would help occupational therapists and other health professionals to create rehabilitation programs focused on the recovery of hand function in stroke patients. However, future studies should consider a sample of more stroke subjects and incorporate an inertial sensor system to assess hand motion.

CHAPTER 6
Classification Models in Post-stroke patients based in Human Hand Motion

6.1. Overview

In this chapter, we present the development of Machine Learning models for the classification of Action Research Arm Test (ARAT) activities between Healthy and post-stroke subjects with similar scores. For this purpose, we used three classification algorithms: Support Vector Machine (SVM), Random Forest (RF), and K-N Neighbors (KNN). The performance of each of the classification models was evaluated with the metrics: Precision, Accuracy, Recall, F1-score, and AU-ROC. In addition, due to data class imbalance, the three models were balanced using the Borderline-SMOTE oversampling algorithm, and their performance were compared with the 5x2cv combined F-test. Finally, the performance of the classification models before and after class balancing was compared using the paired t-test to select the best one.

6.2. Introduction

In the previous chapters, we measured the extension and flexion angles of eleven finger joints in healthy subjects (Chapter 4) and stroke patients (Chapter 5) during the performance of the Action Research Arm Test (ARAT) using the CyberGlove II®. The information obtained allowed us to construct a dataset composed of the flexion and extension angles of 25 healthy individuals during the performance of 400 ARAT activities and 12 post-stroke patients during the execution of 144 ARAT activities completed with an ARAT score of 2 or 3. Therefore, based on this dataset, this chapter presents the development of Machine learning models for classifying ARAT activities with similar scores. In particular, the chapter had two main objectives: I) Develop classification models to predict whether the ARAT activities were performed by a healthy subject or by a subject post-stroke with good upper extremity functionality, based on the hand motion information obtained with the CyberGlove II®. Therefore, a high performance of the classification model will demonstrate that there are differences between the activities of healthy and post-stroke subjects that are not detected by the ARAT scoring method. On the other hand, this chapter have a second objective: II) Evaluate if data class balancing using the Borderline-SMOTE method allows obtaining better performance-classifiers.

6.2. Basic Concepts

6.2.1. Machine Learning

Machine learning (ML) is considered a subfield of computer science where knowledge from artificial intelligence and statistics is applied to the generation of computational models. Contrary to algorithms in traditional programming, ML algorithms can learn automatically and generate a model from input data without being explicitly programmed to produce a particular output [130]. The automatic learning process is performed through training and the data for training is known as training data [131]. Therefore, to generate an accurate model, a large quantity and quality of training data are necessary [131]. Besides, the independent variables or attributes that are introduced into an algorithm are called "features." Actually, the algorithm learns from these features to make a prediction. Therefore, selecting quality features that are relevant, independent, and informative is critical to making an accurate prediction. The model features can be continuous, categorical, or binary [132]. On the other hand, the ML subfield tries to emulate the functioning of the human brain in tasks such as data processing, image recognition, and pattern identification [133]. In recent years it has been used in various clinical applications, for example, in medical diagnosis, disease classification, prediction of clinical outcomes, and treatment response [134]. ML can be classified into three main categories: supervised learning, unsupervised learning, and reinforcement learning.

6.2.2. Classification Models

The classification algorithms belong to supervised learning. In supervised learning, the algorithm learns through a labeled data set (for example, a set of images labeled as containing a dragon or a dinosaur), where each training data sample is presented in the form of an input value with an output label [135]. The algorithm trains a model that, from the input values, can predict the correct response based on the features defined in the process [131]. When the outputs of the prediction model are discrete variables, the model is called a classifier. The classification problems are commonly categorized into binary classification and multi-class classification. In binary classification, the dataset are classified into two classes, while in multi-class classification, the given dataset is classified into more than two classes [136].

The types of classification algorithms according to [137] are as follows:

- Logical Regression
- Naïve Bayes Classifier
- Perceptron
- Support Vector Machine
- K-means Clustering

- Boosting
- Decision Tree
- Random Forest
- Neuronal Networks
- Bayesian Networks

In this thesis, we performed a ML models to classify ARAT activities of healthy and post-stroke subjects. For this purpose, we selected three of the most widely used and best-performing classification algorithms, which are Support Vector Machine (SVM), Random Forest (RF), and K-N Neighbors (KNN). The theoretical background of the classification models used in this thesis is presented below.

6.2.3. Support vector machine (SVM)

Support vector machines (SVM) were developed by Vladimir Vapnik and colleagues [138], SVM are a set of supervised learning algorithms. SVM is one of the most powerful and widely used methods in machine learning. Despite its simplicity, it has proven to be a robust algorithm and can be applied to problems in many areas. These methods are mainly used for classification problems but can also be applied in regression and outlier detection. Among the main advantages of SVM are the following: effective in high dimensional spaces, the optimization problem is convex and provides a unique solution, the model is robust to over-fitting, it is effective even when the number of dimensions is greater than the number of samples, the use of the kernel provides flexibility, and the use of support vectors allows it to provide memory efficiency [139]. The SVM technique's basic idea is to find an optimal hyperplane in a high dimensionality space that separates the data perfectly into two classes. A good separation between the classes allows a correct classification of the test sample, i.e., it is necessary to find the maximal margin of separation to the points closest to this hyperplane [140]. Hence, the vectors (points) that define the hyperplane are the support vectors. Nevertheless, the classes can be linearly separable or not separable (see Figure 6.1).

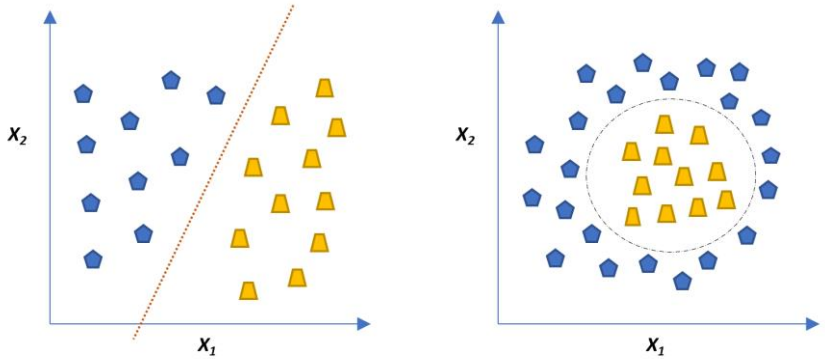

Fig 6.1. Illustration of data with Linear Separation (left); Illustration of data with Non-linear Separation (right).

However, when the data are linearly separable, several separation lines may exist, which would give rise to different separation hyperplanes (see Figure 6.2). Therefore, selecting an incorrect hyperplane may result in classification problems with real data (overfitting), so the algorithm may not generalize well (see Figure 6.2). In contrast, the optimal hyperplane is the one where the maximum margin is found, i.e. where the separation between classes is as wide as possible (see Figure 6.3).

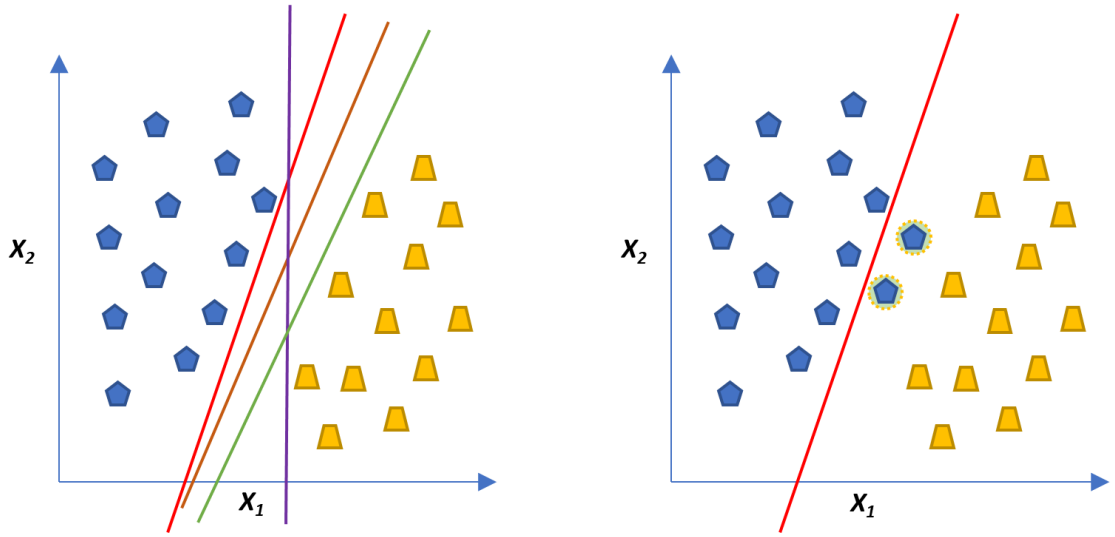

Fig 6.2. Example of different separation hyperplanes (left); Example of over-fitting problem with training and classification data (highlighted in yellow) (right).

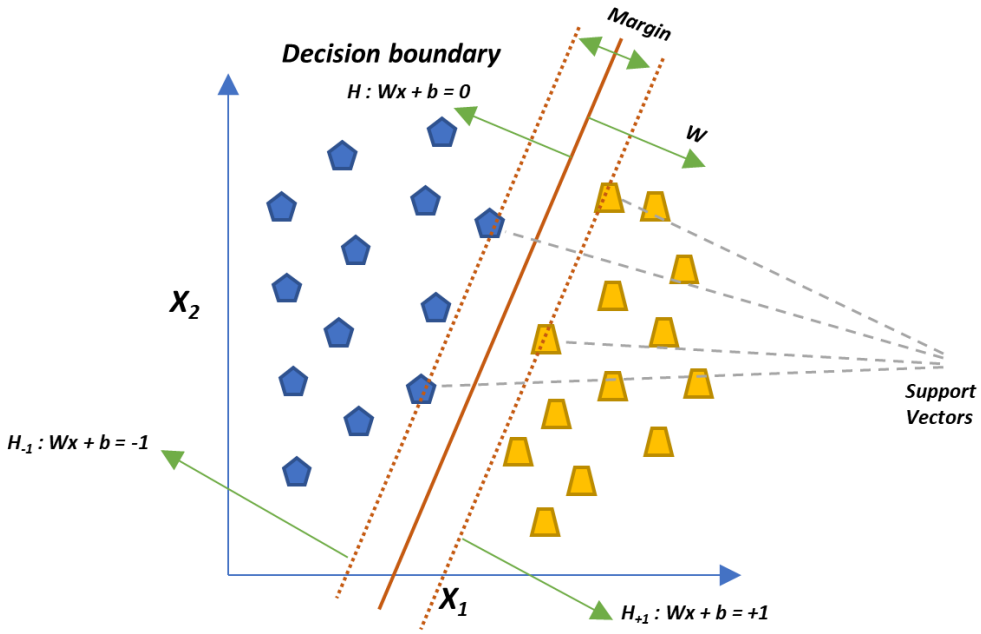

Fig 6.3. Example of Optimal Separating Hyperplane and its associated maximum margin; Hyperplane and decision boundary are equivalent at small dimension space.

However, most of the time, the data are not linearly separable. Hence, the Soft margin and Kernel Trick methods are used to find the separating hyperplanes. The soft margin o also called support vector classifier, is a method used in cases where the data are linearly quasi-separable, relaxing the degree of class separability. This technique creates a soft margin that tolerates the classification errors of some samples at the cost of suffering a penalty. The soft margin handles a fitting parameter called C that controls the trade-off between training errors or overfitting and rigid margins.

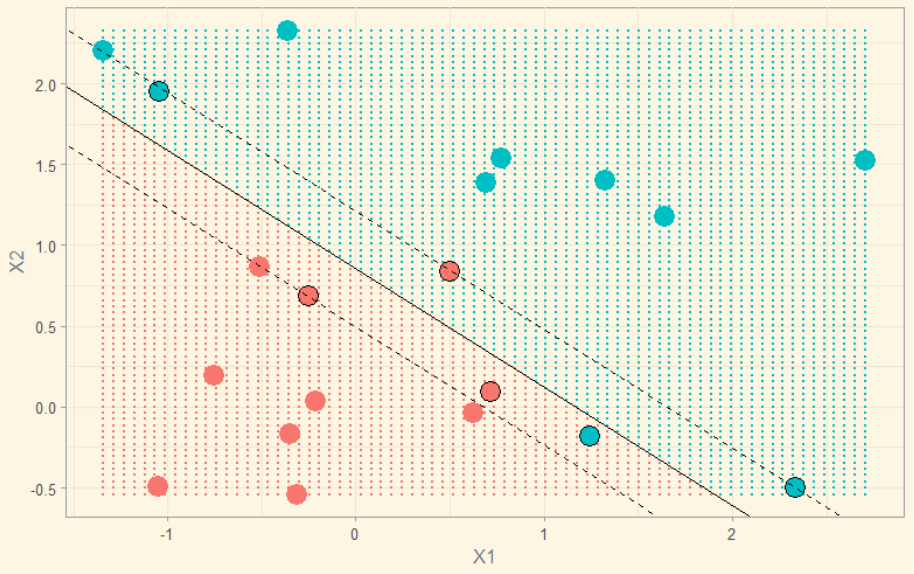

Fig 6.4. Example of Soft-Margin in SVM.

On the other hand, the Kernel method is suitable for problems with data that are not linearly separable. This technique consists of transforming low-dimensional training sets to a higher-dimensional space, so that the data become linearly separable. Therefore, it allows to obtain a more accurate classifier [141]. Among the most commonly used kernels for use with SVMs are:

Lineal

The linear kernel is one of the most commonly used when data is linearly separable. This kernel is primarily used when there are a large number of features in a data set.

$$k(x_i x_j) = (x_i^{\mathrm{T}} x_j)$$

Polynomial (parameters p y c)

The Polynomial kernel represents the similarity training samples in a feature space over polynomials of the original variables.

$$k(x_i x_j) = (x_i^{\mathrm{T}} x_j + c)^p$$

Radial basis function kernel (RBF) (tunable parameter σ2)

Radial Basis Function (RBF) Kernel is one of the most widely used kernels due to its similarity to the Gaussian distribution. This kernel is a Radial Basis Function, with the support vectors as centers. Therefore, SVM is used to find the number (and location) of centers needed to form the RBF network with the highest expected generalization performance [142]. Figure 6.5 illustrates an example of the Radial Basis Function (RBF) kernel SVM.

$$k(x_i x_j) = \left(-\frac{||x_i - x_j||^2}{2\sigma^2}\right)$$

where,

1. σ is the variance and our hyperparameter

2. $||x_i - x_j||$ is the Euclidean distance between two points X_1 and X_2

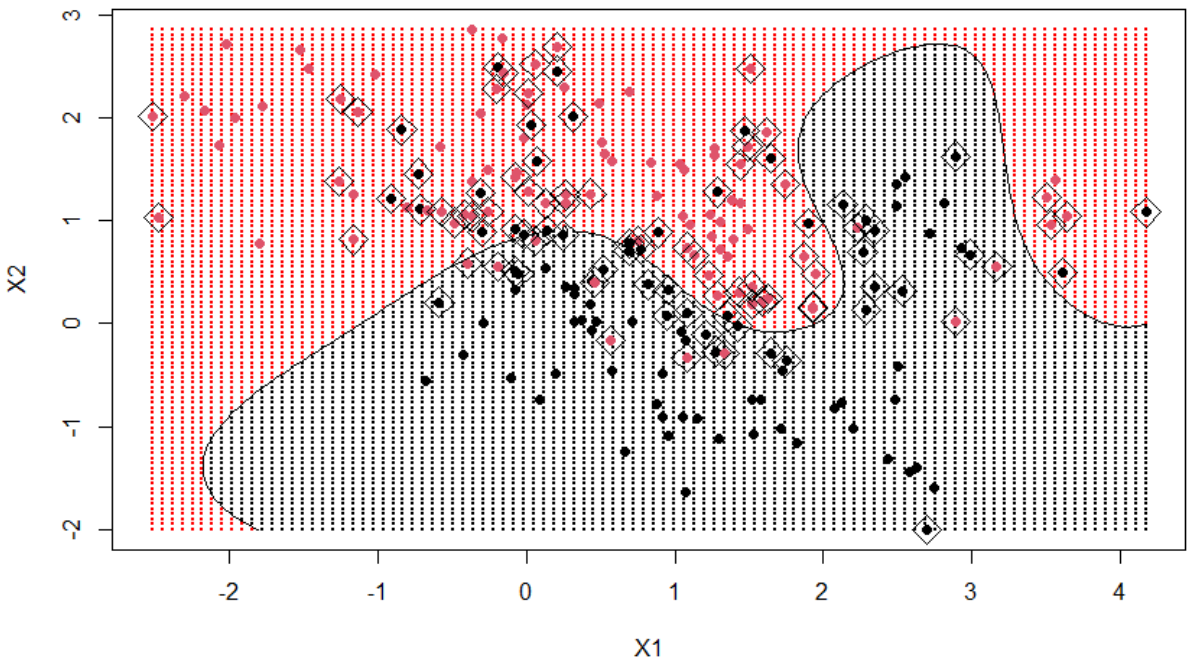

Fig 6.5. Example of Non-Linear SVM; Kernel= Radial basis function (RBF).

6.2.4. K-Nearest Neighbor Classification

The technique K-Nearest Neighbor (KNN) belongs to the supervised language and is commonly used for classification problems but is also applied in regression problems. The KNN classification algorithm is intuitive and relatively simple to use. The operation of this method is based on the fact that when a new

data point is introduced to the algorithm with a given value of *k*, a search for the *k* nearest neighbors of the data point is performed. Then, the nearest neighbors are found by calculating the distance between the introduced data point and the existing data points. The distance can be calculated using various techniques such as Euclidean distance, Manhattan distance, and cosine distance [143]. Finally, the KNN algorithm among these *k* neighbors, count the number of the data points in each category to select the group to which the new data point belongs. Importantly, the *k* value selected has important impact on the performance of KNN algorithm. A big *k* decreases the variance caused by random error, but running the risk of ignoring small but important patterns [144]. On the other hand, KNN is also called a lazy learner that memorizes the complete training dataset and not require training. However, the process of classify a new point, require a lot of memory and CPU resources. Additionally, KNN is a non-parametric algorithm so that if more instances are introduced, the learning changes drastically. Therefore, the learning does not depend on the given data, which is a feature of a non-parametric algorithm. The main advantages of KNN are the following: Simplicity, No training time, non-linear decision boundary, Robust to noisy training data, hyper-parameter tuning easy, and include different distance metrics [145]. Figure 6.6. illustrates the classification process in KNN. The green circle encloses the two objects considered for k=2; the unknown object is classified in the class 1 because the two neighbors belong to class 1. In contrast, the red circle encloses the eight objects considered for k=8; therefore, the unknown object is classified in the class 2 because five of the eight neighbors belong to class 2.

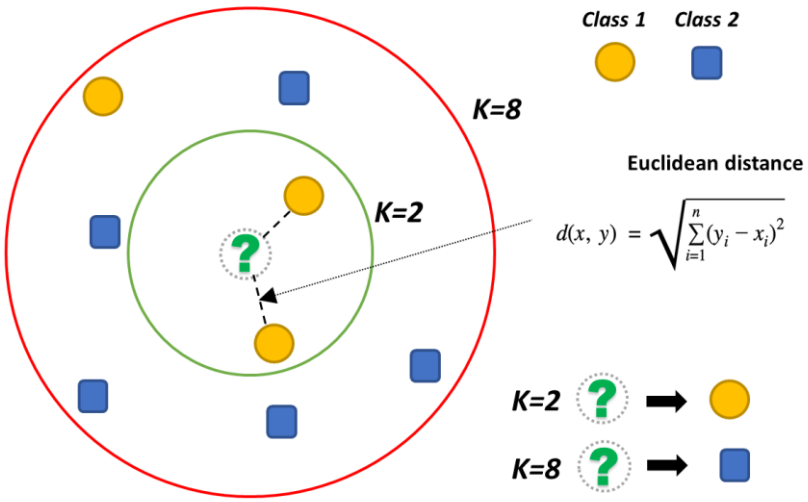

Fig 6.6. Illustration example of K-Nearest Neighbor (KNN) algorithm.

6.2.5. Random Forest

The Random Forest (RF) algorithm was first introduced by Breiman [146]. The RF is one of the most popular tree-based supervised learning algorithms. Moreover, this algorithm is the most flexible and easy to use to solve classification and regression problems. Random forests build hundreds of decision trees to perform the classification process[147]. The RF algorithms use the ensemble technique called Bootstrap

Aggregation or Bagging. Bagging technique selects a random sample from the data set, which is referred to as bag, and the rest which are left out of the sample are referred to as out-of-bag (oob) samples [147]. Therefore, each tree is generated from the samples provided by the original data with a replacement known as row sampling. This step of row sampling with replacement is called bootstrap [148]. Each tree is then trained independently, which generates a particular result. The forest selects the final classification based on majority voting after combining the results of each of the trees. The step of combining all the results and generating a classification based on the majority vote is known as aggregation. Thus, the aggregation step helps to reduce the variance. In addition, the oob (out-of-bag) data is used to obtain the OOB Error, which serves as a validation error and is essentially in the validation set because there is no need for cross-validation. Finally, the main advantages of RF are the following: the accuracy of RF is generally very high, can handle large datasets efficiently, present estimates for variable importance in classification, forests generated can be stored and reused, and RF include methods for balancing error in unbalanced data sets[147]. Figure 6.7 shown the classification process in RF.

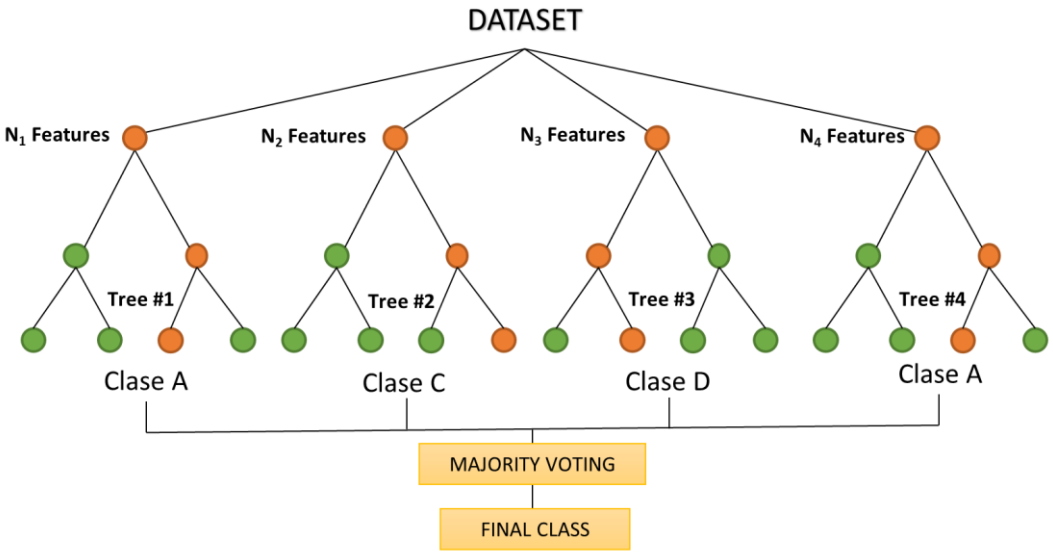

Fig 6.7. Conceptual diagram of the Random Forest algorithm.

6.3 Methods

6.3.1. Programming Language

This project was implemented on Spyder (Python 3.9), an Integrated Development Environment (IDE) specially designed for Python. The three classification models were developed using the scikit learn library, also called sklearn. The sklearn is a python library used to implement machine learning models. In this library, we can implement several classification algorithms and offers the following advantages: simple, effective, free software, and user-friendly [149]. On the other hand, working with Python allows us to perform data analysis and manipulation with the Panda library and make 2D plots with the Matplotlib library.

6.3.2. Data pre-processing

The dataset used in the classification model is composed of the flexion and extension angles of the finger joints of each subject during each ARAT test. The data collection and statistical analysis procedure for this data set were presented in the previous chapters. In the dataset each sample was labeled according to the class to which each activity belonged (Control=0; Stroke =1). There are 800 cases in class '0' and 288 cases in class '1'. Table 6.1 shown the structure of the dataset used in the model.

Table 6.1 Dataset variables

y1	x1	x2	x3	x4	x5	x6	x7	x8	x9	x10	x11	x12	x13	x14
0	Test 01	GRASP	Extension	4.47	13.51	1.73	-16.75	7.72	8.02	3.93	-17.50	3.16	8.64	2.13
1	Test 12	GRIP	Flexion	18.42	17.87	-23.39	28.44	9.41	27.20	10.76	11.30	13.52	21.26	4.42
0	Test 13	GRASP	Extension	6.70	13.78	0.65	20.91	13.05	22.22	11.41	13.85	12.03	20.11	3.68
1	Test 04	PINCH	Flexion	13.85	15.30	7.08	17.12	10.53	19.67	8.00	13.23	10.31	18.02	4.89

y1= response of the dataset; x1-x14 = features of the dataset

In the dataset we identify input and output variables, the input is known as feature, and the output is known as response (discrete variable). The dataset has 14 features; the first three correspond to "Activity," "Subtest," and "Motion," and the remaining eleven correspond to the angles of the finger joints. On the other hand, the output variable is the class to which the subject corresponds {0-Control,1-Stroke}. Hence, the categorical features in the dataset were transformed into binary values using one-Hot encoding method with sklearn. Then, the features corresponding to the finger joints were standardized using Sklearn's StandardScaler function. There were no missing values in the dataset and therefore the 1088 samples were used in the classification models.

6.3.3. Training and testing sets

As mentioned previously, a classification model is trained using a training data set. Therefore, we split our dataset into two parts a training set and test set. To perform this process, we use the sklearn function (train_test_split). In each classification model we used 75% of the data as training set and the remaining 25% as test set. The dataset was not split into the validation set because we used the GridSearchCV technique for tuning the hyperparameters of our algorithms. This technique performs the cross-validation process as detailed below. Finally, the training set is fitted to each of the classifier models to subsequently perform the hyperparameter tuning.

The following functions from sklearn were used for the development of each of the classifiers.

- *from sklearn.neighbors import KNeighborsClassifier()*
- *from sklearn.ensemble import RandomForestClassifier()*
- *from sklearn.svm import SVC ()*

6.3.4. Tuning hyperparameters

Machine learning models have hyperparameters. Hyperparameters are user-adjustable parameters that can vary in quantity from one model to another. Therefore, proper selection of parameter values allows for finding the optimal model performance. However, some models have many possible combinations of hyperparameter values, so adjusting them manually is not the best alternative. There are several computational methods to find the optimal hyperparameters of the model. This process is also known as hyperparameter tuning. Two of the most commonly used are Grid Search CV and Randomized Search CV. We decided to use the GridSearchCV this technique uses all possible permutations of the hyperparameters of a given model. The performance of each model is then evaluated, and the best-performing model is selected. In addition, GridSearchCV has the advantage of including cross-validation. Cross-validation is a technique to identify different problems during model training, such as the occurrence of overfitting. To do this, GridSearchCV will split the training data into training and test partitions to tune the hyperparameters on these data[149]. Next, the model will be fitted with the full training data with the best parameters found. Finally, the model is evaluated with the test data set aside at the beginning of the process (unseen data). However, using all possible combinations consumes a large amount of memory, but in our thesis, we did not handle Big data. The GridSearchCV method is available in the sklearn class and can be initiated by creating an object of GridSearchCV () as is shown below [149]:

hyp = GridSearchCV (estimator, param_grid, cv, scoring)

estimator = The model selected (SVM, RF, KNN);

param_grid = Dictionary with parameters names (str) as keys and lists of parameter settings to try as values;

cv = Number of folds for K-fold cross-validation;

scoring = The performance measure. For example, ‘r2’ for regression models, ‘precision’ for classification models.

6.3.5. Classification metrics

One of the most important steps in machine learning is evaluating the model performance. Different metrics exist for regression and classification models. Since in regression, results are continuous values and in classification, results are discrete values, the evaluation metrics are distinct. However, in this thesis, we focus on classification models. Evaluation metrics within classification models can be applied in two phases. Firstly, in the training phase, to produce a more accurate prediction result in the future evaluation of the classification model. Then, in the testing phase, evaluation metrics are used to measure the efficacy of the classifier when tested on unseen data[150]. Therefore, knowing the different metrics and making the proper selection is crucial to improving the model's performance. The most commonly used metric in classification is accuracy [150], but there are others that are important for evaluating classification models. Therefore, to evaluate the performance of the classification models, we will discuss the metrics used in this

Thesis: Confusion matrix (not a metric but fundamental to the others), Precision, Accuracy, Recall, F1-score, AU-ROC, and the Classification Report.

Confusion Matrix

A confusion matrix is a useful tool for analyzing the performance of classification models when tested on unseen data. Furthermore, it is not exactly a performance metric, but is a basis on which other metrics evaluate the results. A confusion matrix is a cross table of true labels versus model predictions. Each row of the confusion matrix represents instances of an actual class, and each column represents instances of a predicted class [150]. Typically, it is used for binary classification problems but can also be applied to multi-class Classification problems. In Figure 6.8 a binary confusion matrix of 2x2 is shown.

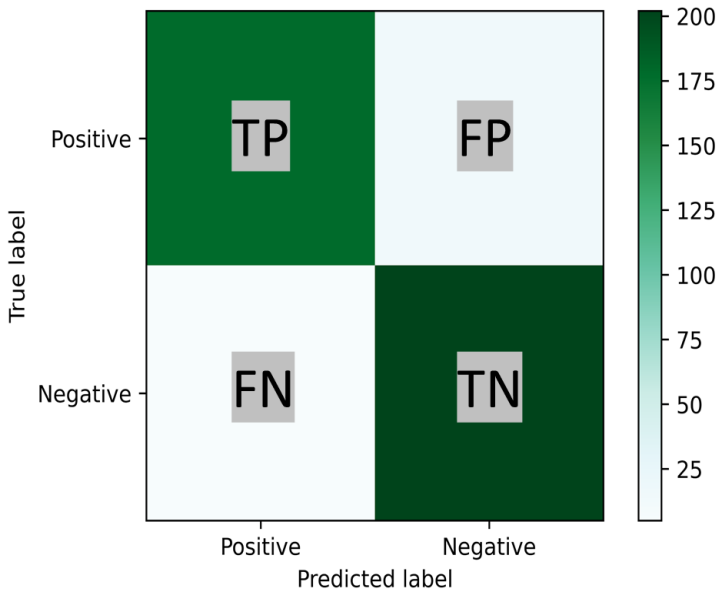

Figure 6.8. Confusion Matrix Binary Classification; TP and TN represent the number of positive and negative instances that are correctly classified. For its part, FP and FN represent the number of misclassified negative and positive instances, respectively.

Accuracy

Accuracy measures the ratio of the number of correct predictions over the total number of predictions. Therefore, accuracy measures how often the classifier correctly predicts. This can be calculated using the below formula:

$$\frac{TP + TN}{TP + FP + TN + FN}$$

Precision

Precision: measure the positive instances that are correctly predicted from the total predicted instances in a positive class. This can be calculated using the below formula:

$$\frac{TP}{TP + FP}$$

Recall

Recall is used to measure the fraction of positive instances that are correctly classified. Therefore, the recall must be as high as possible and It can be calculated using the below formula

$$\frac{TP}{TP + FN}$$

F1-Score

F-score or F1-Score evaluates the recall and precision at the same time. Therefore, F-score is maximum if the recall is equal to the precision. This can be calculated using the below formula:

$$2 \times \frac{Recall \times Precision}{Recall + Precision}$$

Multi-class Metrics

In contrast, the metrics Precision, Recall and F-score in multi-class classification are calculated as the arithmetic mean of the individual class metrics [151]. The formulas are as follows:

$$Macro\ Averaged\ Precision = \frac{\sum_{k=1}^{K} Precision_k}{K}$$

$$Macro\ Averaged\ Recall = \frac{\sum_{k=1}^{K} Recall_k}{K}$$

$$Macro\ Averaged\ F1Score = 2 \times \frac{Macro\ Averaged\ Precision \times Macro\ Averaged\ Recall}{Macro\ Averaged\ Precision^{-1} \times Macro\ Averaged\ Recall^{1}}$$

AUC-ROC (Area under Receiver operating characteristics curve)

The Receiver Operating Characteristic (ROC) curve is graph used to evaluate the performance of binary classification algorithms, i.e., between two classes. Contrary to the other metrics, the ROC curve provides a graphical representation. The ROC curve is obtained by plotting the true positive rate (TPR) (y axis) against the false positive rate (FPR) (x axis) for a single classifier. In the other hand, The Area Under the Curve (AUC) is a metric that allows to summarize the information displayed with the ROC curve. Therefore, the higher the AUC value (closer 1), the better performance of the binary classifier in a given classification test [152]. An illustration of the ROC curve is shown in Figure 6.9.

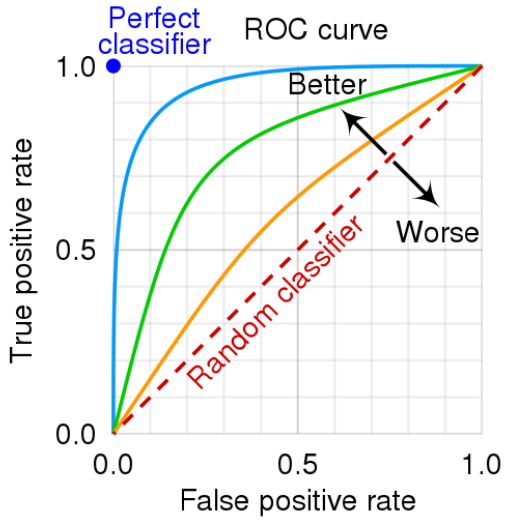

Figure 6.9. Example of distinct receiver operating characteristic curves (ROC).

Classification Report

The classification report displays the following metrics: precision, recall, and f1-score. In addition, the report includes the support value, which is the number of samples of the true response that lies in each class. Therefore, these metrics provide a better understanding of the overall performance of the trained model. This report can be used in both binary and multi-class classification.

6.3.6. Over-sampling Data

In this thesis, the classes in the data set are slightly unbalanced. Therefore, the imbalanced data problem of classification models is commonly solved with oversampling and undersampling techniques. The advantage of oversampling over undersampling is that no samples are lost from the original training set, since all data from the minority and majority classes are preserved [153]. However, in a large dataset, the time and memory consumption could be very large and costly in oversampling. Since the dataset in our thesis is not huge and the imbalance is mild, we do not face this problem. Therefore, we selected an

oversampling technique. We decided to use the Borderline-SMOTE algorithm motivated by the results in studies of arrhythmia detection[154], estimation brain metastasis [155] and emotions recognition [136].

Borderline-SMOTE is an algorithm derived from SMOTE (Synthetic Minority Over-sampling Technique). SMOTE uses the k-nearest neighbor algorithm to generate new and synthetic data to over-sampled the minority class [156]. In contrast, Borderline-SMOTE generates the synthetic data around the borderline between the two classes, unlike SMOTE, where synthetic data is created randomly in all the minority samples [157].

The procedure of Borderline-SMOTE is as follows: First, we calculate the nearest neighbors in the minority class N in all the training set samples. Next, we identified the nearest neighbors; if the majority correspond to the majority class, the samples are put in a set called Danger. The samples in Danger correspond to the borderline data of the minority class. Then, we selected a random N nearest neighbors for each sample in Danger to create the synthetic data. Therefore, we calculate the distance between the sample and its N nearest neighbors and multiply by a random number between 0 and 1. Finally, the synthetic samples of the minority class are generated:

$$Synthetic = p_j + r_j * dif_j, \qquad j = 1,2, \dots, s$$

Where p_j represents the samples in Danger, r_j represents a random number between [0,1], and dif_j represents the distance between the samples and the N nearest neighbor.

6.3.7. Statistical Analysis

The three classification models (RF, SVM, KNN) were compared to determine which has the best performance. First, we evaluated the performance of the three classification models with different evaluation metrics such as Accuracy, Precision, Recall, F1-score, and AUC-ROC in the testing set. Next, the models were evaluated using k-fold cross-validation with five folds and two replicates, giving ten scores for each model. Then, the scores between models were compared with the 5x2cv combined F test [158] using the MLxtend library by Sebastian Raschka [159], which provided the f-statistic and p-value. Subsequently, we evaluated the performance of the three classification models with the evaluation metrics after balancing the data classes using the technique Borderline-SMOTE. The scores between the three models were compared using the 5x2cv combined F test. Finally, each classification model was compared before balancing and after balancing using the paired t-test. The statistical analysis was conducted using the software Anaconda (Anaconda Inc, *Austin, TX, USA)* with Python 3.9. A p-value of less than 0.05 was considered statistically significant for all the statistical analyses.

6.4. Results

In this section, the results of the performance of the classification models Random Forest (RF), K-nearest Neighbor (KNN), and Support Vector Machine (SVM) are presented.

6.4.1. Hyperparameters selection

The GridSearchCV technique was applied to each of the classification algorithms (RF, KNN, SVM) used in this thesis. The hyperparameter values obtained were used to evaluate each classifier in the prediction of results with the test set.

First, the hyperparameters of the SVM model were evaluated and the results were as follows.

SVM: {'C': 10, 'gamma': 0.1, 'kernel': 'rbf'}

Then, the hyperparameters of the KNN model were evaluated and the results were as follows.

KNN: {'leaf_size': 20, 'metric': 'minkowski', 'n_neighbors': 10, 'p': 3, 'weights': 'distance'}

Finally, the hyperparameters of the RF model were evaluated and the results were as follows.

RF: {'max_depth': 50, 'min_samples_leaf': 1, 'min_samples_split': 3, 'n_estimators': 500}

6.4.2. Performance of the Classification Models in the Dataset

Random forest

The Random forest (RF) classifier showed a high accuracy of 93% and a high precision of 96.5%. In contrast, the recall of 76.4% and the f1-score of 85.3% were low. On the other hand, the classification report presented in Table 6.2 shows that the recall and the f1-score values were higher in the control class but were lower in the stroke class. In contrast, the precision was higher in the stroke class, as is shown in the confusion matrix in Figure 6.10.

Table 6.2. Random Forest model classification report

Classes	Precision	Recall	F1-score	Support
Control	0.92	0.99	0.95	200
Stroke	0.96	0.76	0.85	72

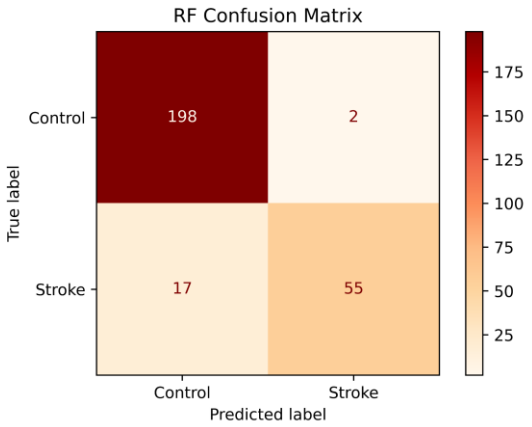

Fig 6.10. Random Forest (RF) Confusion Matrix

K-nearest neighbor

The K-nearest neighbor (KNN) classifier presented a high precision of 95.3% and an accuracy of 87.9%. In contrast, the recall of 56.9 % and the f1-score of 71% were low. The Table 6.3. shown that the recall and f1-score were higher in the control class. While the precision was low in the control class as is shown in Figure 6.11.

Table 6.3. K-nearest neighbor model classification report

Classes	Precision	Recall	F1-score	Support
Control	0.86	0.99	0.92	200
Stroke	0.95	0.57	0.71	72

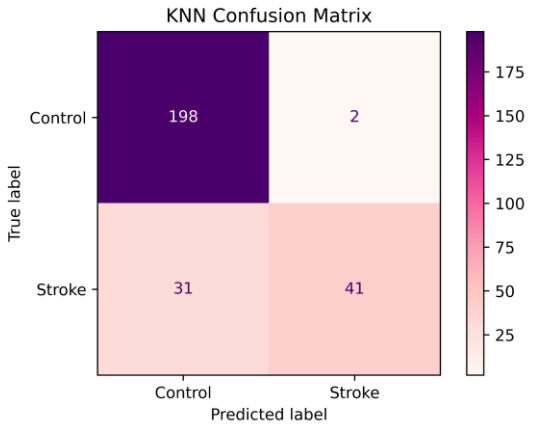

Fig 6.11. K-nearest neighbor (KNN) Confusion Matrix.

Support Vector Machine

The Support Vector Machine (SVM) classifier showed a high precision of 98.3% and a high accuracy of 94.5%. In contrast, the SVM classifier showed a recall of 80.5% and an f1-score of 88.5%. However, the classification report in Table 6.4 showed high values in precision, recall, and f1-score in the control class and in the precision of the stroke class, as is shown in the confusion matrix in Figure 6.3.

Table 6.4. Support Vector Machine model classification report

Classes	Precision	Recall	F1-score	Support
Control	0.93	0.99	0.96	200
Stroke	0.98	0.81	0.89	72

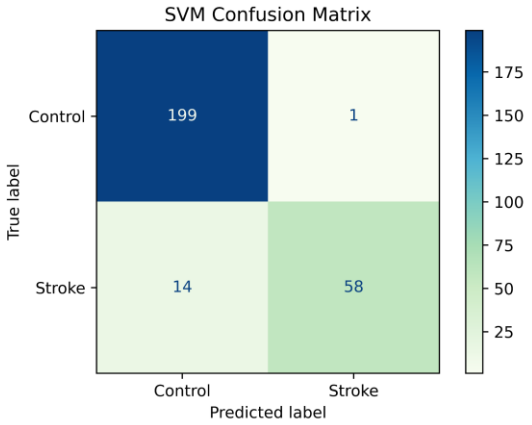

Fig 6.12. Support Vector Machine Confusion Matrix.

6.4.3 Comparison of classification models

Table 6.5 shows the mean values and deviation standard of several evaluation metrics for the RF, SVM, and KNN classifiers. The results showed that the three models have similar precision and no significant differences were found among the three classifiers ($p > 0.05$). The SVM classifier showed significantly higher accuracy and f1-score than the KNN classifier. In contrast, no significant differences ($p > 0.05$) were found in accuracy and f1-score between the SVM and RF classifiers. In addition, the SVM classifier showed a significantly higher recall and AUC than the RF and the KNN classifiers.

Table 6.5. Comparison of classification models in different evaluation metrics

Evaluation Metric	RF	SVM	KNN	RF − SVM		RF − KNN		SVM − KNN	
	Mean ± SD	***Mean ± SD***	***Mean ± SD***	***f***	***p***	***f***	***p***	***f***	***p***
Precision	0.961 ± 0.02	0.969 ± 0.03	0.951 ± 0.02	1.459	0.355	1.788	0.271	1.421	0.366
Accuracy	0.933 ± 0.01	0.958 ± 0.01	0.913 ± 0.01	2.917	0.124	2.2	0.199	26.388	0.001^{***}
Recall	0.781 ± 0.04	0.872 ± 0.04	0.710 ± 0.07	8.959	0.013^{*}	1.089	0.513	45.417	0.00^{***}
F1-score	0.861 ± 0.02	0.917 ± 0.02	0.811 ± 0.04	3.789	0.077	1.7	0.29	36.179	0.00^{***}
AUC	0.980 ± 0.01	0.984 ± 0.03	0.939 ± 0.02	5.445	0.038^{*}	8.15	0.016^{**}	11.754	0.007^{**}

RF= Random Forest; SVM= Support Vector Machine; KNN= K-nearest Neighbors; SD = standard deviation; *f*= *f* statistic; *: p <= .05; **: p <= .01; ***: p <= .001

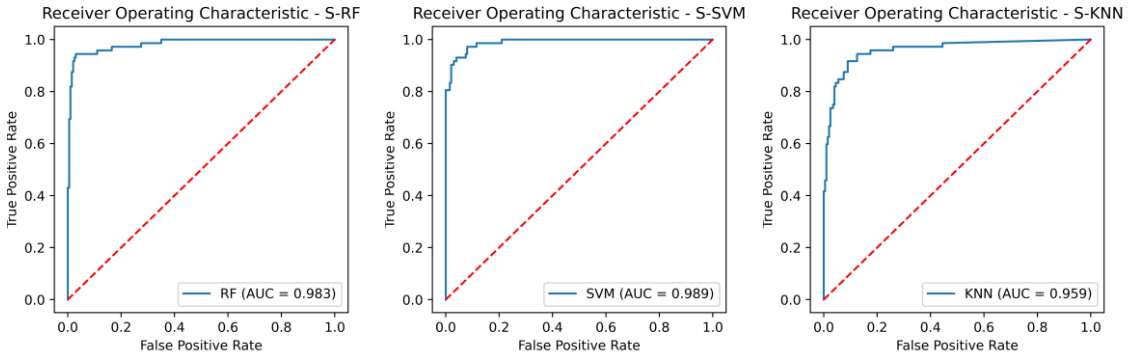

Figure 6.13. The receiver operating characteristic curves (ROC) of the three classification models in the test set.

Borderline-SMOTE Data Balancing

The dataset in this thesis presented a mild case of imbalanced data between the two classes (control and stroke) as is show in Figure 6.14. The results presented earlier in this chapter showed a high accuracy in the three classifiers. However, the accuracy metric is not a good indicator when there are imbalanced classes, as in this case. In contrast, the classifiers KNN and RF showed a lower recall especially in the classification of subjects of the control class. Therefore, to optimize the performance of the classifiers, we decided to use the Borderline-SMOTE algorithm for data oversampling. Figure 6.15 shown the classes after the data balancing with Borderline-SMOTE.

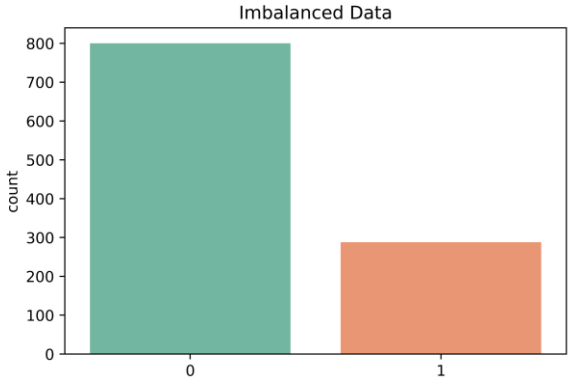

Figure 6.14 Distribution of each class in the dataset; 0=Control and 1=Stroke.

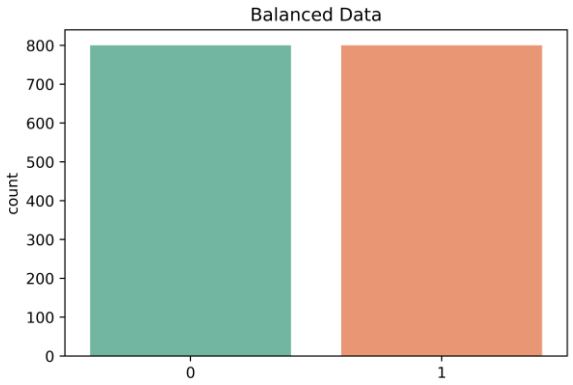

Figure 6.15. Distribution of each class in the dataset after Borderline-SMOTE; 0=Control and 1=Stroke.

6.4.4. Classification Models with Borderline-SMOTE

The three classification models showed an improvement in the classification of both classes (control and stroke), as is shown in Table 6.6 after data balancing with Borderline-SMOTE. Previously, the classification models showed difficulty in classifying subjects with stroke due to the class imbalance. The improvement was remarkable, particularly in the metrics of Recall and f1-score. The overall performance of the classification models in the test set was evaluated with the following evaluation metrics: Accuracy,

Precision, Recall, F1-score, and ROC AUC. The results were as follows: The SVM classifier showed a precision of 98%, while the RF classifier showed a precision of 96.4%, and the KNN classifier showed a precision of 86.3%. On the other hand, the KNN presented a recall value of 98% but analyzing the classification report in Table5 we observed a low recall value of 84% in the control class. In contrast, the SVM classifier presented a recall value of 97.5% and the RF presented a recall of 94% and both classifiers had a uniform recall value in the two classes. In addition, the SVM classifier showed the highest f1-score of 97.7 %, while the RF classifier showed a f1-score of 95.2% and the KNN classifier showed a f1-score of 91.8%. Finally, the Receiver Operating Characteristic (ROC) curve and the AUC (area under the ROC curve) of the three classifiers is shown in Figure 6.16.

Table 6.6. Classification Report of the three classification models after data balancing (Borderline-SMOTE)

Evaluation Metric	RF		SVM		KNN	
	Control	Stroke	Control	Stroke	Control	Stroke
Precision	0.94	0.96	0.98	0.86	0.98	0.98
Recall	0.96	0.94	0.84	0.98	0.98	0.97
F1-score	0.95	0.95	0.91	0.92	0.98	0.98
Support	200	200	200	200	200	200
Accuracy	0.95		0.98		0.91	

RF=Random Forest; SVM= Support Vector Machine; KNN=K-nearest Neighbors

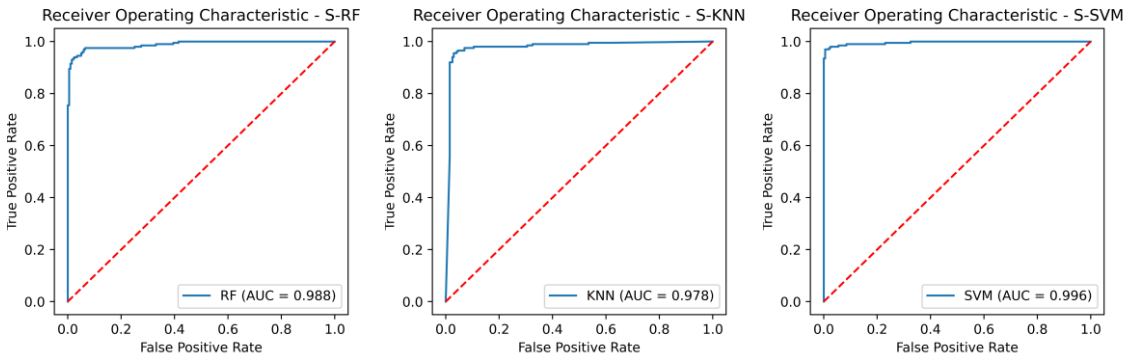

Fig 6.16. The receiver operating characteristic curves (ROC) of the three classification models with Borderline-SMOTE

6.4.5. Performance Comparison between Classifiers after Borderline-SMOTE

Table 6.7 shows the mean values and deviation standard of several evaluation metrics for the RF, SVM, and KNN classifiers using Borderline-SMOTE. As can be seen, the three classification models have a similar and consistent performance. The results showed no significant differences ($p > 0.05$) in accuracy, recall, and f1-score among the three classifiers. However, the RF classifier showed significantly higher precision than the KNN classifier. In contrast, the RF and the SVM classifiers showed a significantly higher AUC than the KNN classifier.

Table 6.7. Comparison of classification models after Borderline-SMOTE in different evaluation metrics

Evaluation Metric	BS_RF	BS_SVM	BS_KNN	BS_RF − BS_SVM		BS_RF − KNN		BS_SVM − KNN	
	Mean ± SD	*Mean ± SD*	*Mean ± SD*	*f*	*p*	*f*	*p*	*f*	*p*
Precision	0.971 ± 0.014	0.968 ± 0.008	0.914 ± 0.021	0.551	0.803	6.083	0.03*	4.049	0.068
Accuracy	0.971 ± 0.010	0.978 ± 0.006	0.948 ± 0.014	1.691	0.293	2.81	0.133	3.88	0.074
Recall	0.970 ± 0.014	0.989 ± 0.007	0.989 ± 0.009	3.403	0.094	3.8	0.077	2.765	0.137
F1-score	0.971 ± 0.010	0.978 ± 0.006	0.950 ± 0.013	1.833	0.261	2.525	0.159	3.668	0.082
AUC	0.996 ± 0.002	0.995 ± 0.004	0.980 ± 0.009	4.074	0.067	7.457	0.019*	7.098	0.022*

BS_RF= Borderline-SMOTE in Random Forest; BS_SVM= Borderline-SMOTE in Support Vector Machine; BS_ KNN= Borderline-SMOTE in K-nearest Neighbors; SD = standard deviation; *f*= *f* statistic; *: p <= .05; **: p <= .01;

6.4.6. Performance comparison of the Classifiers before and after data balancing

In general, the three classification models RF, KNN, SVM showed an improvement after the data balancing process using the Borderline-SMOTE technique in several metrics. In the statistical comparison of the classifiers with unbalanced data and with data balancing, the following results were obtained. In precision metrics, no significant differences were found in the RF and SVM classifiers before data balancing and after data balancing. In contrast, the KNN classifier after data balancing showed significantly lower precision than before balancing, as is shown in Figure 6.17. On the other hand, the RF, SVM, and KNN classifiers showed significantly higher accuracy, recall, f1-score, and AUC after data balancing, as is shown in Figure 6.18-6.21.

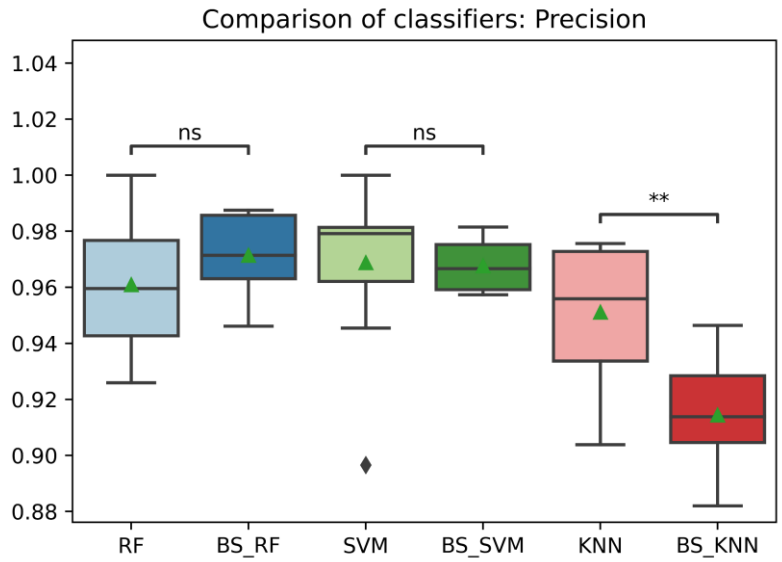

Figure 6.17. Comparison of Precision between Classification models with imbalanced and oversampled data. RF=Random Forest; BS_RF= Borderline-SMOTE in Random Forest; SVM= Support Vector Machine; BS_SVM= Borderline-SMOTE in Support Vector Machine; KNN=K-nearest Neighbors; BS_ KNN= Borderline-SMOTE in K-nearest Neighbors; ns: p > 0.05; **: p <= .01.

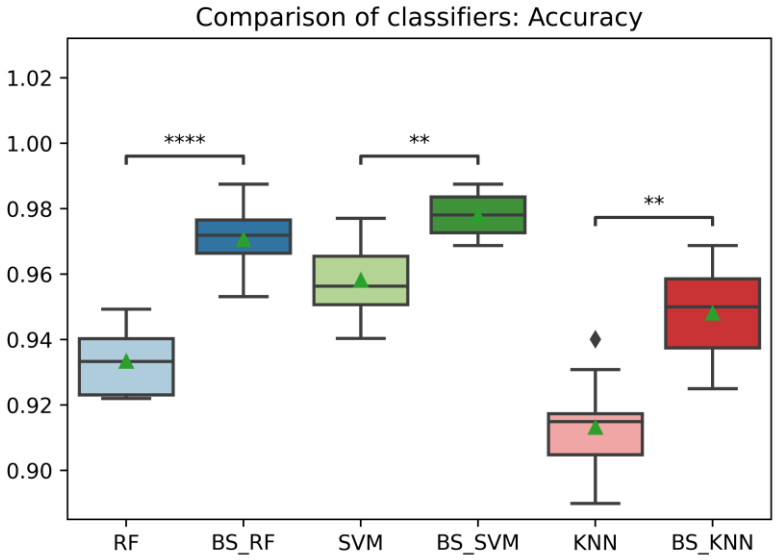

Figure 6.18. Comparison of Accuracy between Classification models with imbalanced and oversampled data. RF=Random Forest; BS_RF= Borderline-SMOTE Random Forest; SVM= Support Vector Machine; BS_SVM= Borderline-SMOTE Support Vector Machine; KNN=K-nearest Neighbors; BS_ KNN= Borderline-SMOTE K-nearest Neighbors; **: p <= .01; ****: p <= .0001.

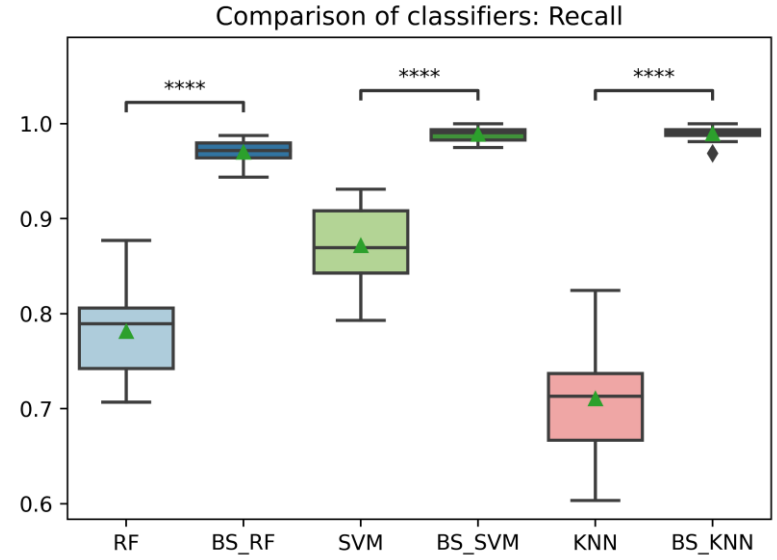

Figure 6.19. Comparison of Recall between Classification models with imbalanced and oversampled data. RF=Random Forest; BS_RF= Borderline-SMOTE Random Forest; SVM= Support Vector Machine; BS_SVM= Borderline-SMOTE Support Vector Machine; KNN=K-nearest Neighbors; BS_ KNN= Borderline-SMOTE K-nearest Neighbors; ****: p <= .0001.

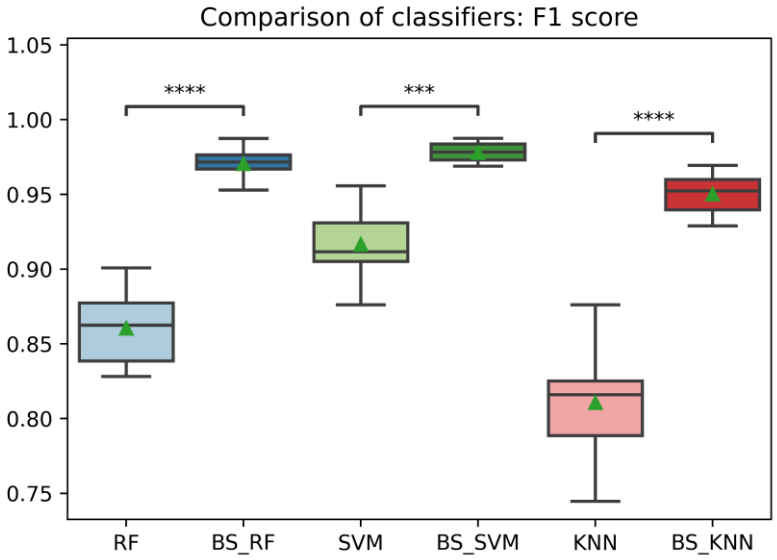

Figure 6.20. Comparison of F1-score between Classification models with imbalanced and oversampled data. RF=Random Forest; BS_RF= Borderline-SMOTE Random Forest; SVM= Support Vector Machine; BS_SVM= Borderline-SMOTE Support Vector Machine; KNN=K-nearest Neighbors; BS_ KNN= Borderline-SMOTE K-nearest Neighbors; ***: p <= .001; ****: p <= .0001.

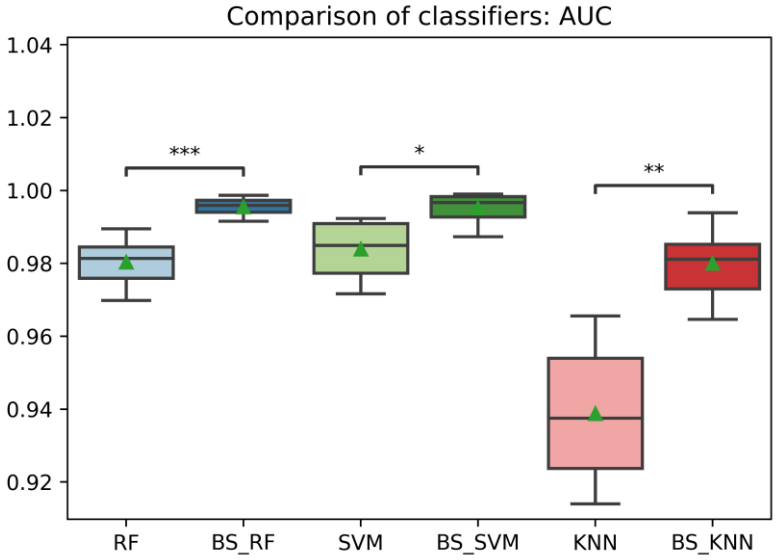

Figure 6.21. Comparison of AUC between Classification models with imbalanced and oversampled data. RF=Random Forest; BS_RF= Borderline-SMOTE Random Forest; SVM= Support Vector Machine; BS_SVM= Borderline-SMOTE Support Vector Machine; KNN=K-nearest Neighbors; BS_ KNN= Borderline-SMOTE K-nearest Neighbors; *: p <= .05; **: p <= .01; ***: p <= .001

6.5. Discussion

In this Thesis, three binary classification models were developed using the following algorithms: Support Vector Machine (SVM), Random Forest (RF), and K-nearest neighbor (KNN). We used as features the angles of flexion and extension of 11 finger joints during the performance of the activities of the Action Research Arm Test (ARAT) to classify activities between two classes: healthy subject (0= Control) and

post-stroke patients (1= Stroke). Importantly, the activities included in the dataset of the stroke group obtained a score of 2 – 3 on the ARAT. While in all the activities included in the dataset of the control group, a score of 3 was obtained. Therefore, based on the ARAT score all tasks were completed and there is not much difference between the tasks in one group and the other. In this way, using completed tasks based on the ARAT score, the performance of the classifier is evaluated.

The result showed that the Support Vector Machine (SVM) classifier had the best performance in the test set before data balancing with a Precision of 98.3%, an Accuracy of 94.5 %, a recall of 80.5%, f1-score of 88.5% and an AUC of 0.989. In addition, the Recall and AUC were significantly higher than the RF and KNN classifiers. However, the recall values in three classifiers were low especially in the stroke group. The lower recall showed that the model was classifying stroke patients as healthy subjects as is shown in the confusion matrices in Fig 4-5. Besides, we detected a mild imbalance between classes, so we decided to use the oversampling technique Borderline-SMOTE. The results showed that after Borderline-SMOTE the three classifiers showed significantly higher accuracy, recall, f1-score, and AUC. In the recall, there was an increase in the RF (17.6 %), SVM (17%), and KNN (41.1 %). However, the KNN classifier showed a recall of 84% in the Control class while the RF and SVM classifiers had a balanced recall in both classes. In addition, the precision of the KNN was significantly lower after data balancing. Finally, all the classification model showed and AUC > 0.95. In fact, the RF and SVM showed the best performance after data balancing and no significant differences were found in any metric between the two classifiers. However, the SVM showed a high accuracy, recall and f1-score and therefore a more balanced performance. Hence, The SVM was the model with the best performance after data balancing with Borderline-SMOTE and before data balancing.

The results in our thesis showed that after data balancing using Borderline-SMOTE the classification models showed an improved performance as in other research. Reddy et al. applied the Borderline-SMOTE algorithm on convolutional neural networks (CNN) to detect arrhythmias using electrocardiogram signals. Their results showed a significantly higher f1-score and accuracy after the use of Borderline-SMOTE [154]. The results of our thesis were similar, where the three classification models obtained significantly higher accuracy, recall and f1-score after using the Borderline-SMOTE technique. On the other hand, Chang et al. presented a study for emotion recognition with electroencephalogram (EEG) signals using data augmentation with the Borderline-SMOTE method [136]. They compared traditional machine learning methods, and their results showed that SVM and XGBoost had better performance in average accuracy and average macro f1-score than decision tree and KNN models. Our thesis obtained similar results where the SVM algorithm showed higher accuracy and f1-score than the KNN and RF models. However, our study used a binary classification analysis, and in Chang et al. study, a multiclass classification method was used. Moreover, there are few studies that combine machine learning with the ARAT test. Dutta et al. developed an SVM classifier with an accuracy of 92% to predict ARAT scores in patients with different degrees of disability. They used a glove with six flex sensor and three force sensors and a motion processing unit [60].

The difference with our study was that we analyzed healthy subjects and patients with good recovery after the rehabilitation process. In addition, the activities we analyzed were completed tasks with a high score. Therefore, we decided to analyze whether the information provided by a data glove with 18 flexion sensors would allow us to classify subjects in each group with good performance. In contrast, Rheme et al. used an SVM model to predict good and poor motor outcomes of stroke patients using ARAT, grip force index, and magnetic resonance imaging (fMRI) [160]. However, the outcome of patients with initially moderate impairment could not be predicted with the information of the ARAT and the grip force test. Their results demonstrate that it is difficult to predict in post-stroke subjects with moderate impairments based on the ARAT scoring process. The difference with our thesis is that our study was not based on the ARAT score but on the information obtained with the human hand motion system, which allowed us to differentiate between subjects with a good post-stroke recovery and healthy subjects.

Importantly, the use of human hand motion information allows the development of high-performance Machine Learning models for the classification of activities between healthy subjects and persons post-stroke. However, to achieve these results it was necessary to balance classes using the Borderline-SMOTE algorithm. These differences are not detected by the ARAT scoring process that is limited only to evaluate the quality performance. Therefore, these results are of clinical relevance for occupational therapists and other health care professionals who can use a classification model for the detection of finger joint impairments not only in people post-stroke but also after surgical procedures, hand injuries and other hand disorders. Regardless, it is essential to consider the recall results since the activities of post-stroke patients identified as the control group could have been performed in the same way as a healthy person. Therefore, the bias would not be in the classifier model, but in the fact that there were no significant differences in certain activities between post-stroke patients and healthy subjects.

6.6 Limitations

In this Thesis, we limited to the use of traditional machine learning classifiers but the use of Ensemble Machine Learning methods has shown very good results in clinical studies [161],[164], so that in future work we could implement an ensemble classifier and compare the results. In addition, deep learning has also been used for classification problems in the area of healthcare, especially Convolutional neural networks (CNNs), showing good results in combination with Borderline-SMOTE [136], [154]. Therefore, the use of deep learning should also be considered for future studies. Another limitation we had is that it was not possible to access patient demographic data. This would have allowed us to evaluate the impact of these features on the classification algorithm. Finally, we limited ourselves to evaluating patients with good upper extremity function according to the ARAT score. Therefore, it would be interesting to evaluate subjects with different degrees of upper extremity impairment to perform a classification model to predict ARAT scores based on information from the eleven finger joints.

6.7. Conclusions

The classifiers with unbalanced data showed a low recall and f1-score especially in the stroke class, after the implementation of Borderline-SMOTE the three classifiers showed a significantly higher accuracy, recall, f1-score, and AUC. However, the SVM classifier showed the higher performance with a precision of 98%, a recall of 97.5% and an AUC of 0.996 after data balancing. Therefore, the results showed that classification models based on human hand motion features in combination with the oversampling algorithm Borderline-SMOTE achieve a higher performance. In addition, the high performance of the classifiers showed that there are differences between the activities performed between healthy and post-stroke individuals that are not detected by the ARAT scoring process. Regardless, the recall results can show activities in which people from both classes performed equally well. Furthermore, the classification model based in hand motion information can be used in future work for the detection of finger joint impairments not only in people post-stroke but also after surgical procedures, hand injuries and other hand disorders.

CHAPTER 7
Conclusions and Future Work

7.1 Conclusions

In this chapter we present a general conclusion for this Thesis.

A novelty hand motion system to improve the evaluation of post-stroke patients with the Action Research Arm Test (ARAT) was presented. The hand motion system is composed of a data glove CyberGlove II®, a Force Sensing module based in force sensitive resistors (FSRs), and a Graphical User Interface (GUI) developed in Unity®.

An important database was obtained in healthy subjects of the finger forces and the range of motion of the metacarpophalangeal (MCP) and proximal interphalangeal (PIP) joints of the fingers (index, middle, ring, and little) and Carpometacarpal (CMC), MCP, and interphalangeal (IP) for the thumb. The database is clinically relevant for the psychotherapist and health professionals to establish therapy goals for patients with impairments and post-stroke patients.

The flexion angles and the finger force on healthy subjects depend on the object size and the type of grasp used (power, precision, or pinch). Therefore, the mean total force was higher in the grasp subtest. In this subtest, we found several activities in which the power grip was used. In contrast, flexion angles in Thumb (CMC, MCP), Index MCP, Middle MCP, and Ring MCP finger joints obtained in the pinch subscale were significantly larger. In this subtest, we found several activities in which the pinch grip was used.

Finger joint impairments and compensatory grasping strategies were identified in stroke patients with left (LH) and right (RH) hemiparesis not detected with the ARAT scoring method. RH and LH patients used compensatory strategies involving increased flexion at the PIP joints for decreased flexion in the MCP joints.

Classification models were developed with the oversampling algorithm Borderline-SMOTE to classify ARAT activities between healthy subject or post-stroke subject with similar ARAT scores. The Support Vector Machine (SVM) classifier showed the higher performance with a precision of 98%, a recall of 97.5% and an AUC of 0.996 after data balancing.

The high performance obtained with the classification models showed that there are differences between the activities performed between healthy and post-stroke individuals that are not detected by the ARAT scoring process. In addition, classification models based on human hand motion features in combination with the Borderline-SMOTE oversampling algorithm demonstrated higher performance.

7.2 Future Work

The use of a motion capture system based on inertial measurement units (IMU) will be incorporated into the hand motion system. This will allow us to add to the existing system the analysis and evaluation of the major joints of the upper extremity (wrist, forearm, elbow, shoulder).

Future studies will evaluate the range of motion of abduction and adduction of the MCP finger joints. Studying these movements will allow us to perform a complete grasping evaluation and identify impairments and compensatory strategies in post-stroke patients in this plane of motion.

Use a hand model with 29 DOF developed in a previous study [165] for the simulation in the module of the Graphical User Interface (GUI). In this way, more realistic movements of the fingers, especially the thumb, can be obtained.

Evaluate stroke patients with mild and severe impairment of upper extremity motor function to assess the performance of the proposed hand motion system during the ARAT execution. In addition, the evaluation of stroke patients with different degrees of hand function impairment will allow the development of machine learning models for ARAT score prediction based on finger joint angles, finger strength, and other demographic characteristics of stroke patients.

Develop applications for the rehabilitation in virtual reality (VR) and augmented reality (AR) for people with stroke by incorporating the leap motion sensor into the hand motion system. The compatibility of the GUI developed in unity allows us to upgrade the application easily to these VR and AR platforms.

Bibliography

[1] P. D. (2017). United Nations, Department of Economic and Social Affairs, “World Population Ageing 2017 - Highlights (ST/ESA/SER.A/397).,” 2017.

[2] National Institute of Neurological Disorders and Stroke (NINDS), “NINDS stroke information page,” 2017. [Online]. Available: https://www.ninds.nih.gov/Disorders/All-Disorders/Stroke-Information-Page.

[3] D. Mozaffarian *et al.*, “Heart Disease and Stroke Statistics—2015 Update,” *Circulation*, vol. 131, no. 4, Jan. 2015.

[4] S. Whitehead and E. Baalbergen, “Post-stroke rehabilitation,” *South African Med. J.*, vol. 109, no. 2, pp. 81–83, 2019.

[5] L. Santisteban, M. Térémetz, J. P. Bleton, J. C. Baron, M. A. Maier, and P. G. Lindberg, “Upper limb outcome measures used in stroke rehabilitation studies: A systematic literature review,” *PLoS One*, vol. 11, no. 5, pp. 1–16, 2016.

[6] J. E. Sullivan *et al.*, “Outcome measures for individuals with stroke: Process and recommendations from the American physical therapy association neurology section task force,” *Phys. Ther.*, vol. 93, no. 10, pp. 1383–1396, 2013.

[7] N. Yozbatiran, L. Der-Yeghiaian, and S. C. Cramer, “A standardized approach to performing the action research arm test,” *Neurorehabil. Neural Repair*, vol. 22, no. 1, pp. 78–90, 2008.

[8] N. S. Ward, F. Brander, and K. Kelly, “Intensive upper limb neurorehabilitation in chronic stroke: Outcomes from the Queen Square programme,” *J. Neurol. Neurosurg. Psychiatry*, vol. 90, no. 5, pp. 498–506, 2019.

[9] C. E. Lang, J. M. Wagner, A. W. Dromerick, and D. F. Edwards, “Measurement of Upper-Extremity Function Early After Stroke: Properties of the Action Research Arm Test,” *Arch. Phys. Med. Rehabil.*, vol. 87, no. 12, pp. 1605–1610, 2006.

[10] I. Carpinella, D. Cattaneo, and M. Ferrarin, “Quantitative assessment of upper limb motor function in Multiple Sclerosis using an instrumented Action Research Arm Test,” *J. Neuroeng. Rehabil.*, vol. 11, no. 1, p. 67, 2014.

[11] H. S. Nam, W. H. Lee, H. G. Seo, Y. J. Kim, M. S. Bang, and S. Kim, “Inertial Measurement Unit Based Upper Extremity Motion Characterization for Action Research Arm Test and Activities of Daily Living,” *Sensors*, vol. 19, no. 8, p. 1782, Apr. 2019.

[12] A. Schwarz, M. M. C. Bhagubai, G. Wolterink, J. P. O. Held, A. R. Luft, and P. H. Veltink, “Assessment of Upper Limb Movement Impairments after Stroke Using Wearable Inertial Sensing,” *Sensors*, vol. 20, no. 17, p. 4770, Aug. 2020.

[13] J. P. O. Held *et al.*, “Inertial sensor measurements of upper-limb kinematics in stroke patients in clinic and home environment,” *Front. Bioeng. Biotechnol.*, vol. 6, no. APR, pp. 1–8, 2018.

[14] Y. Xue, Z. Ju, K. Xiang, J. Chen, and H. Liu, “Multimodal Human Hand Motion Sensing and Analysis-A Review,” *IEEE Trans. Cogn. Dev. Syst.*, vol. 11, no. 2, pp. 162–175, 2019.

[15] H. Liu, Z. Ju, X. Ji, C. S. Chan, and M. Khoury, “Human hand motion analysis with multisensory information,” *Stud. Comput. Intell.*, vol. 675, no. May, pp. 171–191, 2017.

[16] L. Dipietro, A. M. Sabatini, and P. Dario, “A survey of glove-based systems and their applications,” *IEEE Trans. Syst. Man Cybern. Part C Appl. Rev.*, vol. 38, no. 4, pp. 461–482, 2008.

[17] T. G. Zimmerman, J. Lanier, C. Blanchard, S. Bryson, and Y. Harvill, “Hand Gesture Interface Device.,” *Proc. - Graph. Interface*, pp. 189–192, 1987.

[18] G. D. Kessler, L. F. Hodges, and N. Walker, “Evaluation of the CyberGlove as a Whole-Hand Input Device,” *ACM Trans. Comput. Interact.*, vol. 2, no. 4, pp. 263–283, 1995.

[19] M. Fröhlich and I. Wachsmuth, “Gesture recognition of the upper limbs — From signal to symbol,” in *Gesture and Sign Language in Human-Computer Interaction. GW 1997. Lecture Notes in Computer Science, vol 1371. Springer, Berlin, Heidelberg*, 1998, pp. 173–184.

[20] M. H. Yun and A. Freivalds, “Analysis of Hand Tool Grips,” *Proc. Hum. Factors Ergon. Soc. Annu. Meet.*, vol. 39, no. 10, pp. 553–557, Oct. 1995.

[21] Cybergloves Systems, “CyberGlove ® II,” *http://www.cyberglovesystems.com/cyberglove-ii*, 2012. .

[22] M. V. Liarokapis, P. K. Artemiadis, and K. J. Kyriakopoulos, “Transformation of human hand positions for robotic hand controlTelemanipulation with the DLR/HIT II robot hand using a dataglove and a low cost force feedback device,” *2013 21st Mediterr. Conf. Control Autom. MED 2013 - Conf. Proc.*, pp. 431–436, 2013.

[23] J. J. Cabibihan, I. Ahmed, and S. S. Ge, “Force and motion analyses of the human patting gesture for robotic social touching,” *Proc. 2011 IEEE 5th Int. Conf. Cybern. Intell. Syst. CIS 2011*, pp. 165–169, 2011.

[24] Y. Xiao, Z. Zhang, A. Beck, J. Yuan, and D. Thalmann, “Human–Robot Interaction by Understanding Upper Body Gestures,” *Presence Teleoperators Virtual Environ.*, vol. 23, no. 2, pp. 133–154, Aug. 2014.

[25] N. Ticó Falguera, “Biomecànica dels dits de la mà com a factor pronòstic de la recuperació funcional de l’extremitat parètica en pacients amb ictus aguts.,” UPC Departament d’Enginyeria Minera, Industrial i TIC, 2016.

[26] E. Peña-Pitarch, J. V. Costa, J. L. Martinez, A. Al Omar, I. A. Larrión, and N. Tico-Falguera, “Introductory Analysis of Human Upper Extremity After Stroke,” *Int. J. Priv. Heal. Inf. Manag.*, vol. 7, no. 1, pp. 45–60, 2018.

[27] R. Boian *et al.*, “Virtual reality-based post-stroke hand rehabilitation,” *Stud. Health Technol. Inform.*, vol. 85, pp. 64–70, 2002.

[28] D. S. Asakawa, J. T. Dennerlein, and D. L. Jindrich, “Index finger and thumb kinematics and performance measurements for common touchscreen gestures,” *Appl. Ergon.*, vol. 58, pp. 176–181, 2017.

[29] C. Carley and C. Tomasi, “Single-Frame Indexing for 3D Hand Pose Estimation,” *Proc. IEEE Int. Conf. Comput. Vis.*, vol. 2015-Febru, pp. 493–501, 2015.

[30] M. Borghetti, E. Sardini, and M. Serpelloni, “Sensorized glove for measuring hand finger flexion for rehabilitation purposes,” *IEEE Trans. Instrum. Meas.*, vol. 62, no. 12, pp. 3308–3314, 2013.

[31] N. G. Tsagarakis, B. Kenward, K. Rosander, D. G. Caldwell, and C. von Hofsten, “‘ BabyGlove ’: A Device to study Hand Motion Control Development in Infants,” *EuroHaptics*, 2006.

[32] R. Ambar, M. Ahmad, A. Mohd Ali, and M. Abdul Jamil, “Arduino based arm rehabilitation assistive device,” *J. Eng. Technol.*, vol. 1, no. October 2017, pp. 5–13, 2011.

[33] B. O’Flynn, J. Torres, J. Connolly, J. Condell, K. Curran, and P. Gardiner, “Novel smart sensor glove for arthritis rehabiliation,” no. December 2016, pp. 1–6, 2013.

[34] S. Bilgin, Y. Üser, and M. Mercan, “Robotic Hand Controlling Based on Flexible Sensor,” *Int. J. Eng. Appl. Sci.*, vol. 8, no. 4, pp. 49–49, 2017.

[35] H. Yamaura, K. Matsushita, R. Kato, and H. Yokoi, “Development of Hand Rehabilitation System for Paralysis Patient – Universal Design Using Wire-Driven Mechanism –,” *IEEE Int. Conf. Robot. Biomimetics*, pp. 7122–7125, 2009.

[36] Y. Park, J. Lee, and J. Bae, “Development of a finger motion measurement system using linear potentiometers,” *IEEE/ASME Int. Conf. Adv. Intell. Mechatronics, AIM*, no. 1, pp. 125–130, 2014.

[37] M. A. Saliba, F. Farrugia, and A. Giordmaina, “A Compact Glove Input Device to Measure Human Hand , Wrist and Forearm Joint Positions for Teleoperation Applications,” no. March, 2015.

[38] Fifth Dimension Technologies, “5DT Data Glove Ultra Series User`s Manual,” *Manual*, 2004.

[39] C. C. Cheng, I. Her, Q. H. Huang, and M. T. Wu, “A tele-monitoring system for performance evaluation of motor task in fMRI environment,” *ISSNIP 2008 - Proc. 2008 Int. Conf. Intell. Sensors, Sens. Networks Inf. Process.*, pp. 369–374, 2008.

[40] Z. J. Tang, S. Sugano, and H. Iwata, “Design of an MRI compatible robot for finger rehabilitation,” in *2012 IEEE International Conference on Mechatronics and Automation*, 2012, pp. 611–616.

[41] E. Fujiwara, C. Y. Onaga, M. F. M. Santos, E. A. Schenkel, and C. K. Suzuki, “Design of a glove-based optical fiber sensor for applications in biomechatronics,” *Proc. IEEE RAS EMBS Int. Conf. Biomed. Robot. Biomechatronics*, pp. 786–790, 2014.

[42] M. A. Conn and S. Sharma, “Immersive telerobotics using the oculus rift and the 5DT ultra data glove,” *Proc. - 2016 Int. Conf. Collab. Technol. Syst. CTS 2016*, pp. 387–391, 2016.

[43] Ramakant, N. E. K. Shaik, and L. Veerapalli, “Sign language recognition through fusion of 5DT data glove and camera based information,” *Souvenir 2015 IEEE Int. Adv. Comput. Conf. IACC 2015*, pp. 639–643, 2015.

[44] P.-C. Hsiao, S.-Y. Yang, B.-S. Lin, I.-J. Lee, and W. Chou, “Data glove embedded with 9-axis IMU and force sensing sensors for evaluation of hand function,” in *2015 37th Annual International Conference of the IEEE Engineering in Medicine and Biology Society (EMBC)*, 2015, vol. 2015-Novem, pp. 4631–4634.

[45] H. Liu *et al.*, “A glove-based system for studying hand-object manipulation via joint pose and force sensing,” *IEEE Int. Conf. Intell. Robot. Syst.*, vol. 2017-Septe, pp. 6617–6624, 2017.

[46] B.-S. Lin, I.-J. Lee, P.-Y. Chiang, S.-Y. Huang, and C.-W. Peng, “A Modular Data Glove System for Finger and Hand

Motion Capture Based on Inertial Sensors," *J. Med. Biol. Eng.*, 2018.

[47] B. O'Flynn *et al.*, "Novel Smart Glove Technology as a Biomechanical Monitoring Tool," *Sensors & Transducers*, vol. 193, no. 10, pp. 23–32, 2015.

[48] A. Nikonovas, A. J. L. Harrison, S. Hoult, and D. Sammut, "The application of force-sensing resistor sensors for measuring forces developed by the human hand," *Proc. Inst. Mech. Eng. Part H J. Eng. Med.*, vol. 218, no. 2, pp. 121–126, 2004.

[49] Q. Ye, M. Seyedi, Z. Cai, and D. T. H. Lai, "Force-sensing glove system for measurement of hand forces during motorbike riding," *Int. J. Distrib. Sens. Networks*, vol. 2015, 2015.

[50] E. Battaglia *et al.*, "ThimbleSense: A Fingertip-Wearable Tactile Sensor for Grasp Analysis," *IEEE Trans. Haptics*, vol. 9, no. 1, pp. 121–133, 2016.

[51] M. Ferre, I. Galiana, and R. Aracil, "Design of a lightweight, cost effective thimble-like sensor for haptic applications based on contact force sensors," *Sensors*, vol. 11, no. 12, pp. 11495–11509, 2011.

[52] M. C. F. Castro and J. Cliquet A., "A low-cost instrumented glove for monitoring forces during object manipulation," *IEEE Trans. Rehabil. Eng.*, vol. 5, no. 2, pp. 140–147, 1997.

[53] F. Vecchi, C. Freschi, S. Micera, A. M. Sabatini, P. Dario, and R. Sacchetti, "Experimental evaluation of two commercial force sensors for applications in biomechanics and motor control," *5th Ann. Conf. Int. FES*, no. May 2014, 2000.

[54] B.-S. Lin, P.-C. Hsiao, S.-Y. Yang, C.-S. Su, and I.-J. Lee, "Data Glove System Embedded With Inertial Measurement Units for Hand Function Evaluation in Stroke Patients," *IEEE Trans. Neural Syst. Rehabil. Eng.*, vol. 25, no. 11, pp. 2204–2213, Nov. 2017.

[55] G. D. Fulk and E. Sazonov, "Using sensors to measure activity in people with stroke," *Top. Stroke Rehabil.*, vol. 18, no. 6, pp. 746–757, 2011.

[56] M. Hoda, Y. Hoda, B. Hafidh, and A. El Saddik, "Predicting muscle forces measurements from kinematics data using kinect in stroke rehabilitation," *Multimed. Tools Appl.*, vol. 77, no. 2, pp. 1885–1903, 2018.

[57] W.-S. Kim, S. Cho, D. Baek, H. Bang, and N.-J. Paik, "Upper Extremity Functional Evaluation by Fugl-Meyer Assessment Scoring Using Depth-Sensing Camera in Hemiplegic Stroke Patients," *PLoS One*, vol. 11, no. 7, p. e0158640, Jul. 2016.

[58] S. Ganeson, R. Ambar, and M. M. A. Jamil, "Design of a low-cost instrumented glove for hand rehabilitation monitoring system," in *2016 6th IEEE International Conference on Control System, Computing and Engineering (ICCSCE)*, 2016, no. November, pp. 189–192.

[59] E. Repnik, U. Puh, N. Goljar, M. Munih, and M. Mihelj, "Using inertial measurement units and electromyography to quantify movement during action research arm test execution," *Sensors (Switzerland)*, vol. 18, no. 9, pp. 1–23, 2018.

[60] D. Dutta, S. Aruchamy, S. Mandal, and S. Sen, "Poststroke Grasp Ability Assessment Using an Intelligent Data Glove Based on Action Research Arm Test: Development, Algorithms, and Experiments," *IEEE Trans. Biomed. Eng.*, vol. 69, no. 2, pp. 945–954, 2022.

[61] E. M. Bochniewicz, G. Emmer, A. McLeod, J. Barth, A. W. Dromerick, and P. Lum, "Measuring Functional Arm Movement after Stroke Using a Single Wrist-Worn Sensor and Machine Learning," *J. Stroke Cerebrovasc. Dis.*, vol. 26, no. 12, pp. 2880–2887, Dec. 2017.

[62] P. S. Lum *et al.*, "Improving Accelerometry-Based Measurement of Functional Use of the Upper Extremity After Stroke: Machine Learning Versus Counts Threshold Method," *Neurorehabil. Neural Repair*, vol. 34, no. 12, pp. 1078–1087, Dec. 2020.

[63] C. M. Kanzler, I. Lamers, P. Feys, R. Gassert, and O. Lambercy, "Personalized prediction of rehabilitation outcomes in multiple sclerosis: a proof-of-concept using clinical data, digital health metrics, and machine learning," *Med. Biol. Eng. Comput.*, vol. 60, no. 1, pp. 249–261, Jan. 2022.

[64] S. Lee, Y.-S. Lee, and J. Kim, "Automated Evaluation of Upper-Limb Motor Function Impairment Using Fugl-Meyer Assessment," *IEEE Trans. Neural Syst. Rehabil. Eng.*, vol. 26, no. 1, pp. 125–134, Jan. 2018.

[65] L. Formstone, W. Huo, S. Wilson, A. McGregor, P. Bentley, and R. Vaidyanathan, "Quantification of Motor Function Post-Stroke Using Novel Combination of Wearable Inertial and Mechanomyographic Sensors," *IEEE Trans. Neural Syst. Rehabil. Eng.*, vol. 29, pp. 1158–1167, 2021.

[66] L. Yu, D. Xiong, L. Guo, and J. Wang, "A remote quantitative Fugl-Meyer assessment framework for stroke patients based on wearable sensor networks," *Comput. Methods Programs Biomed.*, vol. 128, no. 88, pp. 100–110, May 2016.

[67] R. Julianjatsono, R. Ferdiana, and R. Hartanto, “High-resolution automated Fugl-Meyer Assessment using sensor data and regression model,” in *2017 3rd International Conference on Science and Technology - Computer (ICST)*, 2017, no. Mi, pp. 28–32.

[68] P. Otten, J. Kim, and S. Son, “A Framework to Automate Assessment of Upper-Limb Motor Function Impairment: A Feasibility Study,” *Sensors*, vol. 15, no. 8, pp. 20097–20114, Aug. 2015.

[69] C. Tozlu *et al.*, “Machine Learning Methods Predict Individual Upper-Limb Motor Impairment Following Therapy in Chronic Stroke,” *Neurorehabil. Neural Repair*, vol. 34, no. 5, pp. 428–439, May 2020.

[70] S. Del Din, S. Patel, C. Cobelli, and P. Bonato, “Estimating fugl-meyer clinical scores in stroke survivors using wearable sensors,” *Proc. Annu. Int. Conf. IEEE Eng. Med. Biol. Soc. EMBS*, pp. 5839–5842, 2011.

[71] F. Routhier *et al.*, “Clinicians’ perspectives on inertial measurement units in clinical practice,” *PLoS One*, vol. 15, no. 11, p. e0241922, Nov. 2020.

[72] V. I. Iglovikov, A. Rakhlin, A. A. Kalinin, and A. A. Shvets, “Paediatric Bone Age Assessment Using Deep Convolutional Neural Networks,” in *Lecture Notes in Computer Science (including subseries Lecture Notes in Artificial Intelligence and Lecture Notes in Bioinformatics)*, vol. 11045 LNCS, no. December, 2018, pp. 300–308.

[73] J. Hamill and K. Knutzen, *Biomechanical Basis of Human Movement*, 3rd ed. 2009.

[74] P. J. Mansfield and D. A. Neumann, “Structure and Function of the Hand,” in *Essentials of Kinesiology for the Physical Therapist Assistant*, Second., Elsevier, 2019, pp. 141–177.

[75] J. V. and E. D. Nikki Burr, *Hand Anatomy*, 2017th ed. British Association of Hand Therapists (BAHT), 2017.

[76] C. C. Norkin and D. J. White, *Measurement of Joint Motion: A Guide to Goniometry*, Fifth edit. Philadelphia: Philadelphia : F.A. Davis Company, 2016.

[77] J. L. Sancho Bru, “Model biomecànic de la mà orientat al disseny d’eines manuals,” *TDX (Tesis Dr. en Xarxa)*, Apr. 2008.

[78] B. Buchholz, T. J. Armstrong, and S. A. Goldstein, “Anthropometric data for describing the kinematics of the human hand,” *Ergonomics*, vol. 35, no. 3, pp. 261–273, Mar. 1992.

[79] L. Aiello and C. Dean, *An Introduction to Human Evolutionary Anatomy.*, Sixth. Elsevier Academic Press, 2002.

[80] Y. Yang, C. Fermuller, Y. Li, and Y. Aloimonos, “Grasp type revisited: A modern perspective on a classical feature for vision,” in *2015 IEEE Conference on Computer Vision and Pattern Recognition (CVPR)*, 2015, vol. 07-12-June, no. April, pp. 400–408.

[81] L. Richards and P. Palmiter-Thomas, “A Critical Review of Tools, Methods, and Clinical Utility for Grip Strength Measurement,” *Crit. Rev. Phys. Rehabil. Med.*, vol. 29, no. 1–4, pp. 280–302, 2017.

[82] E. Innes, “Handgrip strength testing: A review of the literature,” *Aust. Occup. Ther. J.*, vol. 46, no. 3, pp. 120–140, Sep. 1999.

[83] CyberGlove Systems Inc.©, “CyberGlove II,” 2017. [Online]. Available: http://www.cyberglovesystems.com/cyberglove-ii. [Accessed: 21-Jun-2019].

[84] E. Peña-Pitarch, N. T. Falguera, and J. (James) Yang, “Virtual human hand: model and kinematics,” *Comput. Methods Biomech. Biomed. Engin.*, vol. 17, no. 5, pp. 568–579, 2014.

[85] R. Tubiana, J.-M. Thomine, and E. Mackin, *Examination of the Hand and Wrist*. CRC Press, 1998.

[86] I. Interlink Electronics, “Interlink Electronics FSR Force Sensing Resistors. FSR Integration Guide,” 2019. [Online]. Available: https://www.digikey.es/es/pdf/i/interlink-electronics/interlink-electronics-fsr-force-sensing-resistors-integration-guide.

[87] J. A. Florez and A. Velasquez, “Calibration of force sensing resistors (fsr) for static and dynamic applications,” in *2010 IEEE ANDESCON*, 2010, pp. 1–6.

[88] M. Y. Saadeh, T. D. Carambat, and A. M. Arrieta, “Evaluating and Modeling Force Sensing Resistors for Low Force Applications,” in *Volume 2: Modeling, Simulation and Control of Adaptive Systems; Integrated System Design and Implementation; Structural Health Monitoring*, 2017, no. 2000, pp. 1–11.

[89] C. M. López-Cerón, “Desarrollo de un sistema para la monitorización de contracción muscular en base a un sensor de presión en superficie,” Universidad Politécnica de Valencia (UPV), 2016.

[90] W.-C. Hsu, T. Sugiarto, J.-W. Chen, and Y.-J. Lin, “The Design and Application of Simplified Insole-Based Prototypes with Plantar Pressure Measurement for Fast Screening of Flat-Foot,” *Sensors*, vol. 18, no. 11, p. 3617, Oct. 2018.

[91] ITead Studio, “HC - 05 - Bluetooth to Serial Port Module (Datasheet),” *Datasheet*, 2010. [Online]. Available: https://datasheetspdf.com/pdf-file/1418730/ITead/HC-05/. [Accessed: 10-Jul-2020].

[92] Unity Technologies, “Unity User Manual 2020.3 (LTS),” 2022. [Online]. Available: https://docs.unity3d.com/Manual/index.html.

[93] K. Nizamis, N. Rijken, A. Mendes, M. Janssen, A. Bergsma, and B. Koopman, “A Novel Setup and Protocol to Measure the Range of Motion of the Wrist and the Hand,” *Sensors*, vol. 18, no. 10, p. 3230, Sep. 2018.

[94] I. Carpinella, J. Jonsdottir, and M. Ferrarin, “Multi-finger coordination in healthy subjects and stroke patients: a mathematical modelling approach,” *J. Neuroeng. Rehabil.*, vol. 8, no. 1, p. 19, 2011.

[95] D. A. Winter, R. K. Greenlaw, and D. A. Hobson, “Television-computer analysis of kinematics of human gait,” *Comput. Biomed. Res.*, vol. 5, no. 5, pp. 498–504, Oct. 1972.

[96] D. A. Winter, H. G. Sidwall, and D. A. Hobson, “Measurement and reduction of noise in kinematics of locomotion,” *J. Biomech.*, vol. 7, no. 2, pp. 157–159, Mar. 1974.

[97] D. A. Winter, *Biomechanics and Motor Control of Human Movement*, Fourth. Waterloo,Ontario,Canada: John Wiley & Sons, Inc., 2019.

[98] V. Gracia-Ibáñez, M. Vergara, J. L. Sancho-Bru, M. C. Mora, and C. Piqueras, “Functional range of motion of the hand joints in activities of the International Classification of Functioning, Disability and Health,” *J. Hand Ther.*, vol. 30, no. 3, pp. 337–347, 2017.

[99] V. Gracia-Ibáñez, P.-J. Rodríguez-Cervantes, V. Bayarri-Porcar, P. Granell, M. Vergara, and J.-L. Sancho-Bru, “Using Sensorized Gloves and Dimensional Reduction for Hand Function Assessment of Patients with Osteoarthritis,” *Sensors*, vol. 21, no. 23, p. 7897, Nov. 2021.

[100] N. J. Jarque-Bou, M. Vergara, J. L. Sancho-Bru, V. Gracia-Ibanez, and A. Roda-Sales, “Hand Kinematics Characterization While Performing Activities of Daily Living Through Kinematics Reduction,” *IEEE Trans. Neural Syst. Rehabil. Eng.*, vol. 28, no. 7, pp. 1556–1565, Jul. 2020.

[101] A. Roda-Sales, M. Vergara, J. L. Sancho-Bru, V. Gracia-Ibáñez, and N. J. Jarque-Bou, “Human hand kinematic data during feeding and cooking tasks,” *Sci. Data*, vol. 6, no. 1, pp. 15–17, 2019.

[102] E. Peña-Pitarch, “Virtual Human Hand: Grasping Strategy and Simulation,” Universitat Politècnica de Catalunya, 2007.

[103] National Aeronautics and Space Administration, “Anthropometry and Biomechanics,” 2019. [Online]. Available: https://www.nasa.gov/feature/anthropometry-and-biomechanics. [Accessed: 20-Mar-2019].

[104] B. K. Szabó, “Rigged hand model for the Blender Game Engine,” *Recent Innov. Mechatronics*, vol. 6, no. 1., 2019.

[105] “Blender 3.1 Reference Manual,” 2022. [Online]. Available: https://docs.blender.org/manual/en/latest/index.html. [Accessed: 05-Sep-2019].

[106] J. F. Padilla-Magaña, E. Peña-Pitarch, I. Sánchez-Suarez, and N. Ticó-Falguera, “Hand Motion Analysis during the Execution of the Action Research Arm Test Using Multiple Sensors,” *Sensors*, vol. 22, no. 9, p. 3276, Apr. 2022.

[107] J. Maw, K. Y. Wong, and P. Gillespie, “Hand anatomy,” *Br. J. Hosp. Med.*, vol. 77, no. 3, pp. C34–C40, 2016.

[108] D. Dolan, “Hope Through Research,” *Neurol. Now*, vol. 10, no. 6, pp. 69–71, Dec. 2014.

[109] V. L. Feigin *et al.*, “World Stroke Organization (WSO): Global Stroke Fact Sheet 2022,” *Int. J. Stroke*, vol. 17, no. 1, pp. 18–29, Jan. 2022.

[110] R. Teasell *et al.*, “Stroke rehabilitation clinician handbook,” *Hear. Stroke Found.*, pp. 1–60, 2020.

[111] N. Ticó Falguera, “Biomechanics of fingers hand as a prognostic factor of functional recovery of the upper extremity in patients with severe stroke.,” Universitat Politècnica de Catalunya., 2016.

[112] R. C. Lyle, “A performance test for assessment of upper limb function in physical rehabilitation treatment and research,” *Int. J. Rehabil. Res.*, vol. 4, no. 4, pp. 483–492, Dec. 1981.

[113] S. Shimawaki, Y. Nakamura, M. Nakabayashi, and H. Sugimoto, “Flexion Angles of Finger Joints in Two-Finger Tip Pinching Using 3D Bone Models Constructed from X-Ray Computed Tomography (CT) Images,” *Appl. Bionics Biomech.*, vol. 2020, 2020.

[114] R. Yokogawa and K. Hara, “Manipulabilities of the Index Finger and Thumb in Three Tip-Pinch Postures,” *J. Biomech. Eng.*, vol. 126, no. 2, pp. 212–219, 2004.

[115] J. W. Lee and K. Rim, “Measurement of finger joint angles and maximum finger forces during cylinder grip activity,” *J. Biomed. Eng.*, vol. 13, no. 2, pp. 152–162, 1991.

[116] S. Shimawaki, T. Murai, M. Nakabayashi, and H. Sugimoto, “Measurement of flexion angle of the finger joint during cylinder gripping using a three-dimensional bone model built by X-ray computed tomography,” *Appl. Bionics Biomech.*, vol. 2019, 2019.

[117] T. Murai, S. Uchiyama, K. Nakamura, Y. Ido, Y. Hata, and H. Kato, “Functional range of motion in the metacarpophalangeal joints of the hand measured by single axis electric goniometers,” *J. Orthop. Sci.*, vol. 23, no. 3, pp. 504–510, 2018.

[118] M. C. Hume, H. Gellman, H. McKellop, and R. H. Brumfield, “Functional range of motion of the joints of the hand,” *J. Hand Surg. Am.*, vol. 15, no. 2, pp. 240–243, Mar. 1990.

[119] G. I. Bain, N. Polites, B. G. Higgs, R. J. Heptinstall, and A. M. McGrath, “The functional range of motion of the finger joints,” *J. Hand Surg. Eur. Vol.*, vol. 40, no. 4, pp. 406–411, 2015.

[120] Z. Smahel and A. Klímová, “The influence of age and exercise on the mobility of hand joints: 1: Metacarpophalangeal joints of the three-phalangeal fingers.,” *Acta Chir. Plast.*, vol. 46, no. 3, pp. 81–8, 2004.

[121] L. De Smet, M. Urlus, A. Spriet, and G. Fabry, “Metacarpophalangeal and interphalangeal flexion of the thumb: influence of sex and age, relation to ligamentous injury.,” *Acta Orthop. Belg.*, vol. 59, no. 4, pp. 357–9, 1993.

[122] E. Peña-Pitarch, J. F. P. Magaña, N. Ticó-Falguera, A. Al Omar, I. A. Larrión, and J. V. Costa, “Virtual human hand: Grasps and fingertip deformation,” *Advances in Intelligent Systems and Computing*, vol. 975. pp. 484–492, 2020.

[123] J. F. Padilla-Magaña, E. Peña-Pitarch, I. Sánchez-Suarez, and N. Ticó-Falguera, “Quantitative Assessment of Hand Function in Healthy Subjects and Post-Stroke Patients with the Action Research Arm Test,” *Sensors*, vol. 22, no. 10, p. 3604, May 2022.

[124] P. Aqueveque, P. Ortega, E. Pino, F. Saavedra, E. Germany, and B. Gómez, “After Stroke Movement Impairments: A Review of Current Technologies for Rehabilitation,” in *Physical Disabilities - Therapeutic Implications*, U. Tan, Ed. InTech, 2017, pp. 96–116.

[125] H. Hayashi and H. Shimizu, “Essential motion of metacarpophalangeal joints during activities of daily living,” *J. Hand Ther.*, vol. 26, no. 1, pp. 69–74, 2013.

[126] A. P. Vasen, S. H. Lacey, M. W. Keith, and J. W. Shaffer, “Functional range of motion of the elbow,” *J. Hand Surg. Am.*, vol. 20, no. 2, pp. 288–292, Mar. 1995.

[127] C. E. Lang, S. L. DeJong, and J. A. Beebe, “Recovery of Thumb and Finger Extension and Its Relation to Grasp Performance After Stroke,” *J. Neurophysiol.*, vol. 102, no. 1, pp. 451–459, Jul. 2009.

[128] P. Raghavan, M. Santello, A. M. Gordon, and J. W. Krakauer, “Compensatory motor control after stroke: An alternative joint strategy for object-dependent shaping of hand posture,” *J. Neurophysiol.*, vol. 103, no. 6, pp. 3034–3043, 2010.

[129] V. S. Hedna *et al.*, “Hemispheric Differences in Ischemic Stroke: Is Left-Hemisphere Stroke More Common?,” *J. Clin. Neurol.*, vol. 9, no. 2, p. 97, 2013.

[130] I. El Naqa and M. J. Murphy, *Machine Learning in Radiation Oncology*. Cham: Springer International Publishing, 2015.

[131] Y. Baştanlar and M. Özuysal, “Introduction to Machine Learning,” vol. 1107, M. Yousef and J. Allmer, Eds. Totowa, NJ: Humana Press, 2014, pp. 105–128.

[132] S. B. Kotsiantis, “Supervised machine learning: A review of classification techniques,” *Inform.*, vol. 31, no. 3, pp. 249–268, 2007.

[133] M. Schuld, I. Sinayskiy, and F. Petruccione, “An introduction to quantum machine learning,” *Contemp. Phys.*, vol. 56, no. 2, pp. 172–185, Sep. 2014.

[134] R. Bhardwaj, A. R. Nambiar, and D. Dutta, “A Study of Machine Learning in Healthcare,” in *2017 IEEE 41st Annual Computer Software and Applications Conference (COMPSAC)*, 2017, vol. 2, pp. 236–241.

[135] P. Mehta *et al.*, “A high-bias, low-variance introduction to Machine Learning for physicists,” *Phys. Rep.*, vol. 810, pp. 1–124, Mar. 2018.

[136] Y. Chen, R. Chang, and J. Guo, “Effects of Data Augmentation Method Borderline-SMOTE on Emotion Recognition of EEG Signals Based on Convolutional Neural Network,” *IEEE Access*, vol. 9, pp. 47491–47502, 2021.

[137] T. Oladipupo, “Types of Machine Learning Algorithms,” in *New Advances in Machine Learning*, IntechOpen, 2010.

[138] C. Cortes and V. Vapnik, “Support-vector networks,” *Mach. Learn.*, vol. 20, no. 3, pp. 273–297, Oct. 1995.

[139] L. Auria and R. A. Moro, “Support Vector Machines (SVM) as a Technique for Solvency Analysis,” *SSRN Electron. J.*, 2008.

[140] Y. Gala Garcia, “Algoritmos SVM para problemas sobre big data,” Universidad Autónoma de Madrid, 2013.

[141] C. J. Villagrá-Arnedo, “Sistema predictivo progresivo de clasificación probabilística como guía para el aprendizaje,” Universidad de Alicante, 2015.

[142] D. Boswell, “Introduction to Support Vector Machines,” 2002.

[143] Javatpoint, “K-Nearest Neighbor(KNN) Algorithm for Machine Learning.” [Online]. Available: https://www.javatpoint.com/k-nearest-neighbor-algorithm-for-machine-learning. [Accessed: 20-Apr-2021].

[144] Z. Zhang, “Introduction to machine learning: k-nearest neighbors,” *Ann. Transl. Med.*, vol. 4, no. 11, pp. 218–218, Jun. 2016.

[145] S. B. Imandoust and M. Bolandraftar, “Application of K-Nearest Neighbor (KNN) Approach for Predicting Economic Events : Theoretical Background,” *Int. J. Eng. Res. Appl.*, vol. 3, no. 5, pp. 605–610, 2013.

[146] L. Breiman, “Random Forests,” *Mach. Learn.*, vol. 45, no. 1, pp. 5–32, 2001.

[147] A. Breiman, Leo and Cutler, “Random Forests.” [Online]. Available: https://www.stat.berkeley.edu/~breiman/RandomForests. [Accessed: 06-Jul-2021].

[148] E. R. Sruthi, “Understanding Random Forest.” [Online]. Available: https://www.analyticsvidhya.com/blog/2021/06/understanding-random-forest/. [Accessed: 21-Mar-2021].

[149] “User Guide Scikit-learn.” [Online]. Available: https://scikit-learn.org/stable/user_guide.html. [Accessed: 04-Aug-2021].

[150] H. M and S. M.N, “A Review on Evaluation Metrics for Data Classification Evaluations,” *Int. J. Data Min. Knowl. Manag. Process*, vol. 5, no. 2, pp. 01–11, Mar. 2015.

[151] M. Grandini, E. Bagli, and G. Visani, “Metrics for Multi-Class Classification: an Overview,” pp. 1–17, Aug. 2020.

[152] D. Steen, “Understanding the ROC Curve and AUC.” [Online]. Available: https://towardsdatascience.com/understanding-the-roc-curve-and-auc. [Accessed: 25-Jul-2021].

[153] A. Yun-chung Liu, “The Effect of Oversampling and Undersampling on Classifying Imbalanced Text Datasets,” The University of Texas at Austin, 2004.

[154] S. Reddy, S. B. Seshadri, G. Sankesh Bothra, T. G. Suhas, and S. C. Thundiyil, “Detection of Arrhythmia in Real-time using ECG Signal Analysis and Convolutional Neural Networks,” in *2020 IEEE 21st International Conference on Computational Problems of Electrical Engineering (CPEE)*, 2020, pp. 1–4.

[155] K.-J. Wang, A. M. Adrian, K.-H. Chen, and K.-M. Wang, “A hybrid classifier combining Borderline-SMOTE with AIRS algorithm for estimating brain metastasis from lung cancer: A case study in Taiwan,” *Comput. Methods Programs Biomed.*, vol. 119, no. 2, pp. 63–76, Apr. 2015.

[156] N. V. Chawla, K. W. Bowyer, L. O. Hall, and W. P. Kegelmeyer, “SMOTE: Synthetic Minority Over-sampling Technique,” *J. Artif. Intell. Res.*, vol. 16, pp. 321–357, Jun. 2002.

[157] H. Han, W. Wang, and B. Mao, “Borderline-SMOTE: A New Over-Sampling Method in Imbalanced Data Sets Learning,” in *ICIC’05: Proceedings of the 2005 international conference on Advances in Intelligent Computing*, 2005, pp. 878–887.

[158] Ethem Alpaydın, “Combined5x2 cv F Test for Comparing Supervised Classification Learning Algorithms,” *Neural Comput.*, vol. 11, pp. 1885–1892, 1999.

[159] S. Raschka, “MLxtend: Providing machine learning and data science utilities and extensions to Python’s scientific computing stack,” *J. Open Source Softw.*, vol. 3, no. 24, p. 638, Apr. 2018.

[160] A. K. Rehme, L. J. Volz, D.-L. Feis, S. B. Eickhoff, G. R. Fink, and C. Grefkes, “Individual prediction of chronic motor outcome in the acute post-stroke stage: Behavioral parameters versus functional imaging,” *Hum. Brain Mapp.*, vol. 36, no. 11, pp. 4553–4565, Nov. 2015.

[161] R. Ani, S. Krishna, N. Anju, M. S. Aslam, and O. S. Deepa, “Iot based patient monitoring and diagnostic prediction tool using ensemble classifier,” in *2017 International Conference on Advances in Computing, Communications and Informatics (ICACCI)*, 2017, pp. 1588–1593.

[162] P. K. Srimani and M. S. Koti, “Medical Diagnosis Using Ensemble Classifiers - A Novel Machine-Learning Approach,” *J. Adv. Comput.*, 2013.

[163] F. Li *et al.*, “Multi-Feature Fusion Method Based on EEG Signal and its Application in Stroke Classification,” *J. Med. Syst.*, vol. 44, no. 2, p. 39, Feb. 2020.

[164] T. G. Dietterich, “Ensemble Methods in Machine Learning,” 2000, pp. 1–15.

[165] E. Peña-Pitarch, I. P. de la Bellacasa, J. F. Padilla-Magaña, A. Al Omar, and I. A. Larrión, “Virtual Human Hand: Wrist Movements,” in *Lecture Notes in Networks and Systems*, vol. 264, 2021, pp. 304–311.

List of Publications

This section details the complete list of publications accepted and presented during the Ph.D.:

Journals

Padilla-Magaña, J.F.; Peña-Pitarch, E.; Sánchez-Suarez, I.; Ticó-Falguera, N. Quantitative Assessment of Hand Function in Healthy Subjects and Post-Stroke Patients with the Action Research Arm Test. *Sensors* ***2022***, *22*, 3604. https://doi.org/10.3390/s22103604

Padilla-Magaña, J.F.; Peña-Pitarch, E.; Sánchez-Suarez, I.; Ticó-Falguera, N. Hand Motion Analysis during the Execution of the Action Research Arm Test Using Multiple Sensors. *Sensors* ***2022***, *22*, 3276. https://doi.org/10.3390/s22093276

Conference Papers

Padilla-Magana, J.; Peña-Pitarch, E.; Ticó, N.; A. Al Omar; Alcelay, J. I. Action Research Arm Test with Multisensory Information. 13th International Conference on Applied Human Factors and Ergonomics (AHFE 2022) and the Affiliated Conferences. New York, USA, July 24-28, ***2022***. *Accepted*

Peña-Pitarch, E.; Inmaculada Puig de la Bellacasa; Padilla-Magana, J.; A. Al Omar; Alcelay, J. I. Virtual human hand: wrist movements. Advances in simulation and digital human modeling: proceedings of the AHFE 2021 Virtual Conferences on Human Factors and Simulation, and Digital Human Modeling and Applied Optimization, July 25–29, 2021, USA. Springer. ***2021***. pp.: 304 ~ 311. ISBN: 978-3-030-79762-1. https://doi.org/10.1007/978-3-030-79763-8

Padilla-Magana, J.; Peña-Pitarch, E.; Ticó, N. Evaluación del Movimiento de la mano mediante el controlador Leap Motion. *Memorias 16 Congreso Nacional de Ciencia Tecnología e Innovación*. *Morelia, Michoacán (México).* ***2021***. https://drive.google.com/drive/folders/1iymiZgIt016SNx2xOh68gqHL-gQPcaDs

Padilla-Magana, J. Design of a sensing system to assess post-stroke rehabilitation with the Action Research Arm Test (ARAT). *9º Simposio Becarios CONACYT en Europa: 8, 9 y 10 de diciembre 2020: memorias: proceedings*. **2021**. pp.: 70 ~ 71. https://www.muframex.fr/wp-content/uploads/2021/02/Memorias-9oSBCE-2020-BD.pdf

Padilla-Magana, J.; Peña-Pitarch, E.; Sánchez, I. Simulación de la extremidad superior del cuerpo humano en un entorno virtual para la rehabilitación médica. *14 Congreso Estatal de Ciencia, Tecnología e Innovación. Morelia, Michoacán (México). 30 octubre* ***2019***.

Peña-Pitarch, E.; Padilla-Magana, J.; Ticó, N.; A. Al Omar; Alcelay, J. I.; Vives, J. Virtual human hand: grasps and fingertip deformation. Advances in Additive Manufacturing, Modeling Systems and 3D Prototyping: proceedings of the AHFE 2019 International Conference on Additive Manufacturing, Modeling Systems and 3D Prototyping, July 24-28, ***2019***, Washington D.C., USA. Springer. 2019. pp.: 484 ~ 492. ISBN: 978-3-030-20216-3. https://doi.org/10.1007/978-3-030-20216-3.

Appendix A

Supplementary material for Chapter 5

Table A1.1. Results of Mann–Whitney test of the arc of motion (AROM) with respect to the Control and Right hemiparesis groups.

			aROM			
Finger Joint	**Group**	**N**	**Mean Rank**	**U**	**Z**	***p***
Thumb CMC	C	400	236.2	14,262.0	−1.53	0.125
	RH	80	262.2			
Thumb MCP	C	400	231.8	12,518.0	−3.07	0.002 **
	RH	80	284.0			
Thumb IP	C	400	239.5	15,610.0	−0.34	0.731
	RH	80	245.4			
Index MCP	C	400	238.4	15,146.0	−0.75	0.451
	RH	80	251.2			
Index PIP	C	400	233.1	13,055.0	−2.60	0.009 **
	RH	80	277.3			
Middle MCP	C	400	258.2	8940.0	−6.23	0.000 ***
	RH	80	152.3			
Middle PIP	C	400	230.6	12,029.0	−3.51	0.000 ***
	RH	80	290.1			
Ring MCP	C	400	240.8	15,874.0	−0.11	0.911
	RH	80	238.9			
Ring PIP	C	400	233.9	13,363.0	−2.33	0.020 **
	RH	80	273.5			
Little MCP	C	400	236.8	14,521.0	−1.31	0.192
	RH	80	259.0			
Little PIP	C	400	211.6	4450.0	−10.20	0.000 ***
	RH	80	384.9			

C= control group; RH= right hemiparesis group; *p < 0.05; **p < 0.01; ***p < 0.001; Control vs Stroke Mann–Whitney U test.; N= Number of tests per group

Table A1.2. Results of Mann–Whitney test of the AROM with respect to the Control and Left hemiparesis groups.

			aROM			
Finger Joint	**Group**	**N**	**Mean Rank**	**U**	**Z**	***p***
Thumb CMC	C	400	231.11	12,245	−0.56	0.577
	LH	64	241.17			
Thumb MCP	C	400	223.10	9038	−3.78	0.000 ***
	LH	64	291.28			
Thumb IP	C	400	239.12	10,152	−2.66	0.008 **
	LH	64	191.13			
Index MCP	C	400	232.16	12,665	−0.14	0.892
	LH	64	234.61			
Index PIP	C	400	232.36	12,744	−0.06	0.955
	LH	64	233.38			

Table A1.2. Cont.

			aROM			
Finger Joint	**Group**	**N**	**Mean Rank**	**U**	**Z**	***p***
Middle MCP	C	400	236.83	11,070	−1.74	0.082
	LH	64	205.47			
Middle PIP	C	400	234.35	12,061	−0.74	0.458
	LH	64	220.95			
Ring MCP	C	400	227.78	10,910	−1.90	0.058
	LH	64	262.03			
Ring PIP	C	400	237.09	10,963	−1.84	0.065
	LH	64	203.80			
Little MCP	C	400	251.12	5353	−7.48	0.000 ***
	LH	64	116.14			
Little PIP	C	400	211.14	4257	−8.58	0.000 ***
	LH	64	365.98			

C= control group; LH= left hemiparesis group; *p < 0.05; **p < 0.01; ***p < 0.001; Control vs LH Mann–Whitney U test.; N= Number of tests per group

Table A1.3. Results of Mann–Whitney test of the AROM with respect to the Stroke groups (Left hemiparesis vs Right hemiparesis).

			aROM			
Finger Joint	**Group**	**N**	**Mean Rank**	**U**	**Z**	***p***
Thumb CMC	LH	64	69.84	2390	−0.68	0.494
	RH	80	74.63			
Thumb MCP	LH	64	75.74	2352.5	−0.83	0.404
	RH	80	69.91			
Thumb IP	LH	64	61.88	1880	−2.73	0.006 **
	RH	80	81.00			
Index MCP	LH	64	71.86	2519	−0.17	0.869
	RH	80	73.01			
Index PIP	LH	64	66.38	2168	−1.58	0.115
	RH	80	77.40			
Middle MCP	LH	64	78.67	2165	−1.59	0.112
	RH	80	67.56			
Middle PIP	LH	64	61.84	1878	−2.74	0.006 **
	RH	80	81.03			
Ring MCP	LH	64	78.56	2172	−1.56	0.119
	RH	80	67.65			
Ring PIP	LH	64	61.54	1858.5	−2.82	0.005 **
	RH	80	81.27			
Little MCP	LH	64	50.23	1135	−5.73	0.000 ***
	RH	80	90.31			
Little PIP	LH	64	68.06	2276	−1.14	0.253
	RH	80	76.05			

RH= right hemiparesis group; LH= left hemiparesis group; C= control group; S= stroke group; *p < 0.05; **p < 0.01; ***p < 0.001; Control vs Stroke Mann–Whitney U test.; N= Number of tests per group

Table A1.4. Functional Range of Motion (FROM) for each finger joint

Finger Joints	Groups		
	C	LH	RH
Thumb CMC	4.09 - 32.97	6.36 - 27.68	-33.44
Thumb MCP	6.99 - 32.40	3.70 - 39.78	3.92 - 36.4
Thumb IP	-38.99	1.96 - 28.48	-44.09
Index MCP	6.90 - 61.89	1.53 - 48.93	-42.76
Index PIP	14.36 - 54.36	3.18 - 52.36	12.55 - 63.1
Middle MCP	2.32 - 61.17	-52.65	5.27 - 45.94
Middle PIP	13.17 - 55.02	19.19 - 65.67	21.39 - 75.34
Ring MCP	-61.06	0.90 - 66.38	10 - 61.01
Ring PIP	8.62 - 49.25	9.31 - 50.21	19.24 - 64.42
Little MCP	2.44 - 44.97	16.68 - 43.17	7.74 - 59.47
Little PIP	8.96 - 30.34	15.82 - 60.60	10.83 - 63.46

C= control group; RH= right hemiparesis; LH= left hemiparesis; CMC= carpometacarpal; MCP = metacarpophalangeal; IP = interphalangeal; PIP = proximal interphalangeal; Negative values represent hyperextension; FROM represents the amplitude of the motion.

Table A1.5. Subtest Range of Motion (sROM) during the performance of the Grasp Subtest (All groups)

Finger Joints	C (°)		LH (°)		RH (°)		C (°)		LH (°)		RH (°)	
	E	SD	E	SD	E	SD	F	SD	F	SD	F	SD
Thumb CMC	5.9	7.4	6.7	1	2.0**	7.8	24	7.6	26.1	1.7	22.2	9.1
Thumb MCP	10.4	9.5	9.7	5.6	9.3	10.3	24.3	8.8	26.9	10.3	26.8	12
Thumb IP	-2.6	14.3	7.3***	6.8	6.6**	18.1	13.3	11.9	22.2***	7.2	32.5***	21.1
Index MCP	17.7	15.8	3.8***	18.4	4.7***	17	42.7	11	41.6	13.9	36.5**	12.3
Index PIP	15.6	8.9	5.0***	11.4	13.8	8.6	35.2	10.6	24.6***	17.3	38.6	13.8
Middle MCP	11.9	12.9	-2.0***	12.3	8.4	12.5	43.3	9.9	35.8**	16.5	32.3***	12
Middle PIP	15.9	7.4	20.4	8.3	24.8***	9.8	41.7	9	45.6	12.5	53.1***	12.3
Ring MCP	7.9	11.6	8	12.5	13.5	13.2	35.7	8.9	45.0**	17	43.3**	13.9
Ring PIP	12.3	8.1	10.2	3.9	21.4***	10.9	38.5	9.9	34	10.9	48.8***	13.4
Little MCP	7.3	7.4	17.8***	4.6	10.1	8.4	28.8	9.1	31.3	5.6	36.0**	14.5
Little PIP	11.8	9.7	18.6***	8.2	15	9	22.9	12.7	45.8***	16.2	44.0***	23.3

RH= right hemiparesis group; LH= left hemiparesis group; C= control group; E= extension; F= flexion; SD= standard deviation *p < 0.05; **p < 0.01; ***p < 0.001; Mann–Whitney U test; °=degrees; CMC= carpometacarpal; MCP = metacarpophalangeal; IP = interphalangeal; PIP = proximal interphalangeal;

Table A1.6. Subtest Functional Range of Motion (sROM) during the performance of the Grip Subtest (All groups)

Finger Joints	Control		LH		RH		Control		LH		RH	
	E	SD	E	SD	E	SD	F	SD	F	SD	F	SD
Thumb CMC	9.9	6.9	8.6	1.5	8.8	4.2	30.7	6	27.0*	1.2	28.1	7.6
Thumb MCP	10.6	8.6	9	6.1	8.2	8.8	28.4	9.5	29.8	9.6	28.7	9.8
Thumb IP	-11.6	17.4	4.5***	7.7	3.9***	12.9	18.6	17.9	25.3*	7.9	30.6***	9.7
Index MCP	21.4	11	14.1	17.8	11.9***	13.3	47.8	13.7	41.3	15.2	33.6***	10.2
Index PIP	18.4	10.1	12.2*	13.6	17.7	12	49.9	12.3	48.4	20.4	56.1	14
Middle MCP	17.5	8.7	8.2***	8	14.1*	10.6	48.7	11.8	36.2*	18.1	33.2***	10.1
Middle PIP	19.6	9.5	29.7**	14.5	30.3**	15.9	51.9	10	61.1**	10.8	67.5***	12.3
Ring MCP	16.6	9.4	19.4	11.2	23.2*	9.8	50.7	15.3	60.4	20.2	54.8	11.7
Ring PIP	14.1	7.9	18.4	12.3	25.0**	14.7	46	11	46.5	11.6	57.0**	15.6
Little MCP	12.5	7.4	22.4***	2.7	16.1*	7.2	41.7	12.9	40.6	7.3	51.2*	17.4
Little PIP	11.2	9.7	21.1**	12.4	13.3	13.7	25.2	14.4	53.8***	17.7	49.7***	24.1

RH= right hemiparesis group; LH= left hemiparesis group; C= control group; E= extension; F= flexion; SD= standard deviation *p < 0.05; **p < 0.01; ***p < 0.001; Mann–Whitney U test; °=degrees; CMC= carpometacarpal; MCP = metacarpophalangeal; IP = interphalangeal; PIP = proximal interphalangeal;

Table A1.7. Subtest Functional Range of Motion (sROM) during the performance of the Pinch Subtest (All groups)

Finger Joints	Control		LH		RH		Control		LH		RH	
	E	SD	E	SD	E	SD	F	SD	F	SD	F	SD
Thumb CMC	13.3	6.1	9.2***	1.6	7.2***	7.6	31.7	5.5	27.2***	1.2	30.7	10.6
Thumb MCP	16	8.6	14	6.8	15.4	10.8	28.3	8	34.2**	9.1	33.2	11.2
Thumb IP	-9.6	16.1	8.9***	10.6	7.6***	16.8	9.5	14.4	21.6	10.1	22.4***	13.9
Index MCP	27.1	9.3	24.1	14.8	17.3***	12.1	48.5	14.9	42.5**	11.1	38.5***	13.8
Index PIP	16	8.8	9.2***	10.7	16.6	10.9	35.3	14.4	29.9	14.3	42.2*	17.2
Middle MCP	24	9.3	15.6***	10.6	19.8	12.2	50.9	11.5	37.2***	13.3	41.7**	13
Middle PIP	14.6	8.2	28.7**	9.9	27.9***	17.5	37.4	10.7	52.7***	11.8	62.3***	17.4
Ring MCP	22.6	8.6	25.5	9.6	26.2*	16	48.1	12	50.4	12.9	53.4**	10
Ring PIP	11.2	8	19.6***	10.3	25.8***	15.4	35.4	12.1	41.9**	14.3	58.4***	12.1
Little MCP	8.7	10.3	23.5***	3.8	14.5**	7.3	27.4	10.1	33.6	6.4	35.3***	9.9
Little PIP	10.9	9.2	25.3***	10.3	17.2**	11	19.2	13	50.5	17.1	49.8***	18.1

RH= right hemiparesis group; LH= left hemiparesis group; C= control group; E= extension; F= flexion; SD= standard deviation *p < 0.05; **p < 0.01; ***p < 0.001; Mann–Whitney U test; °=degrees; CMC= carpometacarpal; MCP = metacarpophalangeal; IP = interphalangeal; PIP = proximal interphalangeal;

Appendix B

Supplementary material for Chapter 6

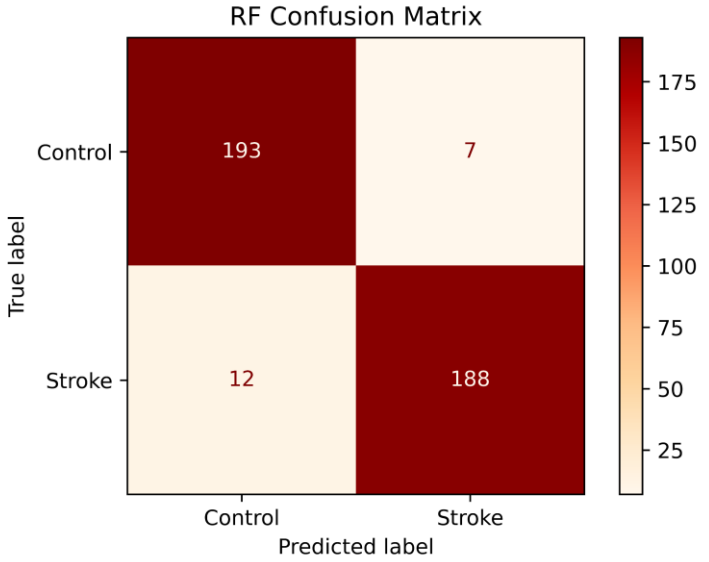

Fig B1. Random Forest Confusion Matrix after Borderline-SMOTE.

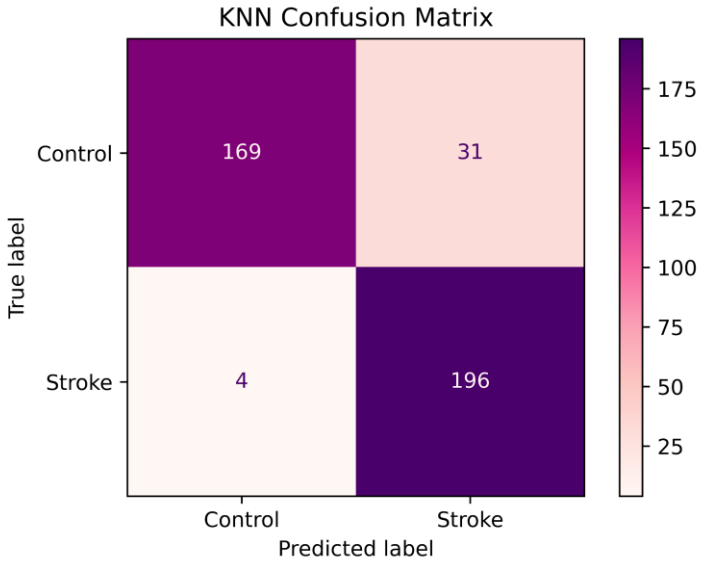

Fig B2. K-nearest neighbor Confusion Matrix after Borderline-SMOTE.

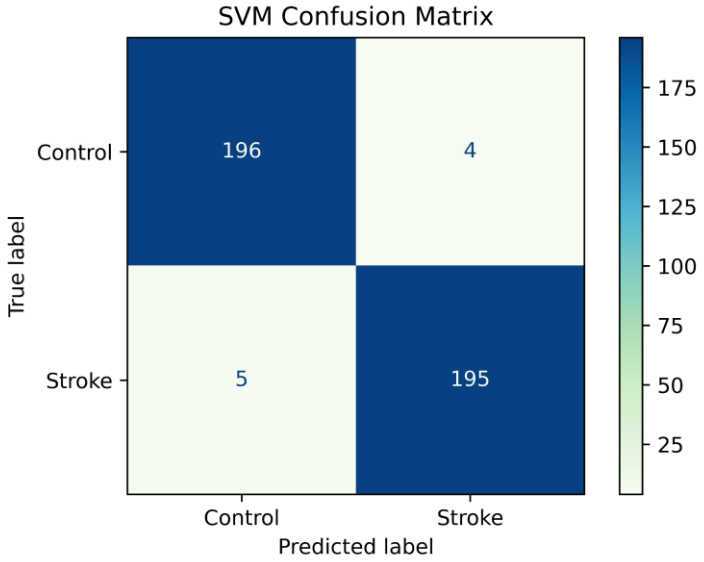

Fig B3. Support Vector Machine Confusion Matrix after Borderline-SMOTE

Table B1.1. Random Forest Paired t-test

Metric	RF	BS_RF	t-statistic	p
Precision	0.961 ± 0.022	0.971 ± 0.014	-1.858	0.096
Accuracy	0.933 ± 0.010	0.971 ± 0.010	-8.153	0.000****
Recall	0.781 ± 0.049	0.970 ± 0.014	-11.281	0.000****
F1-score	0.861 ± 0.024	0.971 ± 0.010	-12.531	0.000****
AUC	0.980 ± 0.006	0.996 ± 0.002	-6.591	0.000****

RF=Random Forest; BS_RF= Borderline-SMOTE Random Forest; *: p <= .05; **: p <= .01; ***: p <= .001; ****: p <=.0001

Table B1.2. Support Vector Machine Paired t-test

Metric	SVM	BS_SVM	t-statistic	p
Precision	0.969 ± 0.029	0.968 ± 0.008	0.107	0.917
Accuracy	0.958 ± 0.011	0.978 ± 0.006	-4.034	0.003***
Recall	0.872 ± 0.044	0.989 ± 0.007	-8.457	0.000****
F1-score	0.917 ± 0.023	0.978 ± 0.006	-7.189	0.000****
AUC	0.984 ± 0.007	0.995 ± 0.004	-3.925	0.003***

SVM= Support Vector Machine; BS_SVM= Borderline-SMOTE Support Vector Machine; ***: p <= .001; ****: p <=.0001

Table B1.3. K-nearest Neighbors Paired t-test

Metric	KNN	BS_KNN	t-statistic	p
Precision	0.951 ± 0.023	0.914 ± 0.021	4.459	0.002***
Accuracy	0.913 ± 0.014	0.948 ± 0.014	-5.137	0.001***
Recall	0.710 ± 0.068	0.989 ± 0.009	-12.884	0.000****
F1-score	0.811 ± 0.039	0.950 ± 0.013	-9.999	0.000****
AUC	0.939 ± 0.018	0.980 ± 0.009	-5.492	0.000****

KNN=K-nearest Neighbors; BS_ KNN= Borderline-SMOTE K-nearest Neighbors; ***: p <= .001; ****: p <=.0001

Appendix C

Participant Information Sheet

HOJA DE INFORMACION PARA EL PARTICIPANTE

TITLE OF THE STUDY: Human Hand Kinematics and Fingertip Force during the Action Research Arm Test

TÍTULO DEL ESTUDIO: Cinemática de la mano humana y fuerza de la punta de los dedos durante el Action Research Arm Test

INVESTIGADORES: Dr. Esteban Peña Pitarch, M.S.M Jesús Fernando Padilla Magaña.

ADSCRIPCIÓN: Universitat Politècnica de Catalunya (UPC).

Escola Politècnica Superior d'Enginyeria de Manresa (EPSEM)

PROGRAMA: DOCTORADO EN AUTOMÁTICA, ROBÓTICA Y VISIÓN.

INTRODUCCIÓN Y PROCEDIMIENTO

Le informamos a través de este documento sobre un estudio de investigación, en el cual está invitado a participar voluntariamente. Para ello le pedimos que lea atentamente esta hoja informativa y que nos consulte la más mínima duda al respecto.

OBJETIVOS:

En este estudio se evaluará a pacientes sanos que no hayan tenido ninguna lesión en la extremidad superior del cuerpo (mano) mediante el Action Research Arm Test ARAT. Con el Objetivo de analizar la cinemática de la mano para determinar el rango de movimiento de las articulaciones mediante el sensor (Cyberglove) y medir la fuerza de agarre a través de sensores de fuerza resistivos (FSR).

BENEFICIOS:

Es posible que de su participación en este estudio no se obtenga un beneficio directo. Sin embargo, Los investigadores de la EPSEM-UPC en colaboración con los médicos rehabilitadores pretenden mediante el análisis de la información obtenida en el estudio: Desarrollar y validar nuevas herramientas para el análisis cinemático y la simulación de la

mano, para su posterior aplicación en el ámbito clínico dentro del área de rehabilitación física. Con el fin de ofrecer un mejor seguimiento, al mejorar la evaluación y la predicción de la evolución de cada paciente. Permitiendo ofrecer planes de rehabilitación más personalizados.

DESCRIPCIÓN DEL ESTUDIO:

El estudio consiste en la colocación de 5 sensores de fuerza resistivos (FSR)en la punta del dedo de la mano dominante, posteriormente se colocará el guante (CyberGlove II) con sensores de flexión. El participante deberá estar sentado en una silla con respaldo firme y sin apoyabrazos. La cabeza en una posición neutral y con los pies en contacto con el suelo. Esta posición se deberá mantener durante todo el periodo de la prueba. EL (ARAT) es una prueba de observación de 19 elementos utilizada por fisioterapeutas y otros profesionales de la salud para evaluar el rendimiento de las extremidades superiores (coordinación, destreza y funcionamiento).

El investigador proporcionara las instrucciones al sujeto para que realice las tareas del Test ARAT que se dividen en 4 subescalas: Grasp, Grip, Pinch y Gross Movement, al tiempo que califica al individuo en función de su desempeño en base a la siguiente escala: 0= sin movimiento, 1= la tarea de movimiento se realice parcialmente, 2= la tarea de movimiento se completa, pero lleva demasiado tiempo, 3= el movimiento se realiza normalmente. Los datos obtenidos por los sensores se almacenarán en una base de datos que posteriormente será analizada por el equipo de investigadores de la Universidad Politécnica de Cataluña. Los datos obtenidos y los resultados publicados respetaran la ley de Protección de datos personales. Esta prueba no durará más de 15 minutos

PROTECCIÓN DE DATOS PERSONALES:

De acuerdo con la Ley 15/1999 de Protección de Datos de Carácter Personal, los datos personales que se obtengan serán los necesarios para cubrir los fines del estudio. En ninguno de los informes del estudio aparecerá su nombre, y su identidad no será revelada a persona alguna salvo para cumplir con los fines del estudio, y en el caso de urgencia médica o requerimiento legal. Cualquier información de carácter personal que pueda ser identificable será conservada por métodos informáticos en condiciones de seguridad por EPSEM. El acceso a dicha información quedará restringido al personal del equipo investigador designado al efecto que estará obligado a mantener la confidencialidad de la información.

De acuerdo con la ley vigente, tiene usted derecho al acceso de sus datos personales; asimismo, y si está justificado, tiene derecho a su rectificación y cancelación. Si así lo desea, deberá solicitarlo al investigador que le atiende en este estudio. De acuerdo con la legislación vigente, tiene derecho a ser informado de los datos relevantes para su salud que se obtengan en el curso del estudio. Esta información se le comunicará si lo desea; en el caso de que prefiera no ser informado, su decisión se respetará. Si necesita más información sobre este estudio puede contactar con el investigador responsable, el/la Dr. Esteban Peña Pitarch Tel. 938732100 ext. 1864. Su participación en el estudio es totalmente voluntaria, y si decide no participar recibirá todos los cuidados médicos que necesite y la relación con el equipo médico que le atiende no se verá afectada.

Consent Form

FORMULARIO DE CONSENTIMENTO DE INFORMACION

TITLE OF THE STUDY: Human Hand Kinematics and Fingertip Force during the performance of the Action Research Arm Test.

TÍTULO DEL ESTUDIO: Cinemática de la mano humana y fuerza de la punta de los dedos durante la realización del Action Research Arm Test.

Nombre(participante):_____**DECLARO** que he leído la hoja de Información y que se me ha entregado una copia, que se me ha dado la oportunidad de hacer preguntas, y que he recibido suficiente información de parte del investigador, quien me ha informado adecuadamente de las condiciones de mi participación en esta investigación. Me han asegurado el tratamiento confidencial de mis datos, además declaro que entiendo que mi participación es voluntaria, por lo que puedo retirarme de la investigación libremente, en cualquier momento durante el experimento y por cualquier motivo, y que:

☐ Otorgo mi consentimiento.

☐ No otorgo mi consentimiento.

Para participar en la investigación que se me ha propuesto, y para que se pueda utilizar la información obtenida durante el experimento con fines puramente de investigación.

DECLARO que cumplo con los siguientes criterios del estudio:

- Mayor de 18 años.
- No eh sufrido ninguna lesión en la muñeca/mano.
- No padezco ninguna enfermedad crónica que afecten el funcionamiento de mi mano.

Fecha y firma del participante

Declaración del investigador responsable

La información contenida en esta solicitud, incluyendo cualquier información que la acompañe, es completa y correcta.

Investigador:

Fecha:

Firma: